

University of Windsor

Scholarship at UWindor

Electronic Theses and Dissertations

Theses, Dissertations, and Major Papers

2004

Addition of hydrogen and oxygen from electrolysis to a gasoline-fuelled spark ignition engine.

Karina Richters
University of Windsor

Follow this and additional works at: <https://scholar.uwindsor.ca/etd>

Recommended Citation

Richters, Karina, "Addition of hydrogen and oxygen from electrolysis to a gasoline-fuelled spark ignition engine." (2004). *Electronic Theses and Dissertations*. 894.
<https://scholar.uwindsor.ca/etd/894>

This online database contains the full-text of PhD dissertations and Masters' theses of University of Windsor students from 1954 forward. These documents are made available for personal study and research purposes only, in accordance with the Canadian Copyright Act and the Creative Commons license—CC BY-NC-ND (Attribution, Non-Commercial, No Derivative Works). Under this license, works must always be attributed to the copyright holder (original author), cannot be used for any commercial purposes, and may not be altered. Any other use would require the permission of the copyright holder. Students may inquire about withdrawing their dissertation and/or thesis from this database. For additional inquiries, please contact the repository administrator via email (scholarship@uwindsor.ca) or by telephone at 519-253-3000ext. 3208.

NOTE TO USERS

This reproduction is the best copy available.

UMI[®]

**Addition of Hydrogen and Oxygen from Electrolysis to a
Gasoline-Fuelled Spark Ignition Engine**

by

Karina Richters

A Thesis

Submitted to the Faculty of Graduate Studies and Research
through Civil and Environmental Engineering
in Partial Fulfillment of the Requirements for
the Degree of Master of Applied Science at the
University of Windsor

Windsor, Ontario, Canada

2004

Copyright © 2004 Karina Richters



National Library
of Canada

Bibliothèque nationale
du Canada

Acquisitions and
Bibliographic Services

Acquisitons et
services bibliographiques

395 Wellington Street
Ottawa ON K1A 0N4
Canada

395, rue Wellington
Ottawa ON K1A 0N4
Canada

Your file *Votre référence*
ISBN: 0-612-92444-0
Our file *Notre référence*
ISBN: 0-612-92444-0

The author has granted a non-exclusive licence allowing the National Library of Canada to reproduce, loan, distribute or sell copies of this thesis in microform, paper or electronic formats.

L'auteur a accordé une licence non exclusive permettant à la Bibliothèque nationale du Canada de reproduire, prêter, distribuer ou vendre des copies de cette thèse sous la forme de microfiche/film, de reproduction sur papier ou sur format électronique.

The author retains ownership of the copyright in this thesis. Neither the thesis nor substantial extracts from it may be printed or otherwise reproduced without the author's permission.

L'auteur conserve la propriété du droit d'auteur qui protège cette thèse. Ni la thèse ni des extraits substantiels de celle-ci ne doivent être imprimés ou autrement reproduits sans son autorisation.

In compliance with the Canadian Privacy Act some supporting forms may have been removed from this dissertation.

Conformément à la loi canadienne sur la protection de la vie privée, quelques formulaires secondaires ont été enlevés de ce manuscrit.

While these forms may be included in the document page count, their removal does not represent any loss of content from the dissertation.

Bien que ces formulaires aient inclus dans la pagination, il n'y aura aucun contenu manquant.

Canada

ABSTRACT

In today's world, people have come to rely on the automobile. Unfortunately, the use of automobiles has had a negative effect on our environment as seen by global warming, acid rain and locally, a great number of ozone action days. It is evident that the use of automobiles is going to continue to grow. Automobile companies are under increasing pressure from environmental organizations and government regulators to develop more environmentally friendly automobiles, while buyers continue to want the performance and reliability of today's car. Therefore, researchers are continuing to experiment with methods to enhance the performance provided from an engine while reducing emissions.

The use of hydrogen has been the focus of many researchers. One of the benefits of using hydrogen is the potential for substantial reduction in emissions. Unfortunately, one of the main obstacles is the development of a hydrogen engine is on-board hydrogen storage. It has been suggested that the use of electrolysis to generate hydrogen on-board a vehicle would solve the current infrastructure problems. This research involved studying the use of an electrolysis unit to produce hydrogen and oxygen, which was then fed into the intake manifold of a gasoline-fuelled spark ignition (SI) engine. Chemical analysis of the electrolysis products confirmed that hydrogen and oxygen were produced in a 2:1 ratio with no evidence of any other by-products. The production rate of the electrolysis products was measured to be approximately 500 mL/min, which on average accounted for 0.12% H₂ by mass of the fuel (gasoline). No significant effect on torque, indicated mean effective pressure, cycle-to-cycle variations or burn duration was noted for the addition of these electrolysis products as compared to the engine run with gasoline only. Emission results for carbon monoxide, nitrogen oxide, and unburned hydrocarbons also showed no effect with the addition of the electrolysis products. Computer simulations conducted showed a small increase in engine power output, and emissions (carbon monoxide and nitrogen monoxide). However, the increase was so small that an effect on the engine was not anticipated.

Family and Friends

ACKNOWLEDGEMENTS

First and foremost, I would like to thank my Co-Advisors, Dr. Henshaw and Dr. Ting for providing me the opportunity to work on this project. Their time spent working with me helped me build knowledge and experience in research. I would also like to thank Dr. Xu and Dr. Zheng for participating on my thesis committee.

Special thanks is given to Bruce Durfy, who gave extraordinary amounts of his time to not only help me with the constant maintenance of the engine but who saw this as an ideal learning opportunity for me as well. His guidance has allowed me to develop the confidence needed to work independently on mechanical repairs. The technical assistance of Pat Seguin and the Technical Support Centre is greatly appreciated.

A very special thanks needs to be given to Tina D'Andrea, whose initial work in this area of research intrigued me to continue. Her support and training were paramount in continuing the research she began. I would also like to thank Mwila (Clarence) Mulenga and Ramiz Ahemad for their help over the months of testing.

In addition to the support I received from those at the University, I could not have completed this thesis without the encouragement of my family and friends. I'd like to especially thank my parents for backing me in the decision to return to school to continue my education after years away and my sister, Celia, and brother, Jim, for their support, which was seen through the jokes made continuously about me still being in school. I've been blessed with too many great friends to name them all but just know that I appreciated your friendship and support through the years.

The financial support of The Natural Science and Engineering Research Council (NSERC), the University of Windsor, and donations by Briggs and Stratton and Global Tech Environmental Products are gratefully acknowledged.

TABLE OF CONTENTS

ABSTRACT	iii
DEDICATIONS	iv
ACKNOWLEDGEMENTS	v
LIST OF FIGURES	x
LIST OF TABLES	xiv
NOMENCLATURE	xvi
LIST OF ABBREVIATIONS	xix
1 INTRODUCTION	1
1.1 Vehicle Contribution to Air Pollution	1
1.1.1 Carbon Dioxide	1
1.1.2 Carbon Monoxide	1
1.1.3 Oxides of Nitrogen	2
1.1.4 Hydrocarbons	2
1.1.5 Ozone	3
1.1.6 Oxides of Sulphur	3
1.1.7 Particulate Matter	3
1.1.8 Reduction in Emissions through the Use of Hydrogen	3
1.2 Objective	4
1.3 Scope	4
2 LITERATURE REVIEW	6
2.1 Spark Ignition Engines	6
2.1.1 Lean Operation	7
2.1.2 Flame Speed	12
2.1.3 Combustion Duration	13
2.1.4 Engine Performance	14
2.2 Hydrogen Addition	16
2.2.1 Flame Speed	18

2.2.2	Combustion Duration	20
2.2.3	Engine Performance	21
2.2.4	Emissions	23
2.2.5	Safety Considerations	24
2.3	Electrolysis	25
2.3.1	Electrolysis Products (Hydrogen and Oxygen) Addition	26
3	SIMULATIONS	28
3.1	Equivalence Ratio Calculation	28
3.2	Simulation Matrix	29
3.3	STANJAN	29
3.4	ENGINE SIMULATION PROGRAM (ESP)	31
3.5	CHEMKIN	33
4	EXPERIMENTAL APPARATUS AND PROCEDURE	34
4.1	Analysis of Electrolysis Products	34
4.1.1	Sample Preparation	34
4.1.2	Calibration	34
4.1.3	Test Procedure	34
4.2	Engine Experimental Set-Up	35
4.2.1	Engine-Dynamometer Set-Up	36
4.2.2	Electrolysis Products Delivery	37
4.2.3	Air Flow	38
4.2.4	Gasoline Delivery	40
4.2.5	Exhaust Delivery/Gas Analysis	40
4.3	Testing Procedure	41
4.4	Equivalence Ratio	42
4.5	Processing Pressure and Crank Angle Data	43
4.5.1	Cylinder Volume Calculation	44
4.5.2	Pressure Signal Conversion Calculation	45
4.5.3	Work Output	46

4.6	Burn Duration Analysis	49
5	RESULTS AND DISCUSSION	51
5.1	Electrolysis Products Analysis	51
5.2	Simulations	51
5.2.1	STANJAN	52
5.2.2	Engine Simulation Program	57
5.2.3	CHEMKIN	59
5.3	Engine Testing	68
5.3.1	Torque	68
5.3.2	Indicated Mean Effective Pressure	72
5.3.3	Coefficient of Variation	76
5.3.4	Burn duration	81
5.3.5	Emissions	96
5.4	Electrolysis Unit Power Requirements	110
5.5	Summary	112
5.5.1	Work	112
5.5.2	Emissions	113
6	CONCLUSIONS AND RECOMMENDATIONS	116
6.1	Conclusions	116
6.2	Recommendations	117
7	REFERENCES	119

APPENDICES

APPENDIX A	Stanjan Procedures	123
APPENDIX B	CHEMKIN	133
APPENDIX C	GC Calibration and Calculations	137
C.1	Calibration using ambient air samples	139
C.2	Calibration using pure hydrogen and oxygen samples	140
C.3	Determination of the composition of electrolysis products	142
APPENDIX D	LabView Code	146
APPENDIX E	Electrolysis Flow Rate Measurements	149
APPENDIX F	Air Flow Measurements	151
APPENDIX G	Uncertainty Analysis	154
G.1	Speed	154
G.2	Torque	155
G.3	Indicated Mean Effective Pressure	155
G.4	Air Flow Rate	156
G.5	Gasoline Flow Rate	159
G.6	Equivalence Ratio	160
G.7	Encoder	162
G.8	Cylinder Volume	163
G.9	Data Acquisition System and Pressure Transducer	164
G.10	Burn Duration	167
G.11	Gas Analysis	168
G.12	Electrolysis Products Flow Rate	169
VITA AUCTORIS		170

LIST OF FIGURES

Figure 2.1	Ideal Air Standard Otto Cycle	6
Figure 2.2	Typical Pressure-Volume Diagram	7
Figure 2.3	Typical emissions trends to equivalence ratio	9
Figure 2.4	Laminar flame speeds for fuels as function of equivalence ratio	12
Figure 2.5	Laminar flame speeds for hydrogen supplemented propane as a function of R_H and ϕ_F .	19
Figure 2.6	Effects of hydrogen addition on BSFC at stoichiometric conditions	22
Figure 2.7	Simplified schematic of the electrolysis of water	25
Figure 4.1	Engine set-up schematic	35
Figure 4.2	Photograph of engine experimental set-up	36
Figure 4.3	Schematic of electrolysis set-up	38
Figure 4.4	Intake Schematic	39
Figure 4.5	Exhaust system designed for use with ENERAC 3000EV Gas Analyser	41
Figure 4.6	Example of p - V diagram	46
Figure 4.7	Trapezoidal method for approximation of area under the curve	47
Figure 5.1	STANJAN modelling results for the effects of the addition of electrolysis products to iso-octane on predicted work	52
Figure 5.2	Adiabatic temperatures at state 3 as predicted by STANJAN for the addition of electrolysis products	54
Figure 5.3	CO concentrations at state 3 as predicted by STANJAN for the addition of electrolysis products	55

Figure 5.4	NO concentrations at state 3 as predicted by STANJAN for the addition of electrolysis products	56
Figure 5.5	Pressure-CAD diagram for engine parameters equal to the Briggs & Stratton Vanguard 20 HP Engine	57
Figure 5.6	p - V diagram provided by the Engine Simulation Program for engine parameters equal to the Briggs & Stratton Vanguard 20 HP Engine	58
Figure 5.7	ESP modelling results for the effects of the addition of electrolysis products to iso-octane on predicted work	59
Figure 5.8	CHEMKIN modelling results for the effects of the addition of electrolysis products to iso-octane on flame speed	61
Figure 5.9	Temperature as distance for equivalence ratios ($\phi=0.7$ to 1.2)	62
Figure 5.10	CHEMKIN modelling results for the effects of the addition of electrolysis products on adiabatic temperatures	62
Figure 5.11	CHEMKIN modelling results for the effects of the addition of electrolysis products on CO concentrations	63
Figure 5.12	CO concentrations as distance from the adiabatic unburned boundary for equivalence ratios ($\phi=0.7$ to 1.2)	64
Figure 5.13	CHEMKIN modelling results for the effects of the addition of electrolysis products on NO emissions	65
Figure 5.14	NO concentrations as distance from the adiabatic unburned boundary	66
Figure 5.15	The effect of electrolysis products addition on torque	69
Figure 5.16	Decrease in torque for the addition of electrolysis products	72
Figure 5.17	The effects of the addition of electrolysis products on IMEP	73

Figure 5.18	Decreases in IMEP for the addition of electrolysis products	76
Figure 5.19	COV_{imep} versus engine speed	78
Figure 5.20	COV_{imep} versus equivalence ratio	80
Figure 5.21	Decreases in COV_{imep} based on the addition of electrolysis products	81
Figure 5.22	Relative pressure versus crank angle for fired and unfired cycle	82
Figure 5.23	$dP/dCAD$ versus crank angle for fired and unfired cycle at 3300 rpm	82
Figure 5.24	Mass fraction burned curves plotted for 16 consecutive cycles (Test 9, without electrolysis products)	83
Figure 5.25	Illustration of the calculation of the 10 to 90 % burn duration	84
Figure 5.26	0-2% burn duration versus speed	86
Figure 5.27	2-10% burn duration versus speed	89
Figure 5.28	10-90% burn duration versus speed	92
Figure 5.29	Location of Peak Burn Rate versus speed	95
Figure 5.30	Carbon monoxide emissions with engine speed	99
Figure 5.31	Decrease in carbon monoxide emissions from the addition of electrolysis products	100
Figure 5.32	Carbon monoxide emissions versus equivalence ratio	101
Figure 5.33	Nitrogen oxide emissions with engine speed	104
Figure 5.34	Decrease in nitrogen oxide emissions from the addition of electrolysis products	105
Figure 5.35	NO emissions versus equivalence ratio	106
Figure 5.36	Hydrocarbon emissions versus speed	108

Figure 5.37	Decrease in hydrocarbon emissions due to the addition of electrolysis products	109
Figure 5.38	Hydrocarbon emissions versus equivalence ratio	111
Figure A.1	Idealized Otto cycle used in STANJAN	123
Figure C.1	Sample of chromatograph produced for ambient air samples used during calibration	138
Figure C.2	Sample chromatograph produced from Varian Chrompack CP-3800 gas chromatograph with thermal conductivity detector (TCD)	145
Figure D.1	LabView User Interphase	146
Figure D.2	LabView code for collecting signals from the three channels	147
Figure D.3	LabView code that sends data to the designated file	148
Figure E.1	Flow rate of electrolysis products versus time	150
Figure F.1a	Flow rate comparison for anemometer and manometer readings (flow rates in L/s)	153
Figure F.1b	Flow rate comparison for anemometer and manometer readings (flow rates in ft ³ /min)	153

LIST OF TABLES

Table 2.1	Comparison of properties for hydrogen, methane, propane and iso-octane	17
Table 3.1	Reactant molar quantities	29
Table 3.2	Engine geometry and operating conditions	32
Table 4.1	Example of LabView data files as viewed in a spreadsheet with some explanation	43
Table 5.1	Calculated volumes of hydrogen and oxygen from electrolysis products	51
Table 5.2	CHEMKIN results as influenced by pressure	67
Table 5.3	Torque results present with fuel and H ₂ flow rates, equivalence ratio and speed for each test	70
Table 5.4	Imep results presented with fuel and H ₂ flow rates, equivalence ratio and speed for each test	74
Table 5.5	COV _{imep} results presented with fuel and H ₂ flow rates, equivalence ratio and speed for each test	79
Table 5.6	0-2% Burn duration results	85
Table 5.7	Summary of test conditions resulting in minimum and maximum burn durations for that test	87
Table 5.8	2-10% Burn duration results	88
Table 5.9	Summary of test conditions resulting in minimum and maximum durations for that test	90
Table 5.10	10-90% Burn duration results	91
Table 5.11	Summary of test conditions resulting in minimum and maximum durations for that test	93
Table 5.12	Location of peak burn rate	94
Table 5.13	Summary of test conditions resulting in minimum and maximum CAD at peak burn rate	96

Table 5.14	Carbon monoxide emissions results	98
Table 5.15	Nitrogen oxide emission results	103
Table 5.16	Hydrocarbon emissions results	107
Table 5.17	Comparison of power requirements and power gain	110
Table 5.18	Comparison of work results for the addition of electrolysis products	112
Table 5.19	Comparison of simulation results and engine testing results for the addition of electrolysis products (CO emissions)	114
Table 5.20	Comparison of simulation results and engine testing results for the addition of electrolysis products (NO emissions)	115
Table C.1	Summary of operating conditions	137
Table C.2	Calculated masses of hydrogen, nitrogen and oxygen from the electrolysis products sample	142
Table C.3	Calculation to determine contribution of O ₂ from electrolysis products	143
Table C.4	Calculated volumes of hydrogen and oxygen from electrolysis products	143
Table C.5	Calculation to determine % of sample unaccounted	144
Table E.1	Electrolysis products flow rate comparison for engine tests	150
Table F.1	Location of pitot tube measurements for equal area method	151
Table G.1	Speed uncertainty calculations for each engine test completed	154
Table G.2	Equivalence ratio uncertainty calculations for each engine test completed	161
Table G.3	IMR 2800P Gas Analyser measurement and range	168
Table G.4	ENERAC 3000E Gas Analyser measurement and range	169

NOMENCLATURE

a	crank radius (m)
a_i	number of different atoms present in the system
A	amplitude
A	cross sectional area (m^2)
B	cylinder bore (m)
c_p	constant-pressure heat capacity of the mixture (ergs/g·K)
c_{pk}	constant-pressure heat capacity of the k th species (erg/g·K)
C_A	mole fraction of air
C_F	mole fraction of fuel
C_H	mole fraction of hydrogen
$D_{k,j}$	multicomponent diffusion coefficient of the species k in species j (cm^2/s)
D_k^T	thermal diffusion coefficient of the k th species (cm^2/s)
h_k	specific enthalpy of the k th species (erg/g)
l	connecting rod length (m)
\dot{M}	mass flow rate (which is independent of x) (g/s)
m_f	mass of fuel (g)
n_R	crank revolutions for each power stroke (for a four stroke engine, $n_R=2$)
n_{ij}	number of i atoms in a j molecule
η_{th}	thermal efficiency
N	engine speed (rev/s)
$\bar{N}_{(j)}$	number of mols in the phase containing species j
P	power (J/s)
P_b	brake power (J/s)
P_{net}	net power (J/s)
p	pressure (kPa)
\bar{p}	average peak pressure (kPa)
Δp	pressure difference (kPa)

Δp_{ci}	change in pressure due to combustion at crank angle i , normalized by V_c (kPa/mm ³)
Δp_i	pressure difference due to combustion at crank angle i (kPa)
p_i	population of i atoms in the system
Q_f	fuel flow rate (L/s)
Q_{air}	air flow rate (L/s)
Q_{HV}	higher heating value (kJ/kg)
R	universal gas constant (0.08205 L·atm/mol·K)
r_c	compression ratio
R_H	relative hydrogen addition
s	stroke variation
S_L	laminar flame speed (cm/s)
T	temperature (K)
V	volume (mm ³)
V_c	clearance volume (mm ³)
V_{max}	maximum volume (mm ³)
V_k	diffusion velocity of the k th species (cm/s)
V_s	swept volume (mm ³)
\bar{W}	mean molecular weight of the mixture (g/mole)
W_k	molecular weight of the k th species (g/mole)
W	work (kJ)
W_{netIN}	net indicated work (kJ)
$W_{grossIN}$	gross indicated work (kJ)
$W_{pumpingIN}$	pumping indicated work (kJ)
x_j	mol fraction of species j
Y_k	mass fraction of the k th species

δ_L	laminar flame thickness (m)
λ	thermal conductivity of the mixture (ergs/cm·K·s)
λ_i	element potential (the “Lagrange multipliers”)
ϕ	fuel/air equivalence ratio
ρ	density (g/cm ³)
η_f	fuel conversion efficiency
η_{th}	thermal efficiency
τ	torque (N·m)
u_k	ordinary diffusion velocity of the k th species (cm/s)
ω_k	thermal diffusion velocity of the k th species (cm/s)
$\dot{\omega}_k$	molar rate of production by chemical reaction of the k th species per unit (mole/cm ² ·s)

LIST OF ABBREVIATIONS

BDC	bottom dead centre
bsfc	brake specific fuel consumption
CAD	crank angle degree
CI	compression Ignition
COV_{imep}	coefficient of variation
HEF	hydrogen energy fraction
imep	indicated mean effective pressure
mbf	mass fraction burned
OSHA	Occupational Safety and Health Administration
pmep	pumping mean effective pressure
sfc	specific fuel consumption
SI	spark ignition
SPE	solid polymer electrolyte
TDC	top dead centre
VOCs	volatile organic compounds
C_8H_{18}	iso-octane
CO	carbon monoxide
CO ₂	carbon dioxide
H ₂	hydrogen
H ₂ O	water

KOH	potassium hydroxide
O ₂	oxygen
OH	hydroxyl radical
N ₂	nitrogen
NO	nitrogen oxide
NO ₂	nitrogen dioxide
NO _x	oxides of nitrogen

1 INTRODUCTION

1.1 VEHICLE CONTRIBUTION TO AIR POLLUTION

In Canada alone, there are 16.8 million light-duty vehicles (cars, vans, sports utility vehicles, and light-duty trucks) traveling an annual distance of approximately 17,000 km [Statistics Canada, 2000]. Under ideal operating conditions a light-duty vehicle using an internal combustion engine will use a fuel (hydrocarbons) and air mixture for combustion emitting carbon dioxide, water and nitrogen. Unfortunately, complete (ideal) combustion is not possible under standard operating conditions, therefore, other products including unburned hydrocarbons, oxides of nitrogen and carbon monoxide are often emitted. The average light-duty vehicle contributed approximately 4480 kg of carbon dioxide, 200 kg of carbon monoxide, 20 kg of volatile organic compounds, 22 kg of oxides of nitrogen, 0.89 kg of oxides of sulphur and 0.27 kg of particulate matter in 2000 [Environment Canada, 2001]. To better understand the need for reduction of automobile emissions a summary is provided below to outline the environmental and health effects related to individual automobile emissions.

1.1.1 Carbon Dioxide

Carbon dioxide is naturally present in the environment. Sources include animal and human respiration, and degradation of materials. Sinks include oceanic and respiration of plants. However, due to the use of hydrocarbon fuels in combustion, carbon dioxide sources outweigh the sinks, causing an imbalance in the atmosphere. This imbalance is contributing to global warming.

1.1.2 Carbon Monoxide

Light-duty vehicles, especially at colder temperatures, are the main source of carbon monoxide (CO), which is a product of incomplete combustion of hydrocarbons [Cooper and Alley, 1994]. Carbon monoxide depletes the hydroxyl radical concentration in the

atmosphere. The hydroxyl radical is considered a natural cleansing agent in the earth's atmosphere. Carbon monoxide also has direct human health effects mainly by reducing the body's ability to carry oxygen and can promote respiratory infections, especially in children and the elderly [Environment Canada, 1998].

1.1.3 Oxides of Nitrogen

Major components of the oxides of nitrogen include; nitric oxide (NO), nitrogen dioxide (NO₂) and nitrous oxide (N₂O). Nitrogen oxide is the dominant oxide of nitrogen formed during combustion and oxidizes into NO₂ in the presence of hydrocarbons and sunlight. NO₂ can further react with hydrocarbons to produce ozone, or with water producing NO₃, a precursor of acid rain [Environment Canada, 1998].

NO affects lung function and is an irritant to mucous membranes. NO slowly oxidizes to NO₂ at room temperature in the presence of O₂ [Schäfer and van Basshuysen, 1995]. NO₂ is a contributor to respiratory problems including: increased sensitivity of asthmatics and bronchitis sufferers, increased respiratory infections in young children and the elderly, and (at high levels) pulmonary edema. Environmental effects of NO₂ include; corrosion of metals, degradation of textiles, rubber and polyurethane, suppressed vegetation growth, increase in ground level ozone and depletion of stratospheric ozone [Environment Canada, 1998].

1.1.4 Hydrocarbons (including VOCs)

Hydrocarbons, including volatile organic compounds (VOCs) contribute to the formation of ground level ozone. Many VOCs, such as benzene, are known carcinogens, and may be neurotoxic [Environment Canada, 1998].

1.1.5 Ozone

Ozone is produced by the oxidation of NO_x and VOCs in the presence of sunlight. Ozone is known to suppress plant growth and at ground level ozone is a global warming agent [Schäfer and van Basshuysen, 1995]. Health effects attributed to ozone include: decrease in lung function, eye irritation, and decrease in immune system efficiency. Ozone may also lead to chronic lung disease [Environment Canada, 1998].

1.1.6 Oxides of Sulphur

Fuels contain small levels of sulphur that when burned (oxidized) produces sulphur dioxide, SO_2 of which a small fraction may be further oxidized to sulphur trioxide, SO_3 [Heywood, 1988]. Sulphur dioxide is an odourless gas that reacts with water to produce sulphuric acid, which contributes to acid rain. SO_2 is an irritant to mucous membranes [Schäfer and van Basshuysen, 1995].

1.1.7 Particulate Matter

Particulate matter can reduce through the air visibility and can cause aesthetic damage to buildings. Health problems are created when small particulate matter ($<10\mu\text{m}$) is inhaled into the lungs causing respiratory infections and decreasing lung function [US Environmental Protection Agency, 2003].

1.1.8 Reduction in Emissions through the Use of Hydrogen

Regulations continue to be modified to enforce a continuing reduction in emissions from automobiles. Therefore, many companies have looked to the use of hydrogen fuel to reduce vehicle emissions and improve performance. Most of the larger automotive companies have prototypes that use on board storage of either liquid or compressed gaseous hydrogen [Crosse, 2003]. The benefits of the use of hydrogen are a substantial reduction in emissions. Unburned hydrocarbons, carbon monoxide and particulate emissions would be limited to those produced by engine oil [Fulton *et al.* 1993]. One of

the main factors limiting the widespread use of the hydrogen engine is uneconomic on-board hydrogen storage.

The infrastructure and training required to handle and store hydrogen would be an enormous capital expense when compared to the existing gasoline and diesel fuels. A possible solution to the problems of safe handling of hydrogen is to produce the hydrogen as needed. Therefore, hydrogen is not stored, reducing the chance of hydrogen leakage and accumulation in closed spaces during storage or filling. For these reasons, the generation of hydrogen on-board a vehicle as needed was considered.

Global Tech Environmental Products Inc. has developed an on-board Hydrogen Power System (HPS), to produce hydrogen and oxygen through electrolysis. The hydrogen and oxygen gas produced are fed into a gasoline-fuelled engine. The company markets the system by guarantying a reduction in exhaust emissions and an increase in horsepower and fuel economy presumably through more complete combustion of the gasoline. A smoother running engine with a longer engine life is also highlighted in their marketing packages. The company claims that they have seen the largest benefits in diesel engines, which are older than two years [Global Tech Environmental Products, 2003].

1.2 OBJECTIVE

The objective of this research is to determine the effects of electrolysis products addition to a small spark ignition gasoline engine. The intention of this investigation is to determine if the addition of the electrolysis products generated by the Global Tech HPS system will reduce emissions and fuel consumption.

1.3 SCOPE

To determine the effects of the electrolysis products, computer simulations along with engine testing was conducted. The computer models; STANJAN, Engine Simulation Program (ESP) and CHEMKIN were used to model the effects of the addition of hydrogen and oxygen (2:1 ratio) with iso-octane fuel on emissions, flame speed and

engine work. The engine testing was completed on a two-cylinder spark ignition gasoline engine to monitor the effects of the electrolysis products from the Global Tech unit on emissions, torque, power and indicated mean effective pressure (imep), burn duration and cycle-to-cycle variation. For both the computer modelling and the engine testing, the results from the addition of electrolysis products were compared to the results from gasoline (iso-octane) only to determine if any benefits are detected by the use of the electrolysis unit.

2 LITERATURE REVIEW

2.1 SPARK IGNITION ENGINES

A spark ignition (SI) engine, as the name indicates uses a spark to ignite a fuel and air mixture. The typical fuel used in a spark ignition engine is gasoline (a mixture of hydrocarbons which is sometimes simulated by iso-octane). A SI engine was used for the experiment section of this research and therefore will be the focus of the literature review.

A SI engine can be designed to operate on a two-stroke or four-stroke mechanical cycle, with the four-stroke engines typically having higher efficiencies [Stone, 1999]. The Briggs and Stratton Engine, which was used in this research, uses two cylinders operating on the four-stroke cycle. This four-stroke cycle is ideally described as the air standard Otto cycle, which consists of four processes. The pressure-volume diagram provided in Figure 2.1 depicts the following processes:

- 1→2 isentropic compression where V_1/V_2 is the compression ratio, r_c .
- 2→3 constant volume combustion
- 3→4 isentropic expansion to original volume V_1
- 4→1 exhaust of combustion products to original pressure at constant volume.

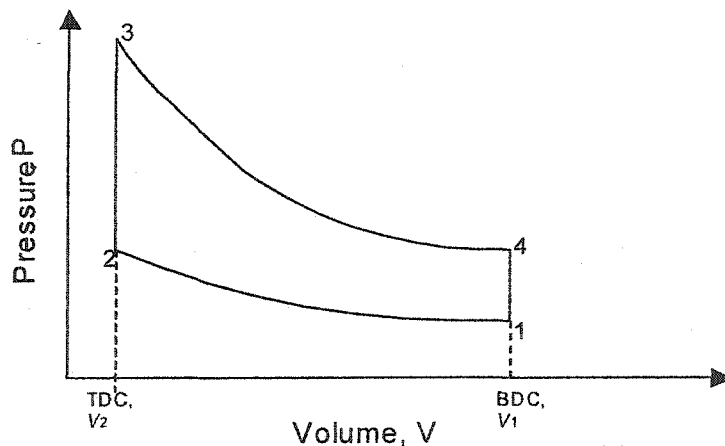


Figure 2.1 Ideal Air Standard Otto Cycle

The ideal air standard Otto cycle assumes that: 1) mixture behaves as an ideal gas with constant specific heat capacity, 2) all processes are fully reversible, 3) no induction or exhaust processes are considered, 4) heat addition is from an external source, 5) heat rejection is to the environment and 6) there is no heat loss to the environment during the cycle except during the exhaust process. However, an actual pressure-volume diagram developed through engine testing would generally look like Figure 2.2. In the Otto cycle, it is assumed that the combustion occurs at minimum volume (TDC), while in a real engine the combustion process occurs over a finite crank angle period (usually between 20 and 70 crank angle degrees) [Heywood, 1988].

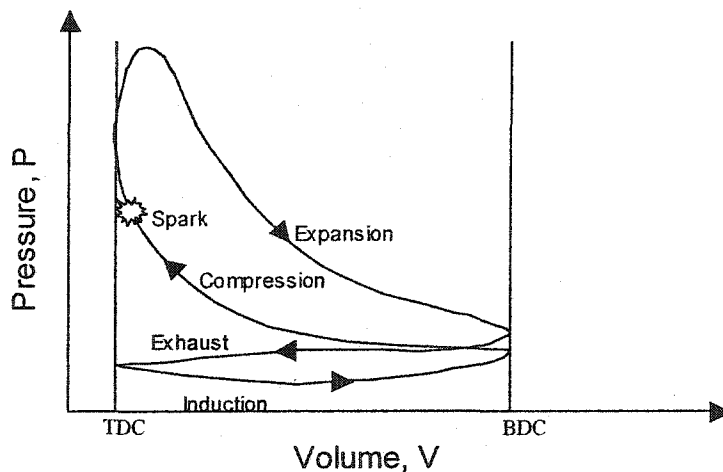


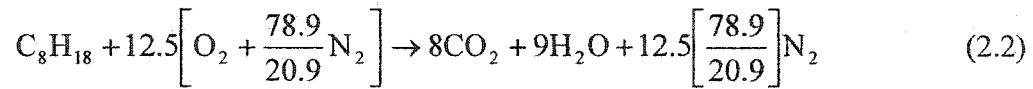
Figure 2.2 Typical Pressure-Volume Diagram

2.1.1 Lean Operation

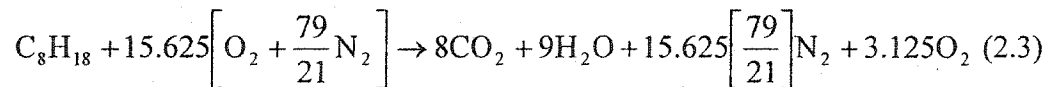
Engines are often described as operating lean, stoichiometric or rich depending on the ratio of air to fuel (A/F) used in combustion. Under stoichiometric conditions, the amount of air supplied is just sufficient to oxidize the fuel. This ratio is usually expressed in terms of the equivalence ratio, ϕ .

$$\phi = \frac{\text{stoichiometric air / fuel ratio}}{\text{actual air / fuel ratio}} \quad (2.1)$$

The chemical equation below is for the stoichiometric combustion of iso-octane in air.



This equation represents complete combustion of one mole of iso-octane fuel with 12.5 moles of oxygen (air is 78.9 % N₂ and 20.9 % O₂). Therefore, the molar stoichiometric air/fuel ratio for this equation is 12.5/1. If the engine combustion chemistry was similar, the actual air/fuel ratio would also be 12.5/1, giving an equivalence ratio of 1. A mixture which has excess air is described as lean and would have an equivalence ratio less than 1.



In this equation the molar ratio of air to iso-octane is increased and the products also include oxygen. From this equation the actual air/fuel ratio is equal to 15.625/1. Therefore, the equivalence ratio is equal to 0.8 ($\phi = 12.5/15.625 = 0.8$). This is a lean fuel mixture. In contrast, a mixture which uses excess fuel compared to air is rich, with an equivalence ratio greater than 1.

Based on engine design and fuel composition there is a limit on how lean or rich a mixture can be prepared and still maintain combustion. At the lean limit of operation, the flame will no longer propagate due to insufficient fuel while at the rich limit of operation there is insufficient oxygen for flame propagation.

Several studies have been conducted to determine the optimum equivalence ratio at which to operate a SI engine. The equivalence ratio can influence emissions and engine performance. The next few subsections will detail the advantages and disadvantages of lean and rich engine operations.

2.1.1.1 Benefits associated with lean operation

Advantages for the lean operation of engines are higher thermal efficiency, lower likelihood of knock and allowance for higher compression ratios while reducing heat transfer [Shrestha and Karim, 1999]. Another fundamental benefit of operating an engine under lean conditions is a reduction in fuel consumption, which translates to a reduction in emissions. Typical variations of emissions compared to equivalence ratio for a spark ignition engine are shown in Figure 2.3 [Stone, 1999].

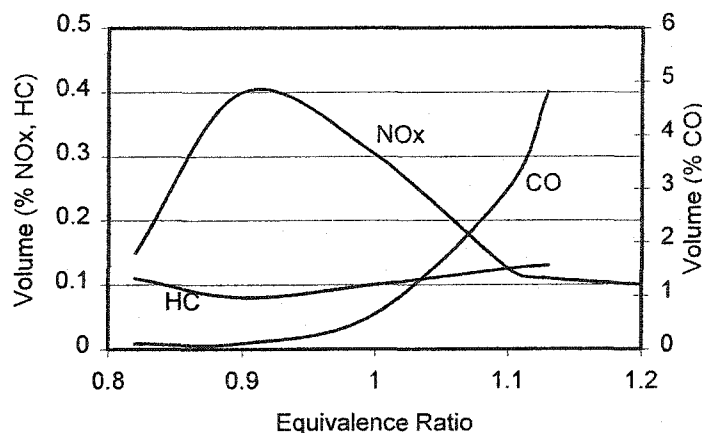


Figure 2.3 Typical Emissions Trends as function of Equivalence Ratios (adapted from Stone 1999)

Carbon Monoxide

As shown in Figure 2.3, carbon monoxide concentration increases with increasing equivalence ratio. The main factor contributing to a higher concentration of carbon monoxide is the decrease in oxygen available for complete combustion. Carbon monoxide is initially formed from the oxidation of the hydrocarbons, with further oxidation of CO to CO₂ [Turns, 2000]. The recombination of CO to CO₂ is primarily dependent on the pressure during the expansion phase [Schäfer and van Basshuysen, 1995]. Higher pressures increase in the rate of oxidation of CO. Even with lean mixtures (excess oxygen) carbon monoxide is present owing to dissociation of CO₂, but the concentration

is reduced with a decrease in combustion temperature. The combustion temperature is reduced the further the combustion is from stoichiometric conditions [Stone, 1999]. Engine related parameters such as ignition timing, compression ratio, and engine speed are insignificant in controlling CO emissions [Schäfer and van Basshuysen, 1995].

Hydrocarbons

Just as carbon monoxide concentrations decrease in the presence of excess air so do the hydrocarbon emissions up to a point. After that point, as mixtures become even leaner, the combustion quality becomes poor and the quench distance increases [Heywood, 1988]. The quench distance is the distance from a cold boundary (such as cylinder walls and crevices) where the flame is extinguished due to heat loss to the metal. The unburned hydrocarbons in these areas would become part of the exhaust, contributing to the hydrocarbon emissions.

Oxides of Nitrogen

The formation of NO_x is more complex because there are three main sources of nitrogen oxide emissions. First, thermal NO is the NO that is oxidized from molecular nitrogen in the air in the postflame zone. Prompt NO is formed in the flame zone. The third main source of nitrogen is fuel NO, which is formed from the nitrogen-containing compounds in the fuel.

The chemistry behind the formation of thermal NO_x is best described by the extended Zeldovich mechanism:



Equations 2.4 and 2.5 will dominate in the presence of excess air (lean mixtures), with Equation 2.6 only significant for rich mixtures due to lower oxygen concentrations [Borman *et al.* 1998]. The chemical kinetics show that the formation of NO is strongly related to the oxygen concentration and the flame temperature [Stone, 1999]. The highest NO_x concentrations occur just lean of stoichiometric where temperature is high and oxygen is available.

In addition to oxygen concentration and flame temperature, the formation of NO_x is also dependent on time. The combustion of lean mixtures is associated with a lower flame speed, which provides a longer time for NO_x formation. Similarly, a reduction in engine speed increases NO_x emissions [Stone, 1999]. On the other hand, operating an engine very lean ($\phi < 0.85$) reduces the combustion temperature resulting in a reduction of NO.

2.1.1.2 Problems associated with lean operation

Problems associated with lean operation are the increased likelihood of poor engine performance caused by slower flame propagation, flame extinction, and increased cycle-to-cycle variations [Shrestha and Karim, 1999]. Other factors affecting the operation of an engine at lean conditions include heterogeneous mixture formation, non-ideal induction systems, and uneven cylinder-to-cylinder distribution [Varde, 1981]. Due to these difficulties most small engines operate near stoichiometric even though the lean limit for gasoline fuel is around an equivalence ratio of 0.6. Three-way catalytic converters in the exhaust of gasoline engines also require the engine to be operated near stoichiometric conditions to maintain high conversion efficiencies of CO, unburned hydrocarbons, and NO_x. Under lean conditions the reduction of NO_x is limited, while under rich conditions, the lack of oxygen limits the oxidation of CO and the unburned hydrocarbons [Schäfer and van Basshuysen, 1995].

2.1.2 Flame Speed

Flames are characterized as either premixed flames or diffusion flames. Premixed flames are so termed because the reactants of combustion are perfectly mixed prior to combustion whereas diffusion flames occur when separate fuel and oxidizer streams combust as they mix. Ideally, the flames generated in spark ignition engines are premixed flames.

A premixed flame can be further classified as laminar or turbulent. The laminar flame speed is the velocity at which the laminar flame propagates into the premixed unburned mixture ahead of the flame and is dependent on pressure, temperature, species concentrations and the mixture transport and thermodynamics properties [Heywood, 1988]. The laminar flame speed (or laminar burning velocity) is dependent on equivalence ratio and peaks just rich of stoichiometric conditions for iso-octane fuel/air mixtures. A comparison of laminar flame speeds is provided in Figure 2.4.

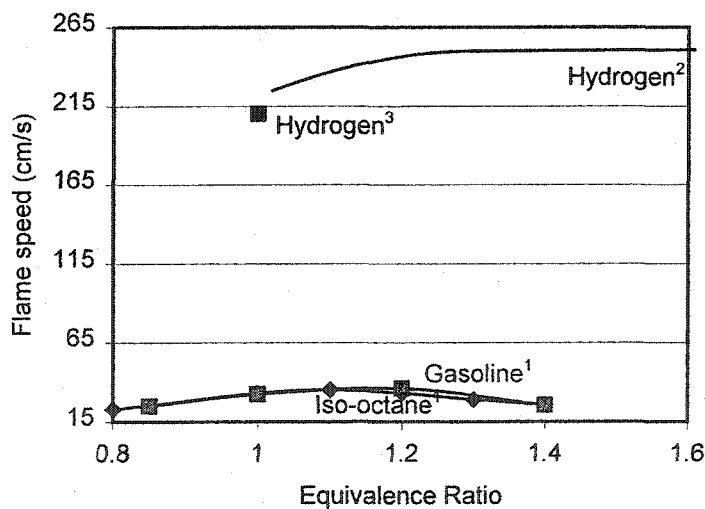


Figure 2.4 Laminar flame speeds for fuels as function of equivalence ratio, at 1 atm and 300K (adapted from ¹Heywood, 1988, ²Strehlow, 1984, ³Turns, 2000).

However, within an engine cylinder the flame is not considered laminar but turbulent. Turbulent flames are directly dependent on the laminar flame speed, S_L , and are generally

characterized by intensity, u' (the root mean square value of the velocity fluctuation) and scale (a measure of the size of eddies found in the turbulent flow) [Borman and Ragland, 1998]. Generally, as turbulence increases so does the burning rate, however, at some point the turbulence may become too great and lead to the extinction of the flame.

2.1.3 Combustion Duration

The combustion process is regularly divided into four stages according to the fuel mass fraction burned (mfb). The four groups are as follows:

1) 0-2% mfb

This is also referred to as the ignition delay period, and includes the initial spark and the development of a flame kernel, usually represented by the interval 0-2% mfb.

2) 2-10% mfb

The flame development phase is usually characterized as the time required after flame initiation to burn 10% of the mass.

3) 10-90% mfb

The bulk of combustion takes place under this category, with the interval representing 10% to 90% mfb. The 10% to 90% mfb is commonly referred to as the combustion duration or rapid burn stage.

4) Flame termination

The extinction of the flame is the final stage.

The mfb percent intervals noted above are somewhat arbitrary, however the intervals above have been used in previous work [Apostolescu and Chiriac, 1996; Sher and Hacoheh, 1989]. In engines, these percentages are sometimes expressed in crank angle degrees. Factors affecting the burn duration include: fuel-air mixture, fuel type, amount of turbulence and cylinder design.

2.1.4 Engine Performance

2.1.4.1 Cycle-to-cycle variations

Cycle-to-cycle variations can be described as the non-repeatability of consecutive engine cycles. The extent of cycle-to-cycle variations is dependent on several factors including; variations in mixture motion, the air/fuel mixture composition and the mixing of residual exhaust gases. Based on the cycle-to-cycle variations, the optimum spark timing is set for the average cycle. Slower burning cycles may not burn completely, leading to losses in power and efficiency. At the other extreme, faster burning cycles, with their over-advanced spark may cause knock [Heywood, 1988]. Knock is characterized by an audible “knocking” sound, which occurs when an unburned gas mixture spontaneously ignites resulting in a rapid pressure rise. Depending on the knock’s intensity and duration, damage to the engine can occur.

Three different approaches have been used to measure the cycle-to-cycle variability. The first involves pressure-related parameters such as maximum cylinder pressure and corresponding crank angle degree (CAD), the maximum rate of pressure rise and the corresponding crank angle and the indicated mean effective pressure. Secondly, the cycle-to-cycle variability has been measured by the burn-rate-related parameters such as maximum heat release rate, maximum mass burning rate, flame development angle (CAD) and rapid burning angle (CAD). The third approach uses the flame front position parameters including the flame radius, flame front area, enflamed or burned volume at given times and flame arrival time at given locations [Heywood, 1988].

Typically the pressure-related parameters are used to measure the cycle-to-cycle variability because of the ease of obtaining and analyzing pressure data. The coefficient of variation (COV) is an important measure of cyclic variability. In terms of the indicated mean effective pressure (imep), the COV_{imep} is the standard deviation of the imep results (σ_{imep}) divided by the average imep and expressed as a percent:

$$COV_{imep}(\%) = \frac{\sigma_{imep}}{imep_{avg}} \times 100 \quad (2.7)$$

A COV_{imep} greater than 10% is usually considered to be the result of a “rough” running engine [Heywood, 1988].

2.1.4.2 Fuel Conversion Efficiency

When describing an engine’s fuel efficiency two terms are often used. The first is the thermal efficiency, η_{th} , calculated by

$$\eta_{th} = \frac{W_c}{m_f Q_{LHV}} = \frac{P}{\dot{m}_f Q_{LHV}} \quad (2.8)$$

where: W_c is the work per cycle

m_f is the mass of fuel inducted per cycle,

Q_{LHV} is the lower heating value,

P is the power,

\dot{m}_f is the fuel flow rate.

The second term calculated is the fuel flow rate per unit power output. This is the specific fuel consumption (sfc), which is inversely proportional to the fuel conversion efficiency, η_{th} , for normal hydrocarbon fuels.

$$sfc = \frac{\dot{m}_f}{P} = \frac{1}{\eta_{th} Q_{LHV}} \quad (2.9)$$

2.1.4.3 Indicated Mean Effective Pressure (imep)

The indicated mean effective pressure (imep) is a measure of the indicated work output per unit swept volume normalized for the number of cylinders and engine speed or the area enclosed in the P - V diagram:

$$imep(N/m^2) = \bar{p}_i = \frac{\text{indicated work output (N} \cdot \text{m) per cylinder per cycle}}{\text{swept volume per cylinder (m}^3\text{)}} \quad (2.10)$$

The terms gross imep and bmep (brake mean effective pressure) are often used to indicate if the pumping work is included in the imep calculation. The bmep does not include the pumping work.

$$imep = bmep + pmep \quad (2.11)$$

The pmep is the pumping mean effective pressure, which is the pumping loss or pumping work divided by the swept volume.

2.2 HYDROGEN ADDITION

The addition of hydrogen as a supplement to a gasoline-air mixture as well as the primary fuel (hydrogen only) in combustion processes has been the focus of several researchers. Several properties of hydrogen make it an attractive fuel alternative when compared to hydrocarbon fuels such as methane, propane and iso-octane (gasoline). A comparison of properties for these fuels is provided in Table 2-1 [D'Andrea, 2003].

Table 2-1: Comparison of Properties for Hydrogen, Methane, Propane and Iso-octane

Properties	Hydrogen	Methane	Propane	Iso-octane (gasoline)
Chemical Formula	H ₂	CH ₄	C ₃ H ₈	C ₈ H ₁₈
Molecular Weight	2.02	16.04	44.1	114.2
Lower Heating Value ² (MJ/mol)	286	802	2043	5100
Lower Heating Value ³ (MJ/kg)	120	50.0	46.4	44
Minimum Ignition Energy ¹ (mJ)	0.02	0.29	0.26	0.24
Flame Speed ^{1,5} (cm/s)	237	42	46	41.5
Diffusion Coefficient ^{1,4} (cm ² /s)	0.61	0.16	0.12	0.05
Quenching Gap ¹ (cm)	0.06	0.2	0.2	0.2

D'Andrea [2003], ¹Bain *et al.*[1998], ²Stone [1999], ³Heywood[1988].⁴At stoichiometric conditions. ⁵At 20°C.

The heating value or calorific value of a fuel is the magnitude of the heat of reaction at constant pressure or at constant volume at a standard temperature (usually 25°C) for the complete combustion of a unit mass of fuel. The term lower heating value or net heating value is used when the water formed is in the vapour phase, while the higher heating value or gross heating value is used when the H₂O is condensed to the liquid phase. Typically, the water in the exhaust is in vapour form, so the lower heating value is used in engine combustion calculations [Turns, 2000]. Hydrogen's inferior heating values mean that the combustion of hydrogen produces less energy per mole than the other fuels. Therefore, an engine operating on a hydrogen-air mixture is expected to have a lower power output than with an equivalent hydrocarbon-air mixture. Hydrogen's other properties, such as high flame speed, high diffusivity, lower ignition energy and reduced quenching gap make it advantageous as a fuel supplement.

2.2.1 Flame Speed

As shown in Table 2.1, hydrogen has a flame speed more than 5 times greater than the iso-octane, propane or methane. Varde [1981] measured the flame speed of hydrogen supplemented gasoline mixtures in a SI engine. The flame speed was measured using ionization probes. The study used two flow rates (7 L/min and 10 L/min) and two engine speeds (1700 rpm and 2000 rpm). For an engine speed of 1700 rpm, the measurements concluded that for lean fuel mixtures (equivalence ratio equal to 0.8) the turbulent flame speed (21 m/s, 23 m/s and 24 m/s) increased as the hydrogen flow rate ($H_2 = 0, 7, \text{ and } 10 \text{ L/min}$) was increased. However, little change was seen for fuel-rich mixture when comparing mixtures with and without the hydrogen supplement.

Milton and Keck [1984] compared laminar flame speeds of stoichiometric mixtures of hydrogen and hydrogen supplemented acetylene, propane, and methane using the constant volume combustion bomb. For hydrogen supplemented propane the flame speed initially accelerates to a value 50% greater than the flame speed of pure propane followed by a reduction in flame speed and then a second rise and fall. This same trend was seen for hydrogen-supplemented methane. No clear explanation was given to explain the double peak. Overall, the addition of hydrogen increased the flame speed by at least 50%. Each experimental flame speed was compared to a calculated value obtained when proportionally averaging the hydrocarbon and hydrogen flame speeds on a molar basis. For all three hydrogen-fuel mixtures the experimental value was less than the predicted value calculated by proportionate averages, with the hydrogen-acetylene experimental values closer to the predicted value. This indicates that the slower burning gases dominated the laminar flame speed.

Yu *et al* [1986] generated a symmetrical counterflow by using two identical aerodynamically shaped nozzles to determine the laminar flame speeds of hydrocarbon-hydrogen and air mixtures. To stabilize the flame an external shroud flow of N_2 was introduced. By varying the velocity of the shroud flow, flame disturbances could be reduced which was important for rich mixtures. This setup improved on the studies

completed by Milton and Keck by allowing for measurements of lean and rich flames as well as flames at stoichiometric conditions. The results of the study showed a strong linear relationship between the laminar flame speed, S_L^0 , and the relative amount of hydrogen addition, R_H , Figure 2.5. The relative amount of hydrogen addition was calculated using

$$R_H = \frac{C_H + C_H / (C_H / C_A)_st}{C_F + [C_A - C_H / (C_H / C_A)_st]} \quad (2.12)$$

where C_F , C_H , and C_A are the mole fractions of fuel (The fuels used were propane and methane), hydrogen and air respectively. S_L^0 was also found to be dependent on the effective fuel/air equivalence ratio, ϕ_F .

$$\phi_F = \frac{C_F / [C_A - C_H / (C_H / C_A)_st]}{(C_H / C_A)_st} \quad (2.13)$$

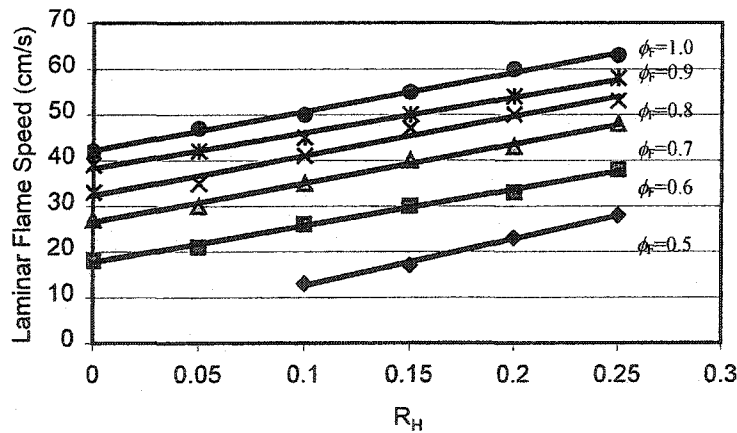


Figure 2.5 Laminar flame speeds for hydrogen supplemented propane as a function of R_H , and ϕ_F (Adapted from Yu *et al.*, 1986).

The laminar flame speed was shown to increase with an increase in the relative amount of hydrogen added to propane. It is expected that a similar increase will be seen with the

addition of hydrogen to iso-octane, as the laminar flame speeds are comparable (propane 46 cm/sec and iso-octane 41.5 cm/sec).

Apostolescu and Chiriac [1996] carried out experiments in a combustion bomb to measure the laminar flame speed for gasoline and hydrogen. A hydrogen addition greater than 10% by mass resulted in an increase of approximately 35% in the laminar flame speed for stoichiometric mixtures. Further experiments were recommended to investigate the influence of smaller amounts of hydrogen.

2.2.2 *Combustion Duration*

A study conducted on a single cylinder SI engine by Rauckis and McLean [1979] investigated the effect of hydrogen-indolene mixtures. The mixtures were characterized by the equivalence ratio and the percent of total fuel energy contributed by hydrogen (HEF – hydrogen energy fraction). The hydrogen energy fraction was varied from 5% to 28%. The most significant reduction in combustion duration was for the 0-2% mfb duration, with a less significant reduction in the 2-10 % mfb duration and relatively little change in the combustion duration stage 10-90% mfb duration. The authors concluded that the principle effect of hydrogen addition was rapid chain-branching oxidation characteristic of hydrogen, which promotes the flame initiation.

Sher and Hacoheh [1989] studied the combustion duration in a gasoline-fuelled SI engine supplemented with gasoline and found that the 0-2% mfb period was significantly reduced with the addition of hydrogen similar to the findings of Rauckis and McLean [1979] for hydrogen supplemented-indolene. The authors believed that the ignition process was also enhanced by the rapid dissociation of the hydrogen molecules to active radicals. This study however, did not support the finding that the effect of hydrogen is more pronounced in lean mixtures as reported by Rauckis and McLean.

Apostolescu and Chiriac [1996] studied the 0-10% mfb and the 10-90% mfb duration, for a hydrogen supplemented gasoline-fuelled SI engine operated on one cylinder. The

addition of hydrogen was shown to shorten both the 0-10% mfb duration and the 10-90% mfb duration. Unlike Rauckis and McLean [1979], Apostolescu and Chiriac [1996] did find a substantial reduction in the 10-90% mfb duration with the hydrogen supplemented gasoline.

2.2.3 *Engine Performance*

2.2.3.1 Cycle-to-cycle Variations

As described in Section 2.1.4.1, the promotion of flame development and propagation rates can reduce the COV_{imep} with optimum spark timing. Therefore, it would be expected that the addition of hydrogen with its higher diffusion coefficient and high flame speed would promote the initial and subsequent flame propagation rates leading to a decrease in the cycle-to-cycle variations.

Varde [1981] randomly selected 200 cycles to determine average peak pressure, \bar{p} , and the peak pressure difference, Δp . Cyclic pressure variations were then represent by the parameter, $\Delta p / \bar{p}$. The results showed a decrease in the pressure variation in the lean mixture region when hydrogen was supplemented to gasoline. Similarly, Apostolescu and Chiriac [1996] reported a significant decrease in cycle-to-cycle variability (based on pressure measurements) with the addition of 5% by weight of hydrogen to gasoline in experiments conducted on a passenger car engine. This correlated with the shortening of the burn duration.

2.2.3.2 Fuel Conversion Efficiency

An improvement in the brake specific fuel consumption (bsfc) was found in the study by Houseman and Hoehn [1974] when gasoline was enriched with hydrogen (3.8 – 11.4 g/min H₂). A 10% improvement in bsfc was found with the modified engine using hydrogen supplemented gasoline over the entire range of engine speeds tested (1000 to 2500 rpm) when compared to the stock engine with gasoline only.

Small quantities of hydrogen (7 and 10 L/min) added to gasoline were noted to decrease the fuel consumption (increase the thermal efficiency) especially in lean mixtures by Varde [1981] in small industrial type SI engines. However, no improvement was seen for rich mixtures.

Hacohen and Sher [1989] introduced hydrogen into the intake manifold at a hydrogen-fuel (gasoline) mass ratio between 2 – 6% and found a significant improvement (10-20%) in the bsfc. Their results are adapted in Figure 2.6 with the bsfc for the hydrogen supplemented fuel compared to the bsfc, which is the brake specific fuel consumption for the engine operated at the same speed and torque but on gasoline only. The authors also noted that the energy conversion gain was most prominent at partial loads. The rate of energy conversion slowed with increased amounts of hydrogen addition with only marginal improvements to the bsfc with hydrogen addition greater than 6%.

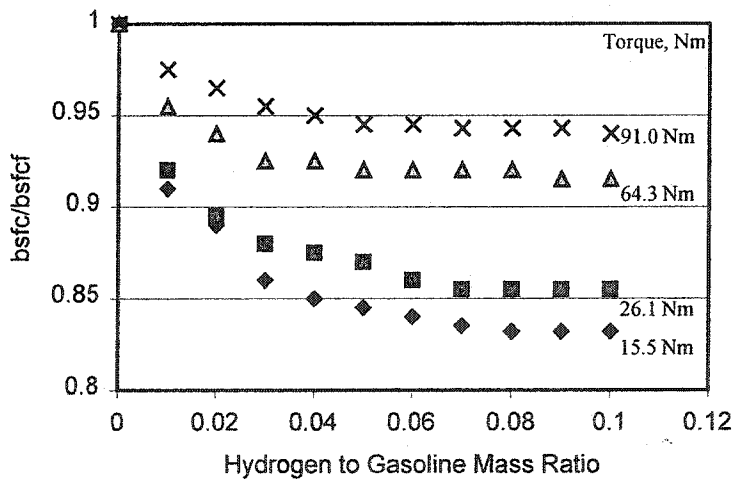


Figure 2.6 Effects of hydrogen addition on bsfc at stoichiometric conditions (Adapted from Hacohen and Sher, 1989).

Two additional studies on SI engines for the addition of hydrogen to gasoline conducted by Apostolescu and Chiriac [1996] and Al-Baghdadi and Al-Janabi [2000] experienced

similar results to those found by Hacothen and Sher, a decrease in the sfc (increase in thermal efficiency) with the addition of up to 6 % by mass of hydrogen.

2.2.3.3 Indicated Mean Effective Pressure (imep)

A study conducted by D'Andrea [2003] used pressure measurements to determine the imep from the same small spark ignition engine as used in this study for gasoline only and hydrogen-supplemented gasoline. The hydrogen was premixed with air and stored in gas cylinders. The supplied gas was delivered to the engine by means of a chamber mounted on the intake. The chamber contained three inlets so the engine could be run from either the compressed air line in the lab or one of the prepared gas cylinders containing 2% hydrogen in air. The imep demonstrated an improvement of 31 – 82% from the addition of 2% hydrogen in air with an equivalence ratio less than 0.78, with negligible effects at equivalence ratios greater than 0.84.

2.2.4 *Emissions*

Stebar and Parks [1974] studied the effects of hydrogen-supplemented fuel in a single-cylinder SI engine operated at 1200 rpm. They concluded that the addition of 10% hydrogen (by weight) extended the lean limit for iso-octane from an equivalence ratio of 0.89 to 0.55 corresponding with a reduction in NO_x emissions. However, they found that hydrocarbon emissions increased.

Similar results were documented by Houseman and Hoehn [1974] for tests conducted on a V-8 SI engine with a modified fuel system. The NO_x emissions for the modified engine with hydrogen-enrichment were found to be only 12% of the NO_x emissions for the stock engine and 5 % of the modified lean-burn engine without hydrogen addition. The hydrocarbon emissions increased with the modified engine with hydrogen-enrichment. The authors speculated that the increase in hydrocarbon emissions was associated with the modified engine running under leaner conditions than the standard engine. Under leaner operating condition the hydrocarbon emissions increase due to wall quenching,

incomplete combustion and lower exhaust temperatures inhibiting post-flame oxidation of the hydrocarbons. The authors also noted that CO emissions decreased with rpm for the modified engine with hydrogen-enrichment whereas the modified engine running on gasoline only had an increase in CO emissions with an increase in rpm.

Emissions measured from a passenger car SI engine by Apostolescu and Chiriac [1996] showed a significant decrease of hydrocarbon emissions with hydrogen addition to lean gasoline mixtures. NO_x emissions tended to increase with hydrogen addition in excess air, which is governed by the relationship between NO_x and temperature. NO_x emissions were reduced only at the highest air-fuel ratios tested. The increase in NO_x emissions is attributed to the higher flame temperatures with hydrogen addition. No substantial difference was reported for CO emissions.

2.2.5 *Safety Considerations*

Many of the properties that make hydrogen attractive as an alternative fuel also add to safety concerns. Hydrogen is classified as a flammable, hazardous gas under U.S. regulation 29 CFR [1993], under the jurisdiction of OSHA (Occupational Safety and Health Administration) because of its wide combustible range, low minimum ignition energy and rapid rate of diffusion. Hydrogen is also the smallest and lightest element, much lighter than air. This is a very significant concern for hydrogen operation indoors but it can be considered a safety feature when used outdoors. Indoors, hydrogen would accumulate near the ceiling or the top of a closed container, which could easily ignite due to hydrogen's low minimum ignition energy, as in the case of the Hindenberg disaster where the suspected ignition source was static electricity [Bain, *et al.*, 1998]. Hydrogen may also displace oxygen in a closed container creating an asphyxiation risk. Hydrogen's high diffusivity, 3-8 times greater than air, allows hydrogen to be diluted quickly in open air to less than the combustible range. Das [1991] estimated that a spill of about 2000 litres of liquid hydrogen would dissipate to below the explosive limit in approximately one minute.

2.3 ELECTROLYSIS

In general, electrolysis is described as the decomposition of water by an electrical current and was first observed by J.W. Ritter in 1798 [Engelhardt, 1904]. The electrical energy must be great enough to overcome the intrinsic negative voltage of the cell and drive a nonspontaneous reaction to give the products hydrogen and oxygen. In the electrolysis of water, this minimum external voltage (decomposition potential of water) is 1.229V. When the external voltage is greater than this value the overall reaction will occur. The electrolysis of water is represented by the following chemical equation:



A simplified schematic of the electrolysis of water is shown in Figure 2.7. Hydrogen gas is formed at the cathode and rises to the surface, similarly oxygen escapes at the anode. The hydroxyl ions (OH^-) move between the cathode and the anode and recombine to form water. The Equations represented in the figure are given below.

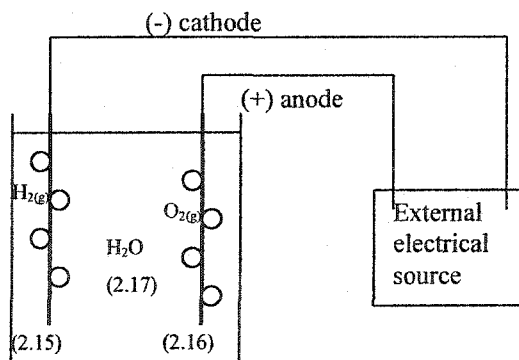


Figure 2.7 Simplified schematic of the electrolysis of water.



Three processes are used in the electrolysis of water: 1) water electrolysis with alkaline aqueous electrolytes, generally potassium hydroxide (KOH), 2) membrane or Solid Polymer Electrolyte (SPE) and 3) high temperature steam electrolysis [Wendt and Plzak, 1991]. For this study the electrolysis unit is a conventional alkaline water electrolysis unit provided by Global Tech. The gas streams are not separated, but H₂ and O₂ are added to the engine together.

2.3.1 *Electrolysis Products (Hydrogen and Oxygen) Addition*

A few studies have been conducted on the effects of hydrogen and oxygen addition on engine combustion. Shrestha and Karim [1999] compared the effects of the addition of hydrogen only and the addition of hydrogen and oxygen to a methane-fuelled spark ignition engine by using a two zone model developed to predict the performance of a gas-fuelled SI engine. The study found that the addition of hydrogen increased the power output for lean mixtures especially, with the concentration of hydrogen in the fuel mixture being about 20–25% by volume. The authors simulated the effects of the addition of hydrogen and oxygen and found that the electrolysis products also improved the power output of the engine. However, the authors determined that the on-board generation of hydrogen by electrolysis while consuming some of the engine output was not a viable option over most of the engine operating range.

Dügler and Özçelik [2000] studied the effects of electrolysis products on four different cars. The cars required no modification and the electrolysis products were fed into the engine through the intake manifold. The authors found a reduction in fuel consumption between 35–40% and a reduction in CO, CO₂ and hydrocarbon emissions of 40–50%. Limited details of the experimental setup and results were provided.

Sobiesiak *et al* [2002] used the computer simulation program CHEMKIN to study the effect of electrolysis products on iso-octane premixed laminar combustion. Based on this computational analysis the flame speed is expected to increase with increasing concentrations of hydrogen and oxygen with the largest increase occurring near

stoichiometric conditions. The adiabatic flame temperature also increases which effectively increases the NO_x emissions. CO emissions were speculated to decrease with the addition of hydrogen and oxygen.

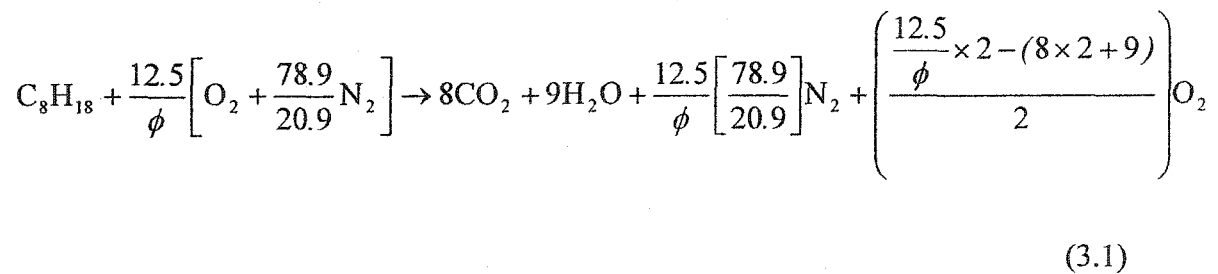
The comparison completed by D'Andrea [2003] for the addition of 2% hydrogen in air to the addition of 2% hydrogen and 1% oxygen in air showed generally insignificant improvement, with a maximum torque increase of 1.7 Nm, a 3-9% increase in the imep and a decrease in the cycle-to-cycle variations (COV_{imep}) of 1%. The extra oxygen had very little effect on engine performance and seemed to play a subtle role in the burn duration, with a decrease in the 0-2% burn duration and peak burn rate but an increase in the 10-90% burn duration for a greater total burn duration. The most significant change found with the addition of hydrogen and oxygen was the increase in NO concentration by at least 500 ppm (representing between a 22% to 86% increase) over the NO concentrations reported for hydrogen addition only. The intent of this thesis research was to use a commercially available electrolysis unit. The hydrogen and oxygen produced by the electrolysis unit was considerably less than the laboratory prepared hydrogen-air mixtures used during D'Andrea's testing.

3 SIMULATIONS

The purpose of this chapter is to demonstrate the use of computer modelling to simulate the effects of hydrogen and oxygen addition, in a 2:1 ratio as produced by electrolysis, to a spark ignition engine. Three software packages were selected for this purpose: STANJAN [Reynolds, 1986], Engine Simulation Program (ESP) [Reynolds and Lumley, 1999] and CHEMKIN 3.7 [Reaction Design, 2002]. The programs were selected based on their ability to either predict emissions or engine performance. In some cases, the simulation results predicted from two programs could be compared. Each program was run using iso-octane as the main fuel with standard air.

3.1 EQUIVALENCE RATIO CALCULATION

Using Equations 2.1 and 2.2 to determine the moles of air required for a desired ϕ value, the stoichiometric air/fuel ratio (12.5) is divided by the ϕ value, or



This equation allows for an approximation of product concentrations, which can be used in the CHEMKIN simulation to speed the computation time.

The addition of electrolysis products is not included in the equivalence ratio since hydrogen and oxygen are produced in stoichiometric proportions.

3.2 SIMULATION MATRIX

Solutions were obtained from STANJAN, ESP and CHEMKIN for the following additions of hydrogen; 1) $H_2 = 0\%$, 2) $H_2 = 0.15\%$ by mass of fuel (8% by volume) and 3) $H_2 = 5\%$ by mass of fuel (75% by volume). To model the effects of electrolysis, oxygen was added at one half the mole concentration of hydrogen in each case. The reactant molar concentrations are presented in Table 3.1.

Table 3.1 Reactant Molar Quantities

ϕ	Reactant Quantities (mol)			
	Fuel		Air/Additional Oxygen	
	Iso-octane	H_2	O_2	N_2
Hydrogen Addition = 0%				
0.7	1	0	17.86	67.18
0.8	1	0	15.63	58.78
0.9	1	0	13.89	52.25
1.0	1	0	12.50	47.02
1.1	1	0	11.36	42.75
1.2	1	0	10.42	39.19
Hydrogen Addition = 0.15% by mass ($H_2 = 7.7\%$ by volume or 0.9% energy content)				
0.7	1	0.084	17.90	67.18
0.8	1	0.084	15.67	58.78
0.9	1	0.084	13.93	52.25
1.0	1	0.084	12.54	47.02
1.1	1	0.084	11.40	42.75
1.2	1	0.084	10.46	39.19
Hydrogen Addition = 5 % by mass ($H_2 = 75\%$ by volume or 28.8% energy content)				
0.7	1	3.00	19.36	67.18
0.8	1	3.00	17.13	58.78
0.9	1	3.00	15.39	52.25
1.0	1	3.00	14.00	47.02
1.1	1	3.00	12.86	42.75
1.2	1	3.00	11.92	39.19

3.3 STANJAN

STANJAN was developed by W.C. Reynolds at Stanford University in 1981 [Reynolds, 1986]. The latest version v.3.89, developed in 1987 was used in this study. STANJAN uses a Fortran source code, run in the DOS mode, to calculate the chemical equilibrium state for the user-specified system and thermodynamic cycle.

To determine the chemical equilibrium state, STANJAN uses the method of element potentials and data from JANAF Thermo-chemical tables [JANAF, 1977]. The method of element potentials relates the mole fractions of each species to quantities called element potentials. There is one element potential for each independent atom in the system [Reynolds, 1986].

STANJAN is limited to one chemical equilibrium analysis per run. Therefore, in order to model an idealized fuel-air Otto cycle, a minimum of five steps need to be completed. They are as summarized:

- Step A: Intake. Reactant molar concentrations are provided along with the inlet temperature. The initial mixture is assumed to be at 300K and 1 atm.
- Step B: Isentropic compression. In this step the compression ratio ($r_c=8.5$) is used to determine the volume compression of the gas.
- Step C: Combustion. The combustion reaction is modeled with an assumption that the reaction is taking place under constant volume. By setting the volume and enthalpy equal to that determined at the end of Step B the adiabatic flame temperature can be computed with the equilibrium products of combustion.
- Step D: Isentropic expansion. It is assumed that the volume returns to the original volume determined in Step A.
- Step E: Exhaust/Blowdown. The exhaust/blowdown step assumes that the volume has returned to the original volume with the products exhausted to return the pressure to the original pressure. This Step is optional as the data is not used in calculations but is used in the development of p - V diagrams.

After each step, STANJAN prints to the output file the calculated pressure (Pa), temperature (K), volume (m^3/kg), internal energy (J/kg), enthalpy (J/kg) and entropy (J/kg-K). Detailed instructions for modeling each of the steps described above are provided in Appendix A.

3.4 ENGINE SIMULATION PROGRAM (ESP)

Engine Simulation Program (ESP), was developed at Stanford by W.C. Reynolds in collaboration with John L. Lumley [Lumley, 1999]. ESP is a Windows based, user friendly program and is available for download from <http://esp.stanford.edu>. The program was developed to simulate the thermodynamic performance of a homogeneous-charge single cylinder SI engine. The effects of turbulence on heat transfer and combustion are considered in this program [Lumley, 1999].

ESP uses a secondary program ESPJAN, derived from STANJAN, that assumes thermodynamic equilibrium and product dissociation. Reactant concentrations and predicted products, such as CO_2 , H_2O , and CO , are inputted into the ESPJAN program. The program calculates the specific enthalpy and energy of the reactants and products in a data table to be used by ESP. Individual product concentrations are not calculated by ESP.

ESP uses ordinary differential equations in energy balance equations designed to analyse the compression stage, expansion stage and the gas exchange stage. The turbulence model uses algebraic equations to relate variables. The program uses the Runge-Kutta method with time steps corresponding to one crank angle degree to solve the differential equations [Lumley, 1999].

ESP was written to aid in engine design by allowing the user to specify the engine geometric parameters including: cylinder bore, stroke and number of cylinders. Other parameters such as spark timing and engine speed can also be modified. ESP default settings were modified to use the parameters of the Briggs and Stratton Vanguard 20 HP engine, which are summarized in Table 3.2.

Table 3.2 Engine Geometry and Operating Conditions

Engine Geometry (modified for Briggs & Stratton Vanguard Engine)	
Cylinder bore, m	7.2E-02
Volume Compression Ratio	8.5E+00
Piston Compression Stroke, m	7.0E-02
Connecting Rod Length, m	1.05E-01
Inlet Ambient Temperature, K	3.0E+02
Exhaust Gas Recirculation Temperature, K	3.0E+02
Exhaust Gas Recirculation Fraction	0.0E+00
Reference Flow Area of Intake Valve (Full Open), m ²	8.72E-04
Reference Flow Area of Exhaust Valve (Full Open), m ²	8.06E-04
Operating Conditions (modified for Briggs & Stratton Vanguard Engine)	
Crank Degrees after Compression TDC where intake opens	335
Crank Degrees after Compression TDC where intake closes	605
Crank Degrees after Compression TDC where exhaust opens	122
Crank Degrees after Compression TDC where exhaust closes	378
Revolutions per minute	3000
Crank Degree after Compression TDC at ignition	699 (set-up of engine) 719 (max. work)
Ambient Temperature	300
Mass Percent EGR	0
EGR return Temperature, K	300
Max. intake valve flow area % of reference	100
Max. exhaust valve flow area % of reference	100
Intake Ambient Pressure, atm	1.00
Exhaust Ambient Pressure, atm	1.00
Flow model: Lumley's coefficients (default settings)	
Discharge coefficient for intake valve	0.645
Discharge coefficient for intake valve backflow	0.868
Discharge coefficient for exhaust valve	0.868
Discharge coefficient for exhaust valve backflow	0.645
Heat transfer model: Stanton number during compression (default settings)	
Stanton number during burn for unburned gas and burned gas	0.0356
Stanton number during expansion	0.0356
Stanton number for in-cylinder heat transfer during gas exchange	0.0356
Stanton number for heat transfer from inlet and exhaust valve flow	0.00237
Heat transfer area above piston at TDC/bore area	1.37
Heat transfer area for intake jet flow/bore area	0.05
Heat transfer area for exhaust jet flow/bore area	0.05
Turbulence model: Lumley's model (default settings)	
Inlet flow turbulent kinetic energy/mean flow kinetic energy	0.2
Exhaust backflow turbulent kinetic energy/mean backflow kinetic energy	0.2
Factor in turbulence dissipation during compression/expansion/gas exchange	0.298
Factor in turbulence dissipation during burn	0.05
Factor in turbulence production during compression/expansion/gas exchange	0.00502
Factor in turbulence production during burn	0.03

3.5 CHEMKIN

CHEMKIN III consists of a collection of programs and subroutine libraries designed to work together to facilitate the formation, solution, and interpretation of problems involving gas-phase and gas-surface chemical kinetics [Kee *et al.* 2001].

The application PREMIX was selected to model adiabatic flame temperatures and pollutant concentrations by simulating a premixed, freely propagating flame. The PREMIX package in conjunction with the CHEMKIN interpreter and the TRANSPORT package work to solve sets of differential equations simultaneously. The priority differential equations used for determining flame propagation under steady state and constant pressure are described in Appendix B.

The chemical mechanism used is a compilation of two mechanisms. The iso-octane mechanism selected for this study was developed by RWTH-Aachen [Peters, 2002]. Unfortunately, this mechanism does not include the chemical reactions that contribute to NO_x formation. Therefore, chemical species and reactions containing nitrogen were selected from the GRI-Mech 3.0 [Smith *et al.*, 1999] and added to the iso-octane mechanism as done by Sobiesiak *et al.* [2002]. The final mechanism including 75 species, and 297 chemical reactions is provided in Appendix B.

4 EXPERIMENTAL APPARATUS AND PROCEDURE

4.1 ANALYSIS OF ELECTROLYSIS PRODUCTS

Chemical analysis was performed on the electrolysis products using a Varian Chrompack CP-3800 gas chromatograph [Walnut Creek, California] with thermal conductivity detector (TCD). A Hayesep A Packed Column [Alltech, Deerfield, IL] was selected for analysis of hydrogen, oxygen and nitrogen. Appendix F is provided to explain in detail the calculations and procedures used in the analysis of the electrolysis products.

4.1.1 *Calibration*

Calibration of the Varian Chrompack CP-3800 gas chromatograph with the Hayesep A column was conducted by injecting different volumes of prepared gases including ambient air samples, oxygen samples and nitrogen samples. The area count for each peak on the produced chromatograph is proportional to the mass, calculations are provided in Appendix F.

4.1.2 *Sample Preparation*

Samples were collected in a 20 mL vial sealed with a rubber septum pierced by two syringes. One syringe went to the bottom of the vial and was attached to the electrolysis outlet tube. The opening of the second syringe was positioned just below the rubber septum and was used as an exhaust. The electrolysis unit was allowed to run for 25 minutes at a flow rate of 480 mL/min. This provided a purge of 600 vial volumes.

4.1.3 *Test Procedure*

The prepared sample vial was placed on Tray 2 and the desired sample volumes of 100 μL and 200 μL entered into the GC controlling computer. The total run time was

approximately 16 minutes. The operating conditions and calculations are provided in Appendix F.

4.2 ENGINE EXPERIMENTAL SET-UP

The engine was previously set-up by D'Andrea [2003] with modifications made for this study to allow for the introduction of the electrolysis products. Modifications were also needed half way through the testing to incorporate a new gas analyser. A schematic of the engine set-up is provided in Figure 4.1 accompanied with a photograph in Figure 4.2. Details of the set-up are provided in the following sub-sections. To summarize the engine set-up, the engine was mounted to a dynamometer and electrolysis products were introduced just above the intake manifold and controlled by a series of valves. A bubble flow meter was used to measure the flow rate of the electrolysis products before being introduced to the engine, and the gasoline flow was measured using a burette. An optical encoder was used to determine crank angle and a pressure transducer was installed on the spark plug to measure the pressure within the cylinder. The data from the encoder and pressure transducer was collected by a computer controlled data acquisition system.

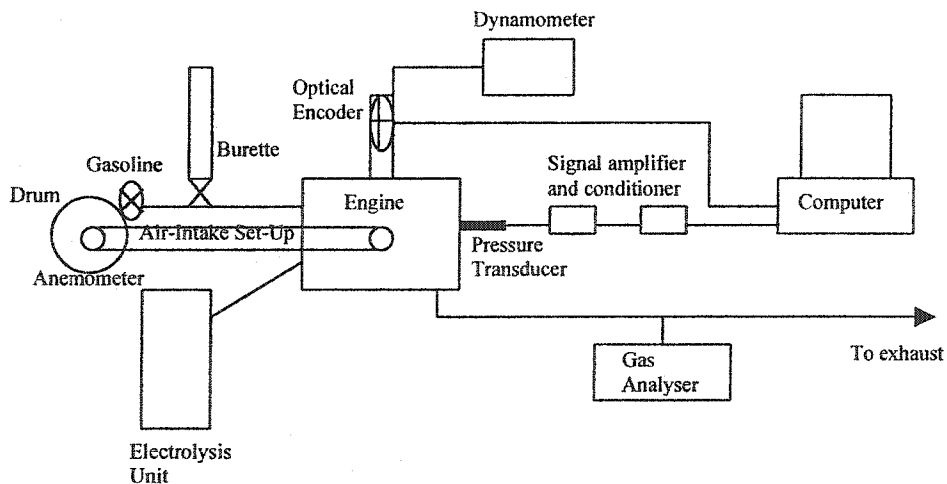


Figure 4.1 Engine Set-Up schematic

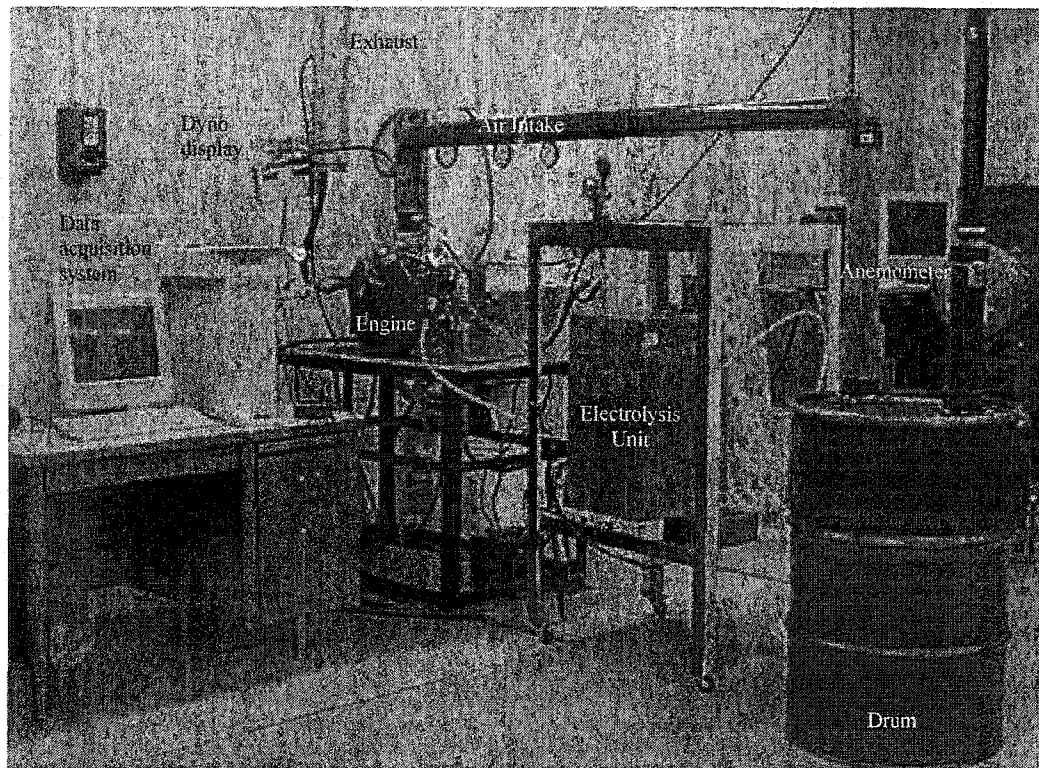


Figure 4.2 Photograph of Engine Experimental Set-Up

4.2.1 Engine-dynamometer Set-Up

A 20 HP, four-stroke, V-twin Briggs & Stratton [Milwaukee, Wisconsin] SI engine was previously mounted to a GoPower [Carrollton, Texas] D-100 water brake dynamometer for experiments conducted by D'Andrea [2002]. The dynamometer provides a load to the engine and reports the torque and speed. D'Andrea [2002] found that at low engine speeds, the engine torque produced was outside the range of the dynamometer. To correct this D'Andrea mounted the engine and the dynamometer on a bench. The shafts were positioned parallel and 30 cm apart. Each shaft was equipped with a sprocket, with the sprockets connected by a chain.

The sprocket on the engine was 1.33 times larger in radius than the sprocket on the dynamometer. Consequently, the dynamometer rotates 1.33 times as fast as the engine. Therefore,

$$\tau_{b,engine} = \tau_{b,dyno} \times 1.33 \quad (4.1)$$

where τ_b = brake torque

The brake power, P_b , produced by the engine is conserved regardless of sprocket size, however, some losses may occur due to the chain.

$$P_{b,engine} = P_{b,dyno} \quad (4.2)$$

An Omega [Stamford, Connecticut] Analog Digital Converter along with LabVIEW software [Omega, Stamford, Connecticut] were used to collect pressure and crank angle measurements. Three channels were used on the data acquisition board. Two channels were used to collect the top dead centre (TDC) signal and a signal of every crank angle degree (CAD) from the BEI [Goleta, California] HS35 optical encoder mounted on the engine's shaft. The third channel was used to collect the pressure signal from the pressure transducer. A spark-plug mounted PCB Piezotronics [Depew, New York] piezoelectric pressure transducer was used to measure the in-cylinder pressure. Before the data acquisition system could collect the pressure data, the charge from the pressure transducer was converted to a voltage using a 422E Series In-Line Charge Amplifier and an ICP signal conditioner [PCB Piezotronics, Depew, New York]. Approximately three pressure measurements were collected for every one CAD signal. The LabVIEW program determined the sampling rate by using the engine speed in rev/min. The speed entered by the user was the displayed speed for the dynamometer at the time of data collection. The LabVIEW user interface and LabVIEW code are given in Appendix D.

4.2.2 *Electrolysis Products Delivery*

Global Tech Environmental Products [Aurora, Ontario] provided the electrolysis unit. The company believes that the engine performance enhancement is better when the electrolysis products are introduced to the engine immediately after generating them. For this reason the electrolysis unit was set as close to the engine as possible. A T-connector and two valves were used to control the flow from the electrolysis unit to the engine as portrayed in Figure 4.3. An aluminium block was designed to fit the intake of the Briggs & Stratton engine and connect to a series of ABS pipes. The first section of ABS pipe included a fitting to attach the tubing from the electrolysis unit as shown in Figure 4.3.

The electrolysis unit required approximately 20 minutes before a steady flow was produced, as detailed in Appendix E. To assure that the electrolysis unit was producing a steady flow of products and to determine the flow rate a mini-Buck Calibrator [A.P. Buck, Orlando, Florida] was used before directing the electrolysis products to the engine.

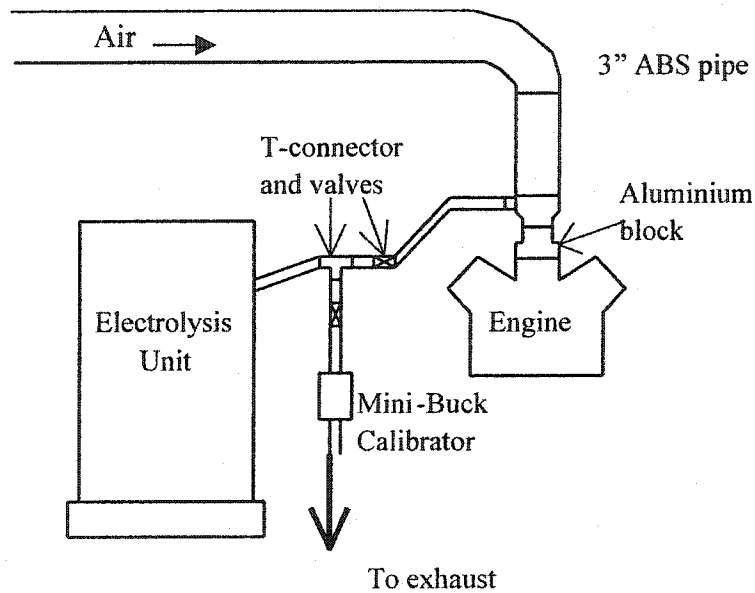


Figure 4.3 Schematic of Electrolysis Set-Up

4.2.3 Air Flow

An Omega [Stamford, CT] Hygro-thermo anemometer HHF710 reports the average air velocity in feet per minute (ft/min). This was used to calculate the air flow rate, Q , into the engine.

$$Q(\text{L/s}) = V\pi r^2 \left(\frac{1(\text{m})}{3.2808(\text{ft})} \right)^3 \left(\frac{1\text{min}}{60\text{s}} \right) \left(\frac{1000\text{L}}{1\text{m}^3} \right) \quad (4.3)$$

where Q = air flow rate (L/s)

V = velocity (ft/min)

r = radius of Omega Hygro-thermo anemometer probe ($r=0.11458$ ft)

During the initial engine tests, the anemometer was located directly above the engine intake. The readings fluctuated erratically due to the effects of the opening and closing of the intake valves. In order to receive a stable reading the anemometer was located downstream of a series of 7.62 cm (3") ABS pipes connected between the engine intake and a large drum as shown in Figure 4.4. The drum was used to dampen the effects of the opening and closing of the intake valves and as a result the anemometer readings represented the average airflow into the engine. These anemometer readings were used to calculate the air/fuel ratio. Based on the calculated air/fuel ratio ($\phi < 0.4$) it was evident that the anemometer readings were too high since the lean limit of iso-octane fuel is $\phi = 0.6$. Therefore, a secondary study was undertaken to determine if the anemometer readings were accurate. In this study, a velocity profile was estimated based on discrete velocity measurements according to the Equal-Area Method using a pitot tube and a manometer. A full description of the procedures and findings are presented in Appendix F.

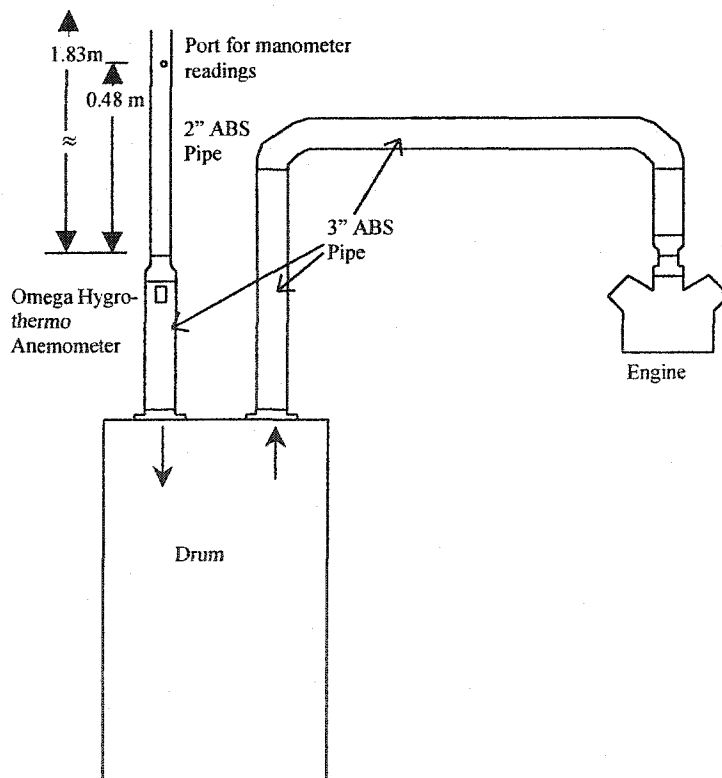


Figure 4.4 Intake Schematic

4.2.4 Gasoline Delivery

The gasoline flow rate was measured using a 50 mL burette. Between the main gasoline supply and the burette was a valve that could be turned off allowing the engine to draw gasoline from the burette only. Burette readings were taken before the main valve was shut off. The burette valve was closed after 30 sec and the main valve reopened. The burette reading after the 30 sec was recorded. The fuel consumption rate was calculated as

$$Q(\text{mL/s}) = \frac{V_2 - V_1}{t} \quad (4.4)$$

where Q = fuel flow rate (mL/s)

V_2 = volume after time t (mL)

V_1 = initial volume (mL)

t = time (s)

4.2.5 Exhaust Delivery/Gas Analysis

Initially exhaust gases were analysed using an IMR [St. Petersburg, Florida] 2800P gas analyser, which measured exhaust and room temperatures as well as concentrations of CO, NO, and O₂ on a dry basis in ppm. During the course of the testing the IMR's NO and CO electrochemical sensors and the T-gas temperature sensor failed. Fortunately, a new ENERAC model 3000EV [Westbury, New York] gas analyser was received. This provided for an opportunity to try the new unit and compare the emission results to those reported from the older IMR unit. To promote a long life for the ENERAC system the exhaust piping was modified to cool the exhaust gases, shown in Figure 4.5. A steel pipe was welded to the existing exhaust manifold and fitted with a compression fitting attaching a copper coil. The other end of the copper coil was attached to a second compression fitting used in conjunction with a gas valve and a T-connector. A second gas valve was used with the T-connector, allowing ambient air to be drawn into the gas probe after testing. The probe was placed inside another steel pipe connected to the

remaining opening on the T-connector. A small piece of rubber hose was placed over the steel pipe and the probe and sealed to prevent air leakage.

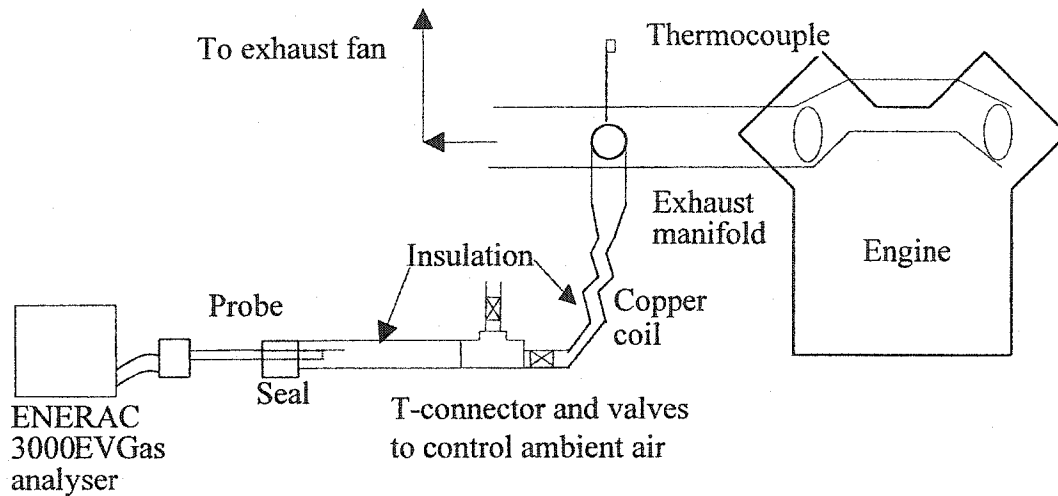


Figure 4.5 Exhaust system designed for use with ENERAC 3000EV Gas Analyser

4.3 TESTING PROCEDURE

Each engine test consisted of three subtests. After letting the engine warm for approximately five minutes, the engine throttle setting was adjusted to $\frac{1}{4}$ throttle and the engine speed was adjusted to the desired rpm by adjusting the load on the engine. The first subtest was the base-line test (Condition 1). The engine was operated without the addition of the electrolysis products. The engine was run under this condition for at least 10 minutes. During this time, emissions results were gathered by either the IMR or ENERAC gas analyser units at a one minute time interval and the LabVIEW program was used to record the pressure and crank angle signals. Gasoline flow rates and air flow rates were also measured and recorded several times during this time. After all required data was collected, flow rate measurements of the electrolysis products were recorded using the mini-Buck calibrator. Once it was determined that the electrolysis unit was producing products at a steady rate, the electrolysis products were redirected to the engine intake (Condition 2). Again, the engine was run for approximately 5 minutes with the addition of the electrolysis products before data was collected. After all data was collected and at

least 10 minutes had passed, the valves controlling the flow of the electrolysis products were switched, and the electrolysis products were once again directed to the mini-Buck calibrator. Flow measurements were recorded and compared against the original measurements and the electrolysis unit was turned off. The last subtest, as with the first, was run without the electrolysis products (Condition 3). Data collection began approximately 5 minutes after the electrolysis unit was shut down ensuring that no electrolysis products were present. When the electrolysis products were not directed to the engine, they were exhausted to a secondary exhaust fan in the room. After approximately 10 minutes, the engine was turned off.

By running the engine with this set-up, the effects of the addition of electrolysis products could be determined without the interference from day-to-day fluctuations in the operation of the engine. The alternative of running the engine without the electrolysis products one day and with the electrolysis products the next day increases the variables that could contribute to significant errors such as, daily environmental variations, quality of fuel, and lack of precise control of the engine (including throttle setting and load).

4.4 EQUIVALENCE RATIO

The measured gasoline flow rates and corrected anemometer air flow rates were used to calculate the equivalence ratio using the equation below,

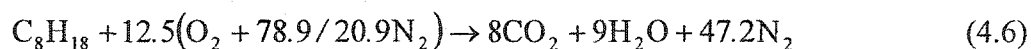
$$\phi = \frac{Q_f / Q_{air}}{(C_f / C_{air})_{st}} \quad (4.5)$$

where Q_f = fuel flow rate (L/s) converted to a vapour at STP

Q_{air} = corrected anemometer air flow rate (L/s) at STP

$$(C_f / C_{air})_{st} = \frac{1}{12.5(1 + 78.9 / 20.9)} = 0.0168, \text{ the stoichiometric fuel/air ratio on a}$$

volume basis for iso-octane obtained from the stoichiometric equation:



The addition of electrolysis products was not included in the equivalence ratio calculation since hydrogen and oxygen are produced in stoichiometric proportions.



4.5 PROCESSING PRESSURE AND CRANK ANGLE DATA

Files saved by LabVIEW consist of three columns of data, which correspond to pressure voltage, CAD and TDC signals. This data, opened in a spreadsheet would be similar to the first three columns in Table 4.1.

Table 4.1 Example of LabView data files as viewed in a spreadsheet. Crank angles calculated in the spreadsheet and supplemental explanations are in bold.

Pressure	Degree	TDC	Crank Angle	Description
volts	Signal	Signal	(°)	
0.499	1.616	0.223		
0.498	4.725	4.688	0	TDC signal identified with a signal strength above 4.0 with a lower pressure volt reading than on the next TDC signal indicates that this TDC signal is associated the 0° CAD.
0.512	0.07	0.238	0.5	
0.502	4.641	0.248	1	Each degree signal above 4.0 indicates a CAD.
0.5	0.084	0.221	1.33	There are 1 to 3 pressure readings between CAD signals.
0.502	0.058	0.232	1.66	
0.499	4.715	0.243	2	
				Approximately 1000 rows of data skipped in preparing this table.
1.185	0.058	0.225	359.5	
1.189	4.717	4.656	360	TDC signal
1.186	0.079	0.229	360.5	
1.186	4.648	0.222	361	

The third column represents the TDC signal. When the crank shaft of the engine passes the TDC the encoder sends a signal, which appears as a peak in voltage. In a four-stroke engine, there will be two TDC signals for each cycle (Figure 2.2), at the beginning of the intake stroke (0°) and at the end of the compression stroke (360°). To determine if the TDC signal corresponded to 0° or 360° , the two pressure voltages were compared. The smaller pressure voltage indicates the beginning of the intake stroke or 0° . Once the 0° signal was confirmed, the three columns of data and approximately 33,500 rows starting with the row directly preceding the 0° signal was copied into a spreadsheet containing functions and macros to calculate several parameters such as work and cycle-to-cycle variations.

4.5.1 Cylinder Volume Calculations

As the piston moves, the volume within the cylinder changes, the minimum volume or clearance volume, V_c , occurs when the piston is at TDC (0° or 360°). The maximum volume, V_{max} , occurs when the piston is at bottom dead centre (BDC), 180° or 540° . For any given crank angle the volume can be calculated using the following equations [Heywood, 1988]:

$$V = V_c + V_s \quad (4.8)$$

$$V_s = (l + a - s)\pi B^2 / 4 \quad (4.9)$$

where l = connecting rod length (Briggs & Stratton 20HP Engine = 0.105 m)

a = crank radius (Briggs & Stratton 20 HP Engine = 0.035 m)

B = cylinder bore (Briggs & Stratton 20HP Engine = 0.072 m)

s = stroke variation

The variation in stroke is related to the crank position, in radians, θ , by the function [Heywood, 1988]:

$$s(\theta) = a \times \cos(\theta) + [l^2 - a^2 \times \sin^2(\theta)]^{1/2} \quad (4.10)$$

4.5.2 Pressure Signal Conversion Calculation

The pressure signal is recorded in LabVIEW in volts and converted to kilopascals using the equation [PCB Piezotronics, 1999]:

$$p(\text{kPa}) = \frac{V_{out} (1\text{pC/mV})(1000\text{mV/V})(6.895\text{kPa/psi})}{1.085\text{pC/psi}(10)} \quad (4.11)$$

where V_{out} = signal voltage (V)

1 pC/mV = in-line amplifier scaling picocolomb per millivolt

1000 mV/V = millivolt to volt conversion

6.895 kPa/psi = kilopascal to pound per square inch conversion

1.085 pC/psi = transducer sensitivity picocolomb per pound per square inch

10 = signal conditioner scaling factor (gain)

Once the volumes for each crank angle are calculated and the pressure signal converted to useful values of kPa, calculations can be completed for work, power, imep and cycle-to-cycle variations.

4.5.3 Work Output

A spreadsheet developed and documented by D'Andrea [2002] was used to produce a p - V diagram, shown in Figure 4.6, and calculate the work output.

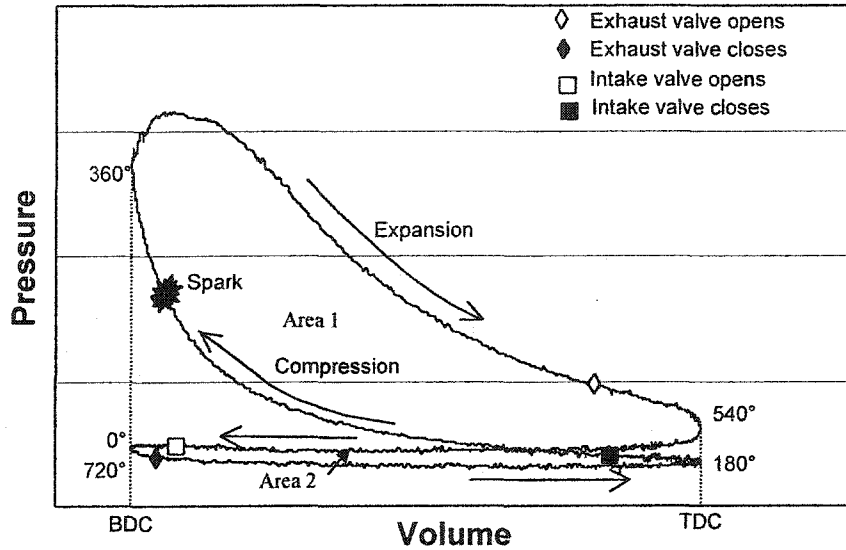


Figure 4.6 Example of p - V diagram

The work delivered to the piston during the entire cycle is referred to as the net indicated work per cycle, W_{netIN} , which is equal to the gross indicated work, $W_{grossIN}$, minus the pumping work, $W_{pumpingIN}$. The gross indicated work is the work delivered to the piston during the compression and expansion stroke only, indicated as Area 1 in Figure 4.6. Area 2 represents the work transferred from the piston to the cylinder gases during the inlet and exhaust strokes, or the pumping work. Therefore, the net indicated work per cycle is equal to Area 1 minus Area 2 and is calculated by the integral [Heywood, 1988]:

$$W = \oint p \times dV \quad (4.12)$$

where W = work (kJ);

p = pressure (kPa);

dV = derivative with respect to Volume.

The spreadsheet performs the integration by finding the area enclosed by the curve, using the trapezoidal method as presented in Figure 4.7. The trapezoidal method simply states that the area under the curve can be approximated from V_2 to V_1 as the sum of the areas of the trapezoids.

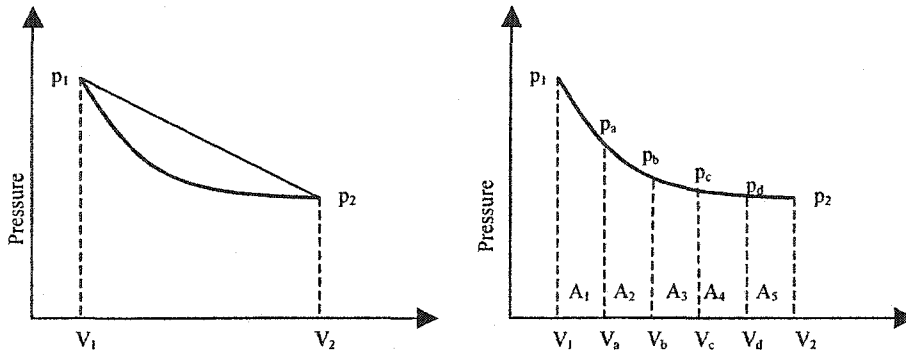


Figure 4.7 Trapezoidal method for approximation of area under the curve

As shown in Figure 4.7 the smaller the increment between volumes the better the approximation for the area under the curve. The area of a trapezoid is calculated by

$$A_i = \frac{1}{2}(P_1 + P_a)(V_a - V_1) \quad (4.13)$$

The total area under the curve is the sum of all areas.

$$A_t = \sum_{i=1}^n A_i \quad (4.14)$$

The spreadsheet was designed to calculate the area within the curve by calculating smaller areas, which were summed at strategic locations along the curve. The pumping work was determined by calculating the total area below the upper boundary of Area 2 and subtracting the area below the lower boundary of Area 2. Similarly, the gross work was calculated by determining the total area below the upper boundary of Area 1, the curve defined by 360 and 540 CAD, and subtracting the area marked by the lower

boundary of Area 1. This procedure was repeated for each cycle entered into the spreadsheet.

The indicated mean effective pressure, $imep$, is a measure of the net indicated work (W_{netIN}) per unit swept volume (V_s).

$$imep(\text{N/m}^2) = \frac{W_{netIN}(\text{N} \cdot \text{m})}{V_s(\text{m}^3)} \quad (4.15)$$

The $imep$ result is usually reported for research purposes since it provides a value independent of the number of cylinders and the size of engine tested, allowing the results to be compared to different engines [Heywood, 1988]. The $imep$ results were averaged over approximately 100 cycles.

The indicated power, P_I , produced by a cylinder is also related to the indicated work per cycle [Heywood, 1988]:

$$P_I = \frac{W_{netIN} N}{n_R} \quad (4.16)$$

where N = engine speed (rev/s);

n_R = crank revolutions for each power stroke (for a four stroke engine, $n_R=2$).

The calculated W_{netIN} and P_{net} are based on the data for one cylinder. Therefore, to determine the total work or power delivered by an engine, the calculated values must be multiplied by the number of cylinders in the engine, in this case 2. This assumes that the work produced in the metered cylinder is equal to that produced in the other cylinder. The indicated power must not be confused with the brake power, P_b . The brake power is calculated based on the dynamometer readings, which excludes power losses such as friction.

4.6 BURN DURATION ANALYSIS

A widely used technique, the burn duration analysis, compares the pressure rise within a cylinder during a fired cycle to an unfired cycle. The pressure rise in a cylinder is caused by two factors: combustion and change in volume due to piston motion. The pressure rise during the fired cycle is expected to be higher due to combustion than the unfired cycle with no combustion occurring where there is only the change in volume due to piston motion. Therefore, the pressure rise due to combustion only or mass fraction burnt (mfb) is calculated by subtracting the pressure rise in the unfired cycle from that of the fired cycle.

A spreadsheet macro developed by D'Andrea [2002] was used to determine the burn duration. Due to variations in pressure from cycle-to-cycle, the program first had to manipulate the data by shifting the pressure traces, so the pressure data was the same for both the fired and unfired cycle at the crank angle where the spark occurred. The difference due to combustion, Δp , was then calculated by subtracting the unfired cycle pressure from the fired cycle pressure at every CAD. The pressure measurements recorded at partial CAD degrees during the fired cycle were not used in the calculation because the number of intermediate readings could vary between 2 to 4 and may not correspond to values for the unfired cycle. The pressure difference due to combustion, Δp , was normalized to the clearance volume, V_c , at TDC, resulting in the pressure rise due to combustion, Δp_c [Stone, 1999]:

$$\Delta p_{ci} = \Delta p_i \times \frac{V_i}{V_c} \quad (4.17)$$

where: Δp_{ci} = change in pressure due to combustion at crank angle i , normalized by V_c (kPa/mm³);

Δp_i = pressure difference due to combustion at crank angle i (kPa);

V_i = volume at crank angle i (mm³);

V_c = clearance volume (mm^3).

The end of combustion was presumed to occur at the maximum Δp_{ci} . Then the fraction of charge burnt was calculated at every CAD by dividing Δp_c by the maximum Δp_{ci} in that cycle. The burn durations; 0 to 2%, 2 to 10%, 10 to 90%, and total burn duration were determined by locating the CAD that corresponds to the required mass fraction burned (eg. 2%, 10%, 90%, end of combustion).

This analysis was completed for approximately 100 cycles for each of the 3 Conditions (without, with and without electrolysis products) within each test. The pressure data for the unfired cycle were collected at the end of each test by momentarily removing the spark plug cap from the spark plug while the engine continued to run. The pressure data was recorded as quickly as possible when the spark plug was removed to minimize the effects of any decrease in rpm. The pressure traces for the unfired cycle were averaged for each CAD for use in the burn duration analysis.

5 RESULTS AND DISCUSSIONS

5.1 ELECTROLYSIS PRODUCTS ANALYSIS

The sample of electrolysis products was analysed twice using different volumes. A detailed description of the process and calculations are provided in Appendix C. Table 5.1 shows that the ratio of H₂:O₂ was on average 2:1, as would be expected from electrolysis.

Table 5.1 Calculated volumes of hydrogen and oxygen from electrolysis products

Sample Volume (μL)	V _{H₂} μL	V _{elecO₂} μL	H ₂ :O ₂
100	67.47	29.65	2.3
200	109.49	60.86	1.8

The chromatogram produced during the electrolysis products analysis also showed the presence of nitrogen, indicating that the sample was contaminated with ambient air. This ambient air was likely introduced into the sample either by inadequate purging of the vial during sample collection or by the GC sample injection process. The second test conducted from the same vial shows a higher volume of N₂, which indicates that during the sample injection process, ambient air is being drawn into the vial.

The chromatograph did not show any peaks other than those for hydrogen, oxygen and nitrogen. Based on calculations in Appendix C, 0.5% (Sample 1, $V=100 \mu\text{L}$) and 11% (Sample 2, $V=200 \mu\text{L}$) of the total volume was unaccounted for by the chromatograph.

5.2 SIMULATIONS

The use of computer models has become important in combustion research. Computer models allow for prediction and extrapolation of experimental results. Unfortunately, each model has limitations. Notwithstanding the model limitations themselves, other factors including; user knowledge of the model and reliable reference data (i.e. chemical

rate coefficients, thermodynamics data) will affect the accuracy of the modeling results. The effect of the addition of electrolysis products to iso-octane on combustion was modelled using STANJAN, Engine Simulation Program (ESP), and CHEMKIN. Details are provided for each model in Chapter 3. The simulation matrix present in Section 3.2 was completed for each model and the results are provided below.

5.2.1 STANJAN

The predicted work and emissions results are presented in the following sections.

5.2.1.1 Predicted Work

STANJAN can be used to predict work by using the internal energy values, as documented in Appendix A. This method assumes that the expansion and compression strokes were adiabatic. The work predicted by the internal energy values calculated in STANJAN is illustrated in Figure 5.1.

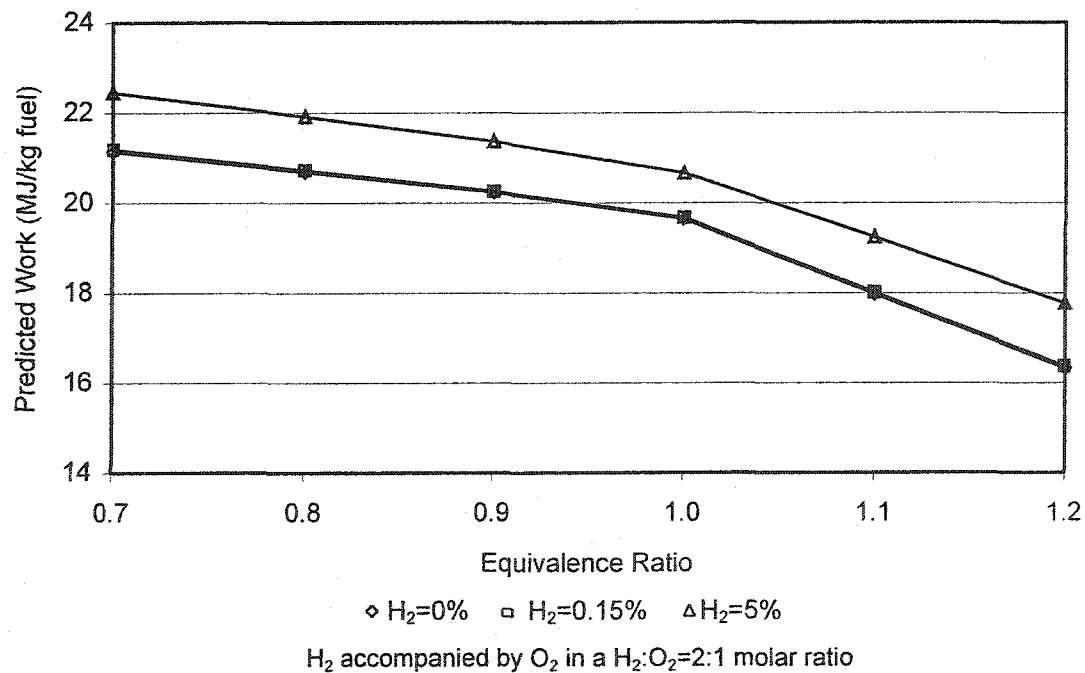


Figure 5.1 STANJAN modelling results for the effects of the addition of electrolysis products to iso-octane on predicted work

As shown in Figure 5.1, the addition of hydrogen at 5% by mass of fuel results in a percent increase in the range of 5-8.5% for work/kg fuel (fuel=iso-octane and hydrogen) when compared to no hydrogen addition. Similarly, an increase in work of approximately 0.2% resulted from the addition of hydrogen and oxygen where the H₂ is present at 0.15% by mass of fuel. This was expected since the hydrogen is added as a supplement for the iso-octane and is not used to replace iso-octane.

5.2.1.2 Emissions

STANJAN reports product concentrations (emissions) as molar fractions, mass fractions and total mols. The products used in the STANJAN analysis included the products associated with complete combustion, CO₂, H₂O and N₂, and those expected for incomplete combustion, NO₂, NO, O₂, C₈H₁₈, HO, O, H₂, CO, and H. The results for the CO and NO concentrations are based on molar fractions after combustion (state 3), which is considered to be closer to the true state of the exhaust gas, rather than the equilibrium state after isentropic expansion (state 4).

Adiabatic Temperature

The adiabatic combustion temperatures predicted by STANJAN are shown in Figure 5.2. Burning only iso-octane the temperatures increase with equivalence ratio with a slight decrease in temperature after $\phi = 1.1$. In support of this finding, the maximum burned-gas temperatures in SI engines occur at $\phi \approx 1.1$ [Heywood, 1988]. The addition of electrolysis products (H₂=0.15% and 5% by mass), increased the adiabatic combustion temperatures an average of 0.14% (4K) and 4.4% (124K). This finding was expected for several reasons. The increase in adiabatic temperatures is expected since the adiabatic flame temperature of hydrogen (3,079K) is greater than the adiabatic flame temperature of iso-octane (2,275K) [Turns, 2000]. The hydrogen and oxygen were added without the associated nitrogen, so burn temperature is enhanced further. As well, the added hydrogen acts as an extra fuel without reducing the amount of iso-octane leading to a higher heating value of the fuel mixture.

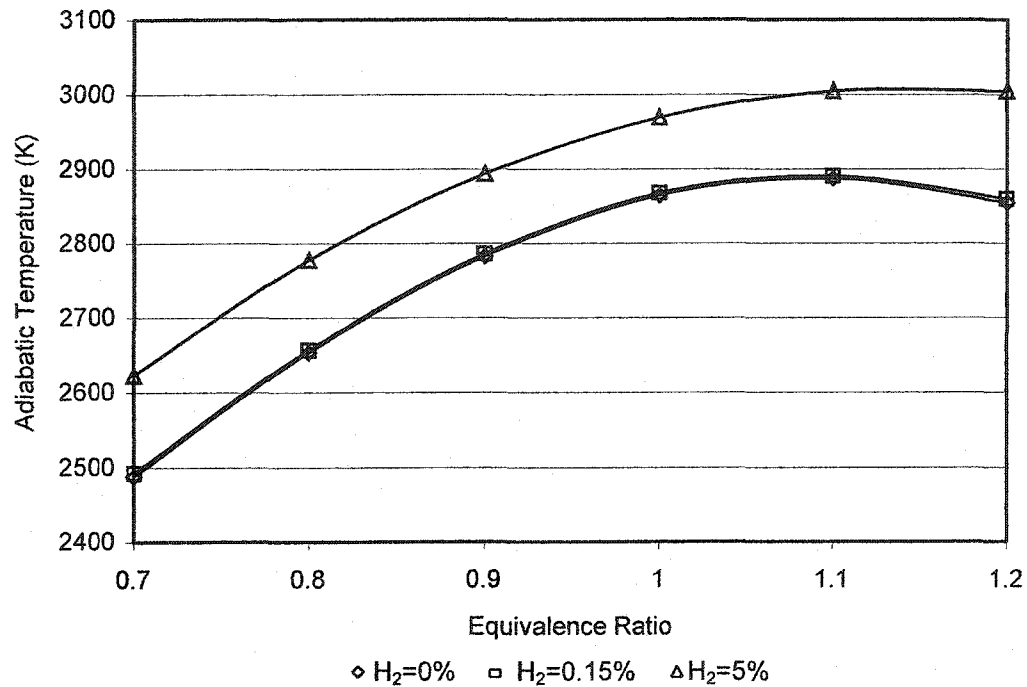


Figure 5.2 Adiabatic temperatures at state 3 as predicted by STANJAN for the addition of electrolysis products

Carbon Monoxide

STANJAN uses the method of element potentials to determine the chemical equilibrium for adiabatic combustion of the fuel-air mixture. This model is useful for predicting the trend in CO emissions as electrolysis products are added and the equivalence ratio varied, since during engine testing it may be difficult to vary the equivalence ratios. With this in mind, the CO results reported by STANJAN are shown in Figure 5.3.

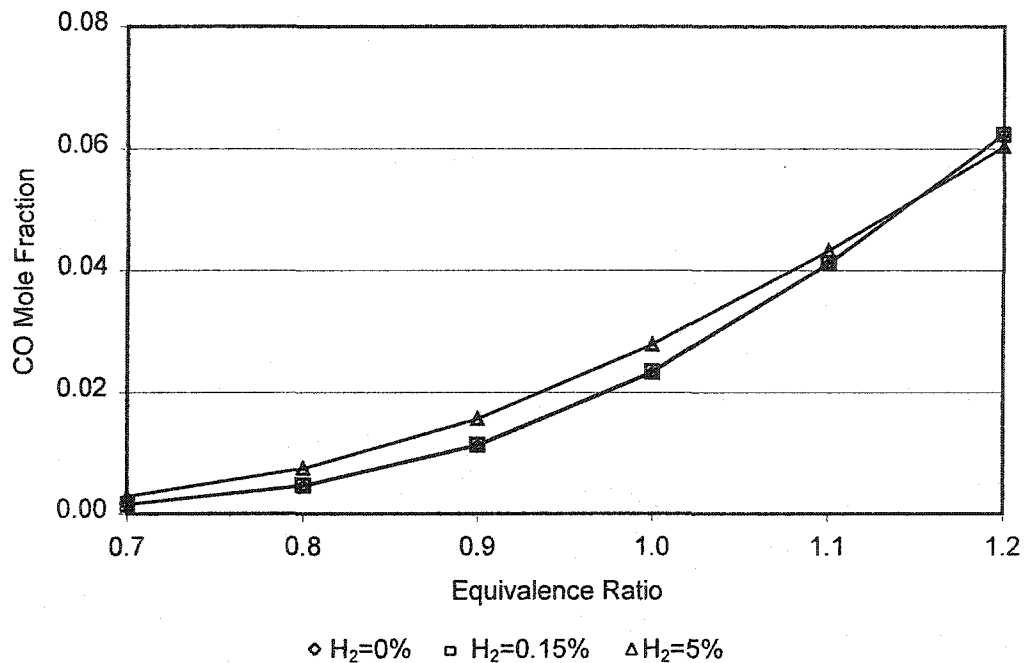


Figure 5.3 CO concentrations at state 3 as predicted by STANJAN for the addition of electrolysis products

CO concentrations are controlled by the equivalence ratio and the flame temperature. The state 3 CO concentrations are greater for hydrogen and oxygen addition than for no addition up to an equivalence ratio of $\phi = 1.15$. At richer mixtures than this the CO concentration decreases with hydrogen and oxygen addition.

Nitrogen Oxide

The NO mole fractions predicted by STANJAN are shown in Figure 5.4. An increase in NO concentrations occur with the addition of electrolysis products with peak concentrations at the equivalence ratio of $\phi = 0.8$, however, the increase is very small for the addition of electrolysis products with H₂=0.15%. NO concentrations are greatly affected by temperature. As discussed, the maximum temperature predicted to occur around an equivalence ratio of 1.1. As the fuel-air mixture becomes leaner, the increasing oxygen concentration initially offsets the decrease in gas temperatures. Therefore, in SI engines the NO concentrations usually peak at equivalence ratios around 0.9 [Heywood,

1988]. The STANJAN results predicted the peak NO concentrations to occur at equivalence ratios equal to 0.8. In engines the NO equilibrium emissions are formed through a complex set of kinetic reactions, which are not included in the STANJAN model.

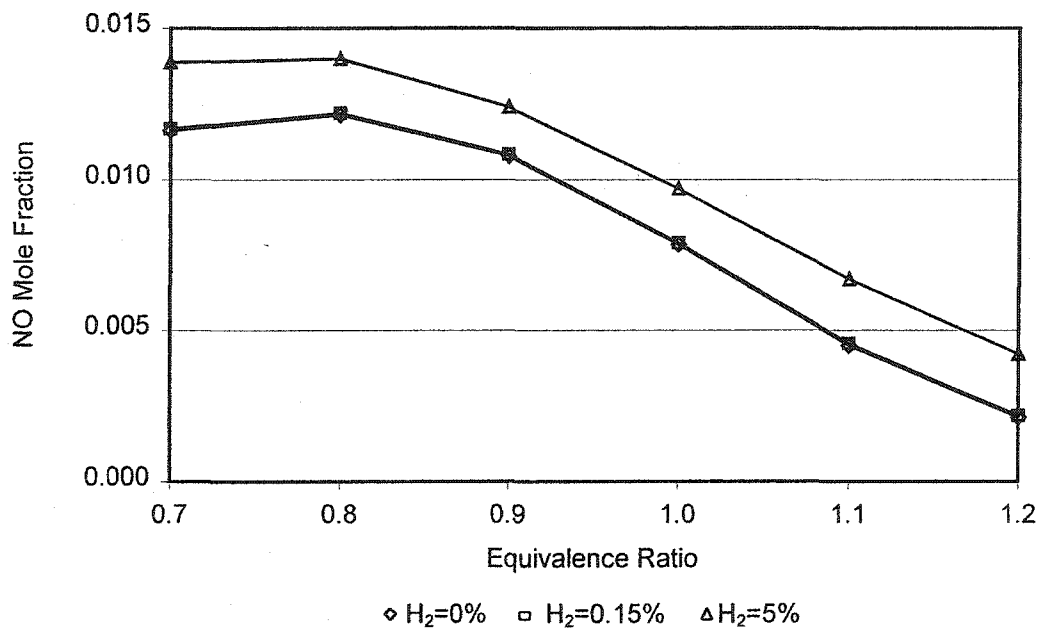


Figure 5.4 NO concentrations at state 3 as predicted by STANJAN for the addition of electrolysis products

Unburned Hydrocarbons

The only hydrocarbon concentration calculated as a product of combustion in STANJAN was iso-octane. Iso-octane concentrations are expected to increase with equivalence ratio, as the amount of air limits the combustion of the hydrocarbons. However, the mole fractions predicted by STANJAN are very small ($<10^{-80}$) and are likely the result of the mathematical uncertainty inherent in computer modelling. STANJAN is incapable of modelling unburned hydrocarbon concentrations properly since it cannot predict other species formed by recombining hydrocarbon fragments. The program is also unable to simulate the effect on unburned hydrocarbons from the quenching of the flame due to boundary layers and crevices. The results, even though unusable, showed that the

addition of electrolysis products resulted in an increase in iso-octane especially under leaner conditions.

5.2.2 ESP

The Engine Simulation Program (ESP) model predicts work output from an SI engine but not the exhaust gas mixture. Real-engine limitations such as the effects of turbulence, engine geometric parameters, spark timing and engine speed were also accommodated.

5.2.2.1 Predicted Work

The modelling was first completed using the spark ignition timing of the Briggs & Stratton engine 699° (21° btdc), which was used for the engine testing component of this research. However, it was noted that, ESP with the default settings predicted that the combustion process was completed before the piston reached top-dead-centre (TDC - 360°), Figure 5.5, and observed as a loop in the p - V diagram provided by ESP, Figure 5.6 [Reynolds, 2002].

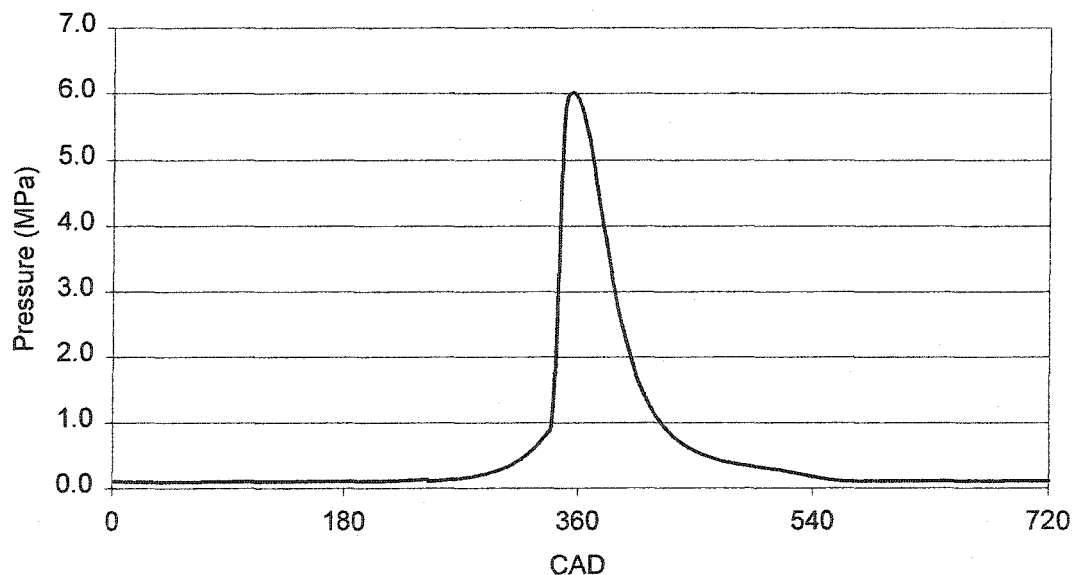


Figure 5.5 Pressure-CAD diagram for engine parameters equal to the Briggs & Stratton Vanguard 20 HP Engine ($\phi=1$, $H_2=0.15\%$)

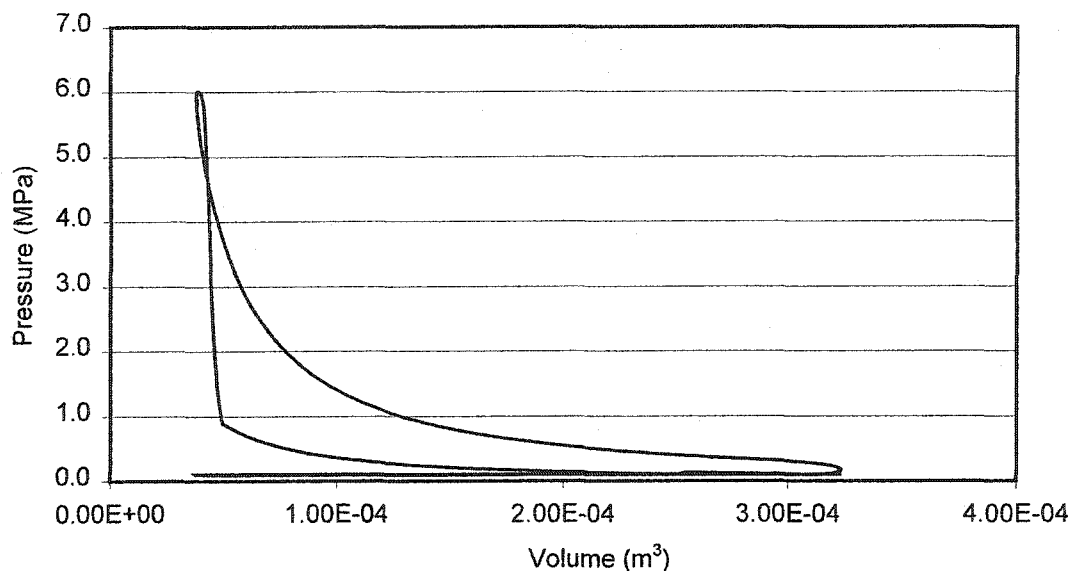


Figure 5.6 p - V diagram provided by the Engine Simulation Program for engine parameters equal to the Briggs & Stratton Vanguard 20 HP Engine ($\phi=1$, $H_2=0.15\%$)

By adjusting the spark timing in the model, it was found that ESP predicted the maximum work/kg fuel to occur with the spark timing of 719° and the loop in the p - V diagram was eliminated. The work presented in Figure 5.7 is the maximum work/kg fuel predicted by ESP at a spark timing of 719° .

As shown in Figure 5.7, the addition of hydrogen at 5% by mass of fuel results in an increase of 4-6% in work/kg fuel when compared to no hydrogen addition. Similarly, a hydrogen addition of 0.15% by mass of fuel results in a percent increase in work of approximately 0.1-0.2%. This increase in predicted work is similar to the increase predicted by STANJAN (0.2% and 5-8.5% for $H_2=0.15\%$ and 5% by mass, respectively).

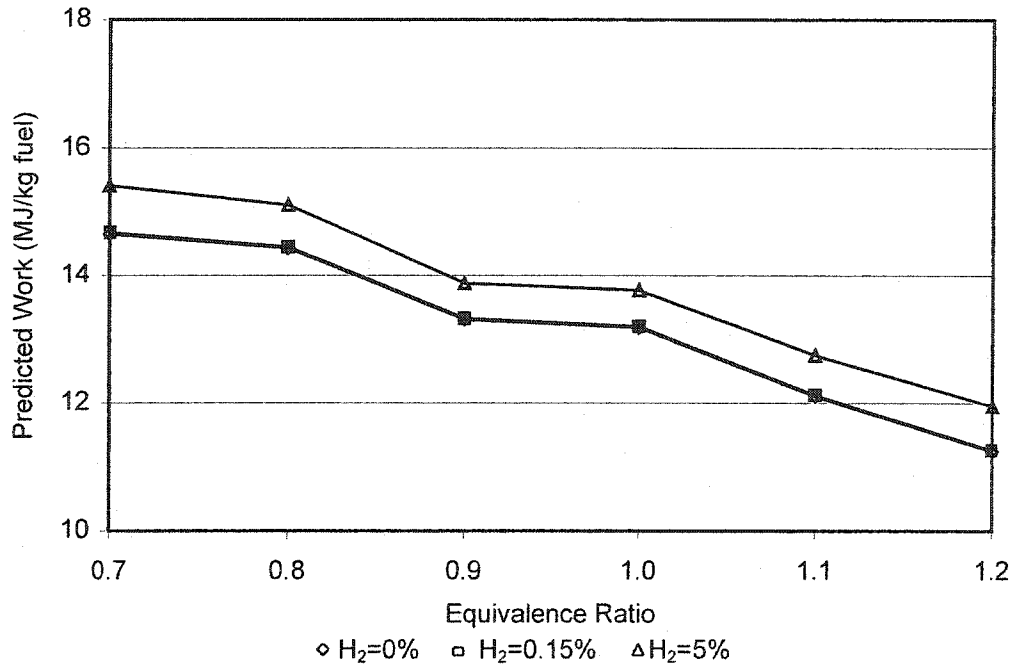


Figure 5.7 ESP modelling results for the effects of the addition of electrolysis products to iso-octane on predicted work

As expected the predicted work results determined by ESP (Figure 5.7) were less than those calculated based on STANJAN results for internal energy (Figure 5.1). The maximum predicted work determined in ESP (5% H₂ addition by mass of fuel and $\phi = 0.7$) was less than the minimum value calculated using the STANJAN simulation (no hydrogen addition and $\phi = 1.2$). These lower values predicted by ESP were expected due to inclusion of heat transfer losses, which are not included in the STANJAN simulation.

5.2.3 CHEMKIN

The application PREMIX was selected to model adiabatic flame temperatures and pollutant concentrations by simulating a premixed, freely propagating flame.

5.2.3.1 Flame Speed

CHEMKIN was used to predict the laminar flame speed under a pressure of 1 atm and temperature equal to 298K. The results provided in Figure 5.8 show that the addition of electrolysis products increases the flame speed. This is expected since the flame speed of hydrogen is 237 cm/s, while the flame speed of iso-octane is 41.5 cm/s, therefore, the addition of hydrogen should increase the overall flame speed of the fuel-air mixture. However, the addition of electrolysis products at $H_2=0.15\%$ by mass shows an increase in flame speed on the scale of 1 to 1.5%. Of the three models used, CHEMKIN is the only model capable of predicting the flame speed of a fuel-air mixture.

5.2.3.2 Emissions

CHEMKIN reports product concentrations in the “exhaust” gas as molar fractions. Simulations were run with initial conditions of 1 atmosphere and an unburned mixture temperature of 298K. All product concentrations reported are at a distance of 10 cm from the adiabatic unburned boundary. At this distance the temperature becomes fairly stable and it is assumed that combustion is completed, see Figure 5.9.

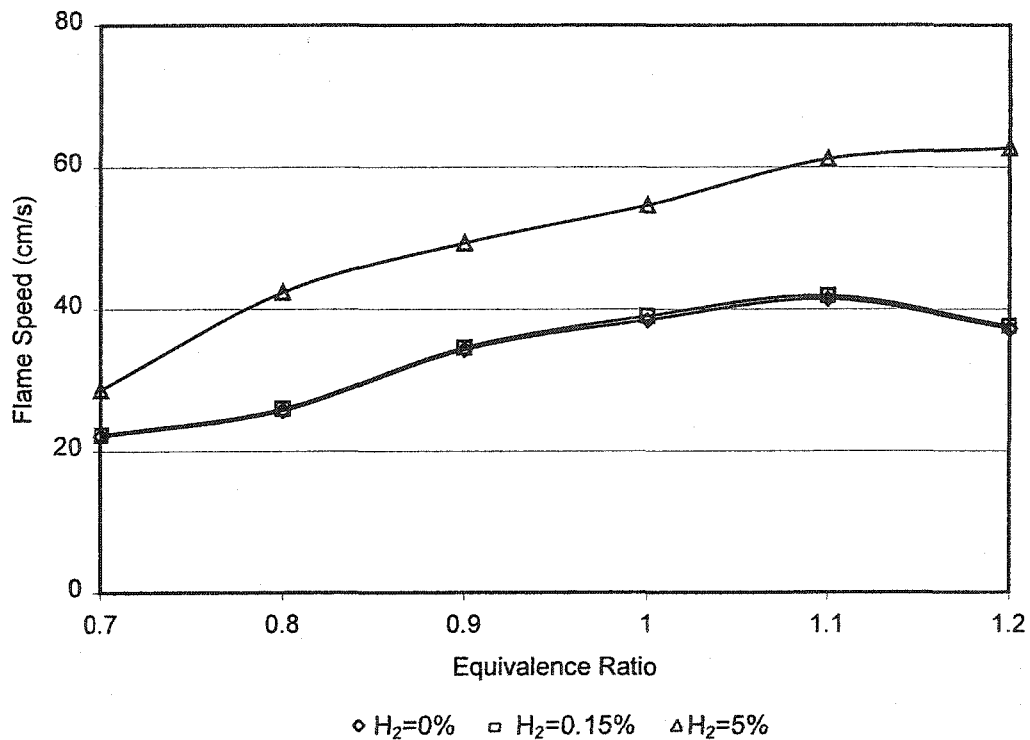


Figure 5.8 CHEMKIN modelling results for the effects of the addition of electrolysis products to iso-octane on flame speed

Adiabatic Temperatures

The adiabatic combustion temperatures determined by CHEMKIN are shown in Figure 5.10. The temperatures increase with equivalence ratio with a slight decrease in temperature after $\phi = 1.0$ for H₂=0% and 0.15%. As discussed in the STANJAN results, the maximum burned gas temperatures in SI engines occur at $\phi \approx 1.1$ [Heywood, 1988]. The addition of electrolysis products (H₂=0.15% and 5% by mass) increased the adiabatic combustion temperatures on an average of 0.04% and 5.3%.

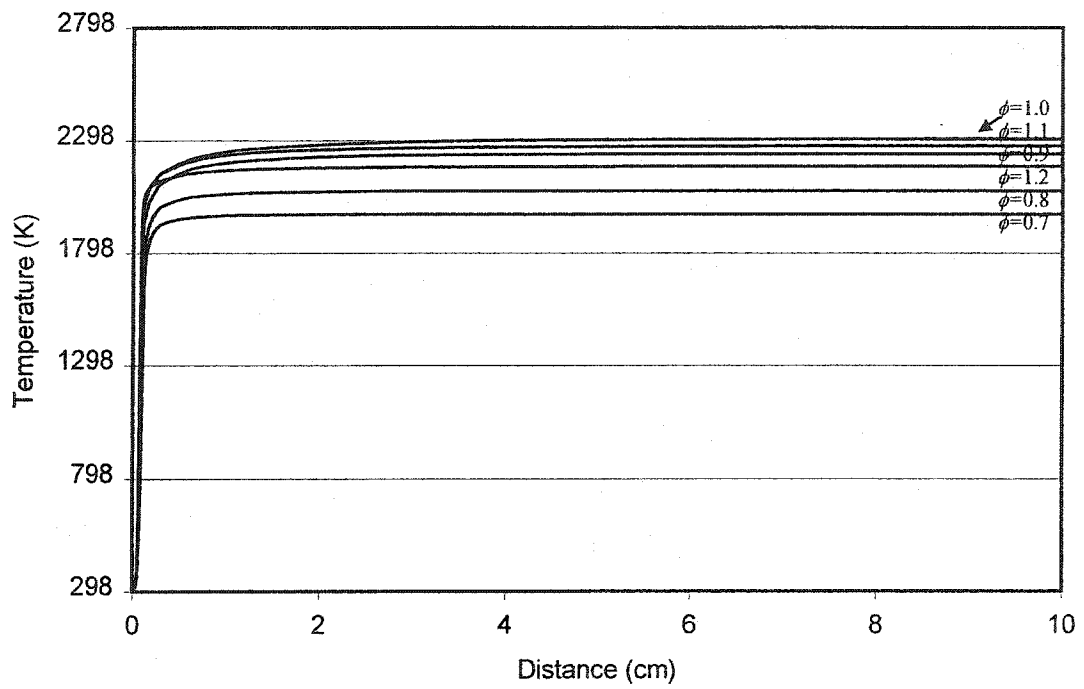


Figure 5.9 Temperature as distance for equivalence ratios ($\phi=0.7$ to 1.2)

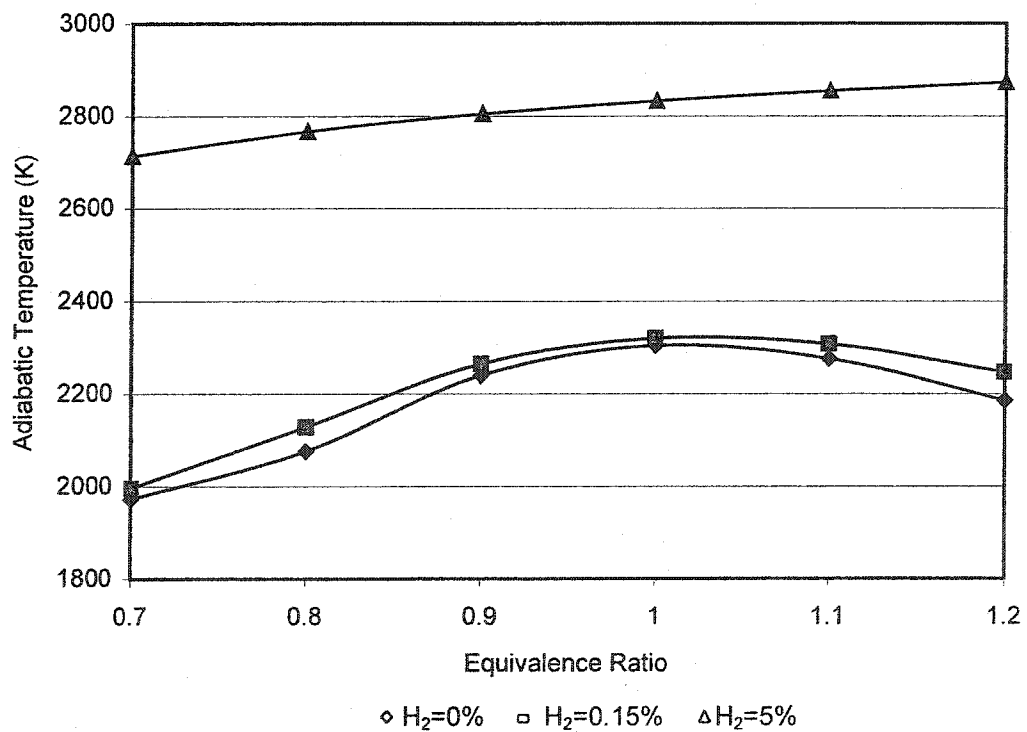


Figure 5.10 CHEMKIN modelling results for the effects of the addition of electrolysis products on adiabatic temperatures (1 atm)

Carbon Monoxide

In contrast to STANJAN, CHEMKIN uses chemical kinetics to determine the emissions concentrations. However, at a distance of 10 cm from the adiabatic flame boundary, the results predicted using chemical kinetics are expected to have reached equilibrium. In general, the CO concentrations increased with an increase in the equivalence ratio. Figure 5.11 shows that the addition of the electrolysis products ($H_2=0.15\%$) increased the CO emissions up to an equivalence ratio equal to 1.0 after which CO concentrations decreased. CO concentrations for the addition of electrolysis products ($H_2=5\%$) were significantly greater than without the electrolysis products for equivalence ratios less than 1.1. For equivalence ratios greater than 1.1 the CO emissions decreased for the addition of electrolysis products ($H_2=5\%$).

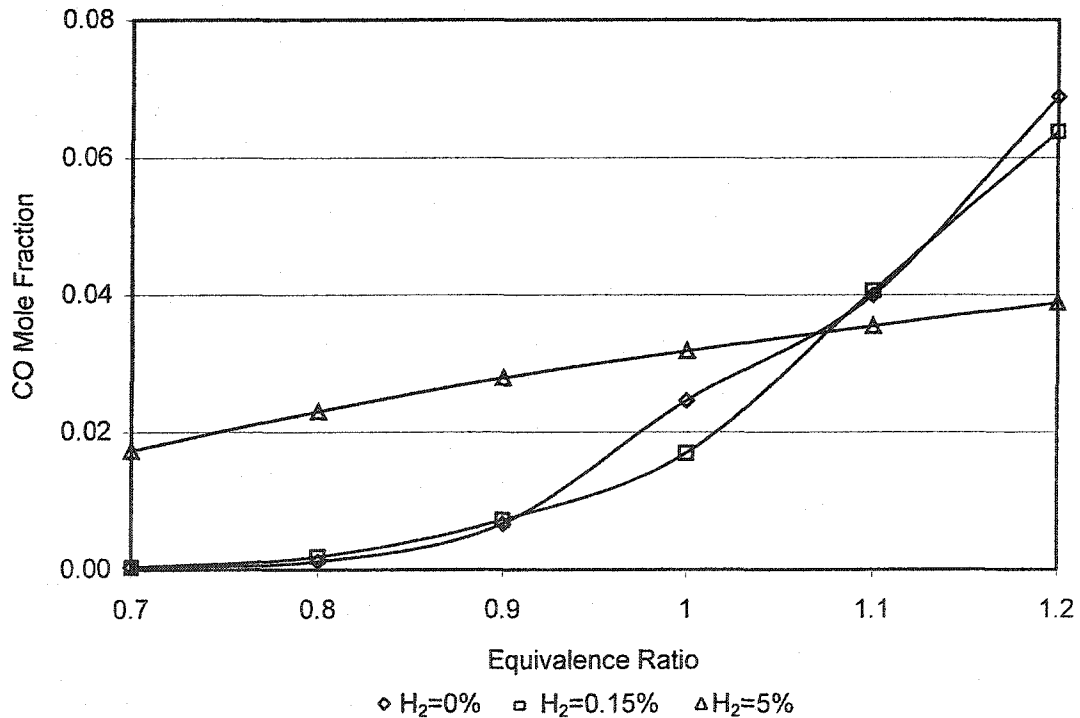


Figure 5.11 CHEMKIN modelling results for the effects of the addition of electrolysis products on CO concentrations (1 atm)

The CO trends and concentrations predicted by CHEMKIN are generally similar to those predicted using STANJAN with the exception that CHEMKIN predicts a reduction in CO concentrations for the addition of electrolysis products ($H_2=5\%$) compared to no addition at higher equivalence ratios ($\phi \approx 1.0$ for $H_2=0.15\%$ and $\phi \approx 1.1$ for $H_2 = 5\%$) instead of 1.2 as predicted by STANJAN. The CO concentrations predicted by CHEMKIN at a 10 cm distance from the adiabatic unburned boundary should be similar to those predicted by STANJAN.

In premixed hydrocarbon-air flames, the CO concentration increases rapidly in the flame zone to a maximum value after the flame, after which the CO concentrations decrease to the equilibrium value for adiabatic combustion. This process is illustrated in Figure 5.12 using the CHEMKIN results plotted against distance from the adiabatic unburned boundary, with an example of temperature versus distance. The temperature at a distance of 10 cm from the adiabatic unburned boundary is constant, see Figure 5.9. It is generally assumed that in postflame combustion, products from a spark ignition engine are close to equilibrium [Heywood, 1988].

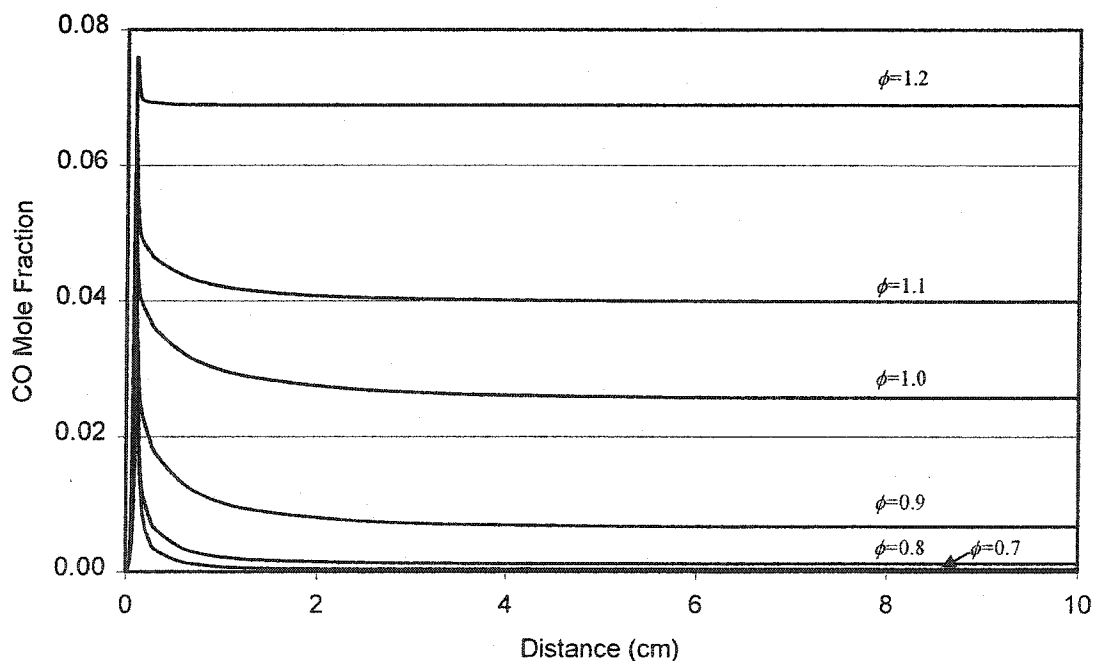


Figure 5.12 CO concentrations as distance from the adiabatic unburned boundary for equivalence ratios ($\phi=0.7$ to 1.2)

Nitrogen Oxide

The NO emission results determined through CHEMKIN simulations are shown in Figure 5.13. The CHEMKIN results show that peak NO concentrations occur around stoichiometric conditions with NO concentrations higher with the addition of electrolysis products. Note that the increase for the addition of the electrolysis products, where $H_2=0.15\%$ by mass is considerably small.

As discussed in the STANJAN results, NO concentrations are greatly affected by temperature, with maximum temperatures predicted around the equivalence ratio of 1.1 in SI engines and predicted by CHEMKIN and STANJAN. The CHEMKIN results predicted the peak NO concentrations to occur near stoichiometric conditions.

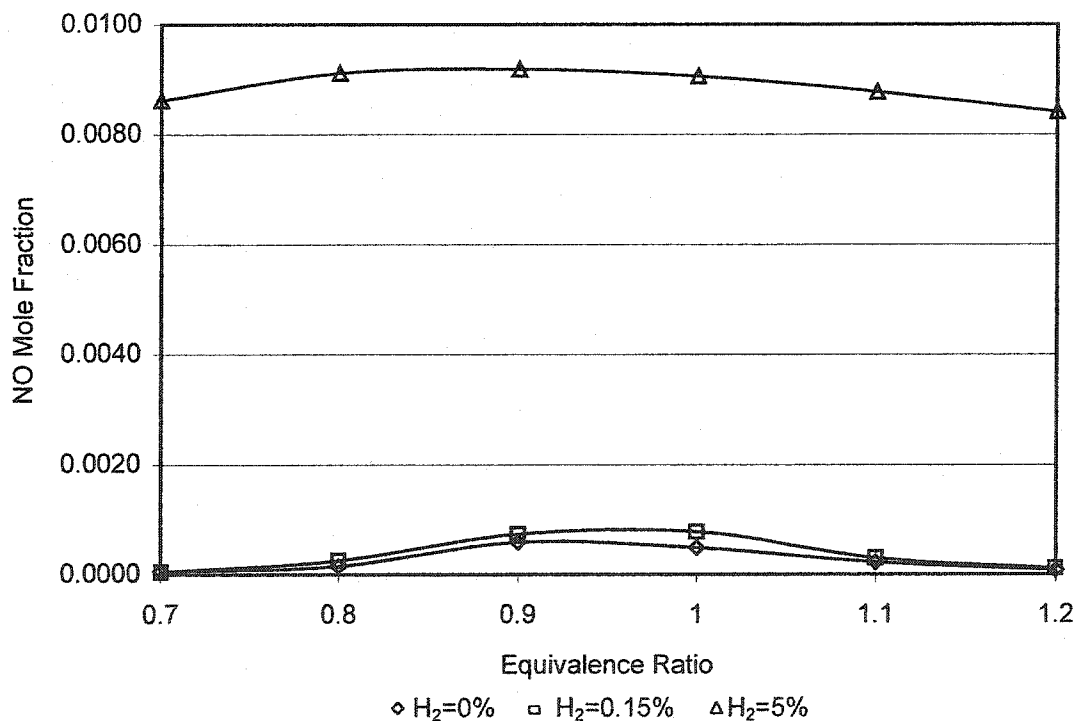


Figure 5.13 CHEMKIN modelling results for the effects of the addition of electrolysis products on NO emissions (1 atm)

As shown in Figure 5.14, NO concentrations increase with increasing distance from the adiabatic unburned boundary. NO forms in both the flame front and the postflame gases. The NO formed in the postflame gases dominates in engines over that formed in the flame front as the flame reaction zone is extremely thin and thus has a relatively short reaction time [Heywood, 1988].

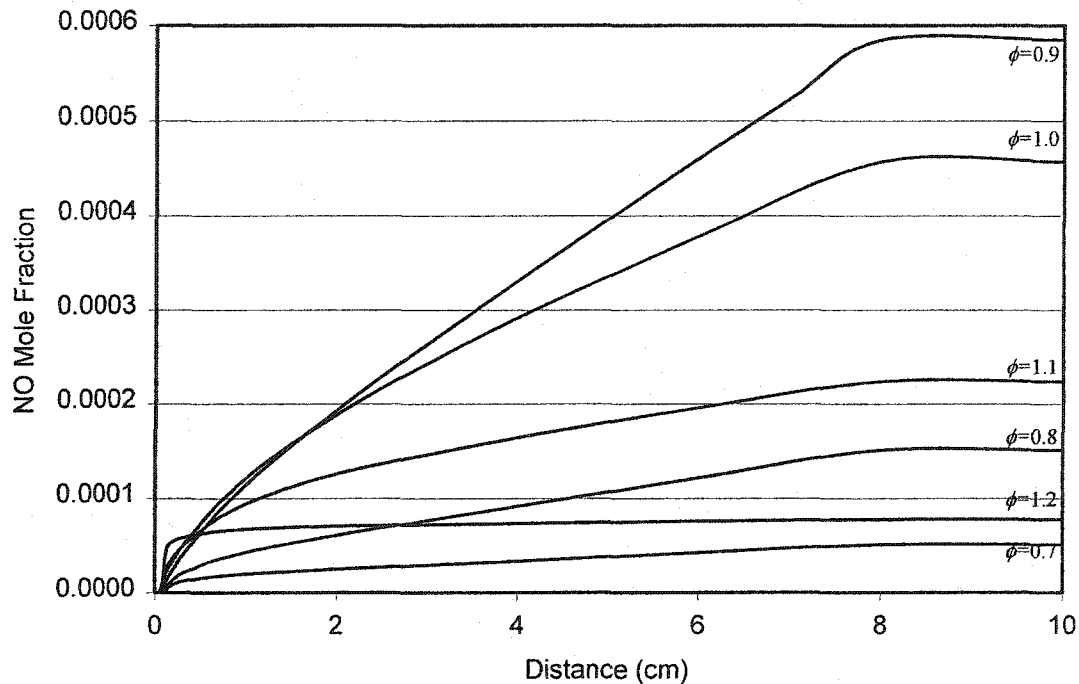


Figure 5.14 NO concentrations as distance from the adiabatic unburned boundary

Unburned Hydrocarbons

The iso-octane results were examined, however, the mole fractions predicted by CHEMKIN are very small ($<10^{-30}$) and are likely the result of the mathematical uncertainty inherent in computer modelling. Unburned hydrocarbon concentrations are expected to increase with equivalence ratio, as the amount of air limits the combustion of the hydrocarbons. The results, even though unusable, showed that the addition of electrolysis products resulted in a decrease in iso-octane concentrations.

Findings for Simulations Completed at Higher Pressures

Attempts were made to use CHEMKIN at pressures determined in STANJAN for state 3. Increasing the pressure, lead to convergence problems. For a pressure of 5 atmospheres simulations were completed for the addition of electrolysis products ($H_2 = 5\%$ by mass of fuel) for equivalence ratios, ϕ , between 0.7 and 1.1. These results are provided in Table 5.2. Other simulations attempted failed to converge.

Table 5.2 CHEMKIN results as influenced by pressure

Equivalence Ratio	Flame speed (cm/s)		CO Concentration (mole fraction)		Adiabatic Temperature (K)		NO Concentration (mole fraction)	
	1atm	5 atm	1atm	5 atm	1atm	5 atm	1atm	5 atm
0.7	28.6	17.7	6.22E-04	2.95E-4	2033	2039	8.99E-05	2.92E-4
0.8	42.3	28.4	4.58E-03	2.41E-3	2246	2262	6.82E-04	2.28E-3
0.9	49.3	34.0	9.61E-03	5.90E-3	2325	2355	1.14E-03	3.35E-3
1.0	54.6	38.8	1.72E-02	1.33E-2	2374	2421	1.31E-03	2.98E-3
1.1	61.1	43.9	4.00E-02	3.88E-2	2399	2428	7.35E-04	9.53E-4

The increase in pressure resulted in a small increase in temperature (between 6 and 47 K) as expected based on simple compression of gases. The formation of NO depends on pressure as well as temperature [Pulkrabek, 1997]. For the increase in pressure from 1 atm to 5 atm, CHEMKIN predicted an increase in NO concentrations (between 25 and 108%). The largest NO concentration increase due to the higher pressure was at $\phi=0.8$. CO concentrations decreased with the increase in pressure by 3–71%, with the greatest percentage reductions at lower equivalence ratios. The increase in pressure from 1 atm to 5 atm is small compared to the pressures predicted in STANJAN (73 atm to 90 atm for state 3). It is expected that with a further increase in pressure, the NO concentrations predicted by CHEMKIN would approach those predicted by STANJAN. Based on the limited results, it would be expected that the CO concentrations predicted by CHEMKIN at higher pressures would diverge from those predicted by STANJAN.

5.3 ENGINE TESTING

Eleven engine tests were completed as outlined in Section 4.6. In the following sections, results from the engine tests will be provided for torque, imep, COV, burn duration, and emissions. In most graphs (excluding the emissions versus equivalence ratio) the symbols represent the test conditions, where a diamond represents the initial condition (Condition 1), the square represents the results for the addition of the electrolysis products (Condition 2), and the circle represents the data after the electrolysis products are removed (Condition 3).

5.3.1 Torque

The torque results are plotted against engine speed in Figure 5.15 with results provided in Table 5.3. Although set to run at a desired rpm, the engine speed did fluctuate during testing. Minimum and maximum rpm values noted during the testing were used to calculate the uncertainty in speed (refer to Appendix G, Section G.1). The x-directional error bars represent the uncertainty in speed for each test. The size of the error bars is a representation of how stable the engine speed was maintained, the smaller the error bar the less the rpm fluctuated during the test. The uncertainty in torque is ± 0.41 N·m based on the Go-Power Systems manufacturer's specifications (Appendix G, Section G.2). The uncertainty in torque is represented by error bars in the y-direction centred around the result for the addition of the electrolysis products. For all tests the equivalence ratio was maintained for all three conditions, varying less than 2.4%, except for Test 10, which had a change in equivalence ratio of 12.2% between Conditions 1 and 3. However, the average uncertainty in equivalence ratio for Test 10 was 0.14, which is greater than the difference in the calculated equivalence ratios for Test 10.

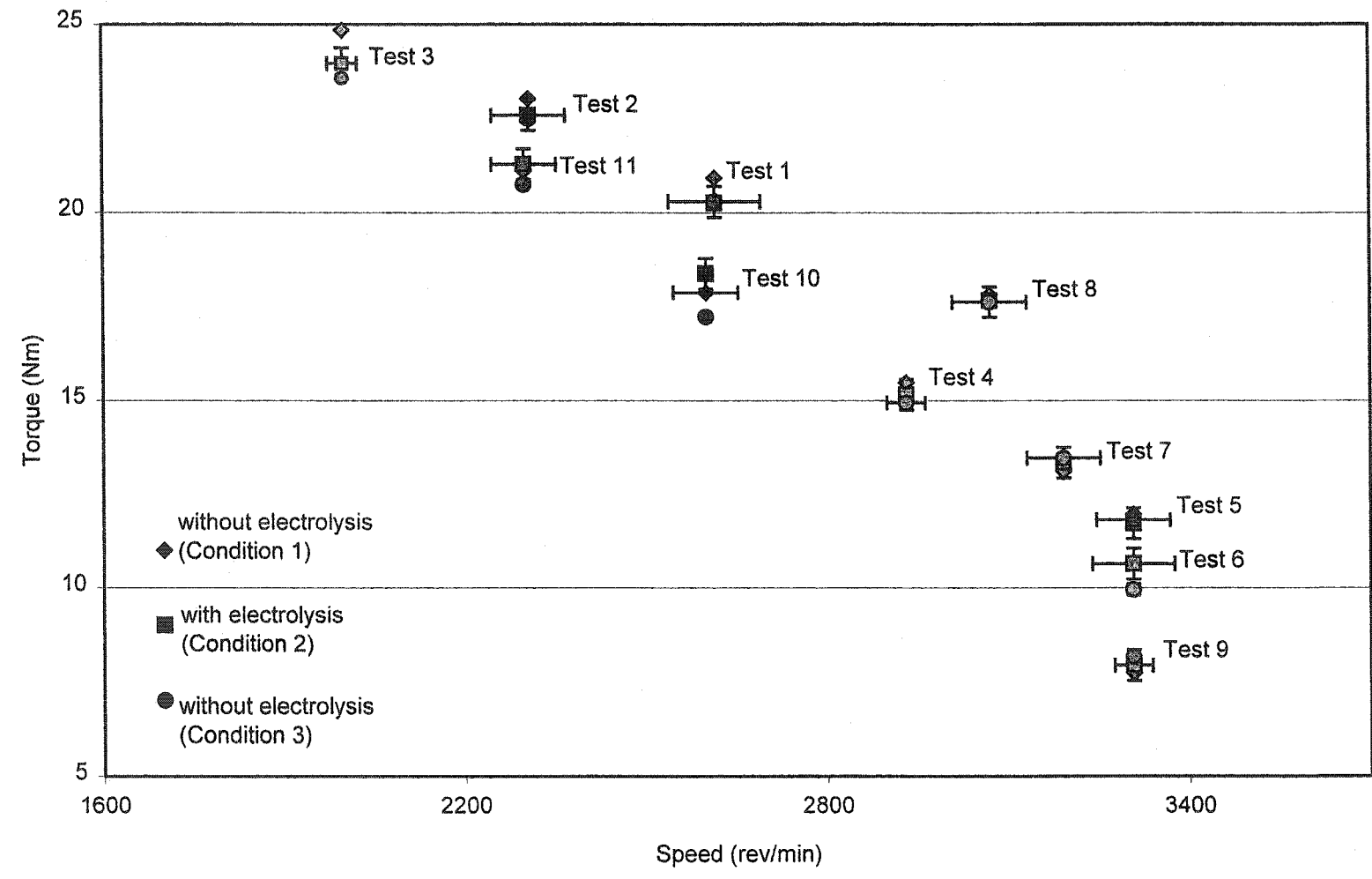


Figure 5.15 The effect of electrolysis products addition on torque

Table 5.3 Torque results presented with fuel and H₂ flow rates, equivalence ratio and speed for each test.

Test	Condition	Speed		Fuel flow rate	H ₂ flow rate			Equivalence ratio (ϕ)	Torque (N·m) $u_r=0.41$
		rev/min	uncertainty (u_{rpm})	L/s	L/s	% by mass	% by volume		
1	1	2620	78	0.083				0.78	20.9
	2			0.084	0.0056	0.12	6.7	0.79	20.3
	3			0.082				0.79	20.3
2	1	2310	62	0.080				0.82	23.0
	2			0.078	0.0055	0.12	7.0	0.82	22.6
	3			0.078				0.82	22.5
3	1	2000	25	0.073				0.81	24.9
	2			0.072	0.0055	0.14	7.7	0.82	24.0
	3			0.069				0.80	23.6
4	1	2930	32	0.087				0.80	15.5
	2			0.086	0.0060	0.12	7.0	0.81	15.2
	3			0.086				0.82	14.9
5	1	3310	62	0.091				0.88	12.0
	2			0.092	0.006	0.11	6.0	0.90	11.7
	3			0.091				0.89	11.8
6	1	3310	70	0.085				0.74	10.0
	2			0.085	0.0056	0.12	6.6	0.75	10.6
	3			0.086				0.76	10.0
7	1	3190	62	0.084				0.80	13.1
	2			0.083	0.0051	0.11	6.2	0.78	13.3
	3			0.084				0.79	13.5
8	1	3050	62	0.086				0.73	17.8
	2			0.085	0.0053	0.11	6.2	0.73	17.7
	3			0.087				0.74	17.6
9	1	3300	32	0.085				0.69	7.7
	2			0.084	0.0053	0.11	6.3	0.70	7.9
	3			0.083				0.69	8.2
10	1	2600	55	0.090				0.82	17.9
	2			0.083	0.0058	0.12	7.0	0.77	18.4
	3			0.078				0.72	17.2
11	1	2300	55	0.083				0.72	21.1
	2			0.081	0.0058	0.13	7.2	0.71	21.3
	3			0.080				0.72	20.7


Notes: 1) Condition 1 represents initial condition, engine run without electrolysis.

Condition 2 represents the addition of electrolysis products.

Condition 3 represents engine run without electrolysis products.

2) Oxygen added in a volume ratio of 1:2 (oxygen/hydrogen).

3) u_{rpm} represents the maximum uncertainty based on calculation in Appendix G.

4)  shading represents the maximum value for the test.

Based on the graphical representation of the results provided in Figure 5.15, as the engine's speed is increased the ability of the engine to do work (torque) decreases.

A torque increase was reported for the addition of electrolysis products in only three of the tests conducted; Test 6 had the greatest increase in torque of 0.6 N·m for a 0.12 % H₂ addition by mass of fuel and an equivalence ratio of 0.75. Tests 10 and 11 also experienced an increase in torque of 0.4 N·m and 0.2 N·m (0.12 % and 0.13 % H₂ addition by mass of fuel and $\phi = 0.77$ and 0.71, respectively). However, for all three tests the increase in torque is less than 2 times the uncertainty factor ($2 \times 0.41 = 0.82$ N·m). For all other tests, the torque was less for the addition of the electrolysis products when compared to either of the other two conditions, including Test 3. Test 3 showed the greatest difference in torque ($\Delta\tau = 1.3$ N·m) between Condition 1 and Condition 3 even though the addition of the electrolysis products resulted in the maximum addition of H₂ (0.14 % H₂ by mass of fuel) amongst all tests. This difference in torque is less than 3 times the uncertainty factor. Based on these results, changes in torque were not consistent for the addition of the electrolysis products and all differences in torque were less than 3 times the uncertainty factor. Figure 5.16 is provided to show the decrease in torque upon adding electrolysis products as calculated between Conditions 1 and 2 ($\tau_1 - \tau_2$) and Conditions 3 and 2 ($\tau_3 - \tau_2$). Clearly, the addition of the electrolysis products had both a positive and negative effects on torque. It is important to note that the load was not changed between Conditions as the speed of the engine remained constant for each Condition.

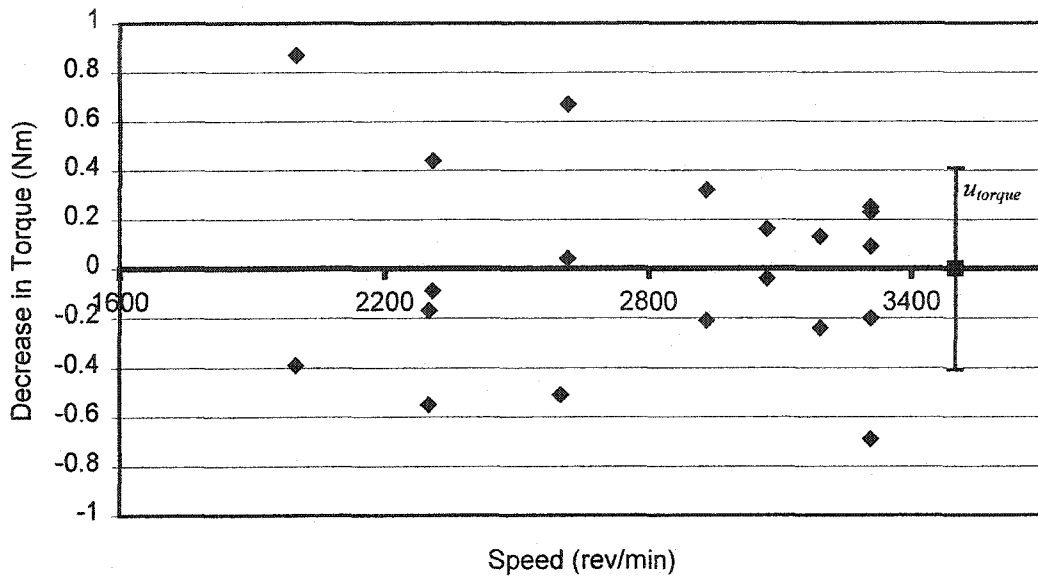


Figure 5.16 Decrease in torque for the addition of electrolysis products

5.3.2 Indicated Mean Effective Pressure

The process of determining the indicated mean effective pressure, imep, is described in detail in Section 4.4.3. Each of the imep values presented in Figure 5.17 and Table 5.4 is the average imep for approximately 100 cycles. Tests 3 and 11 were not included in this analysis as the p - V diagrams produced at these lower speeds (2000 and 2300 rpm, respectively) showed pressures later in the expansion stroke (462° to 540°), which were less than the pressures during the compression stroke (180° to 250°) for the same volume. The likely source of these errors was that at the lower speeds the effects of the second cylinder significantly influenced the data acquired from the first.

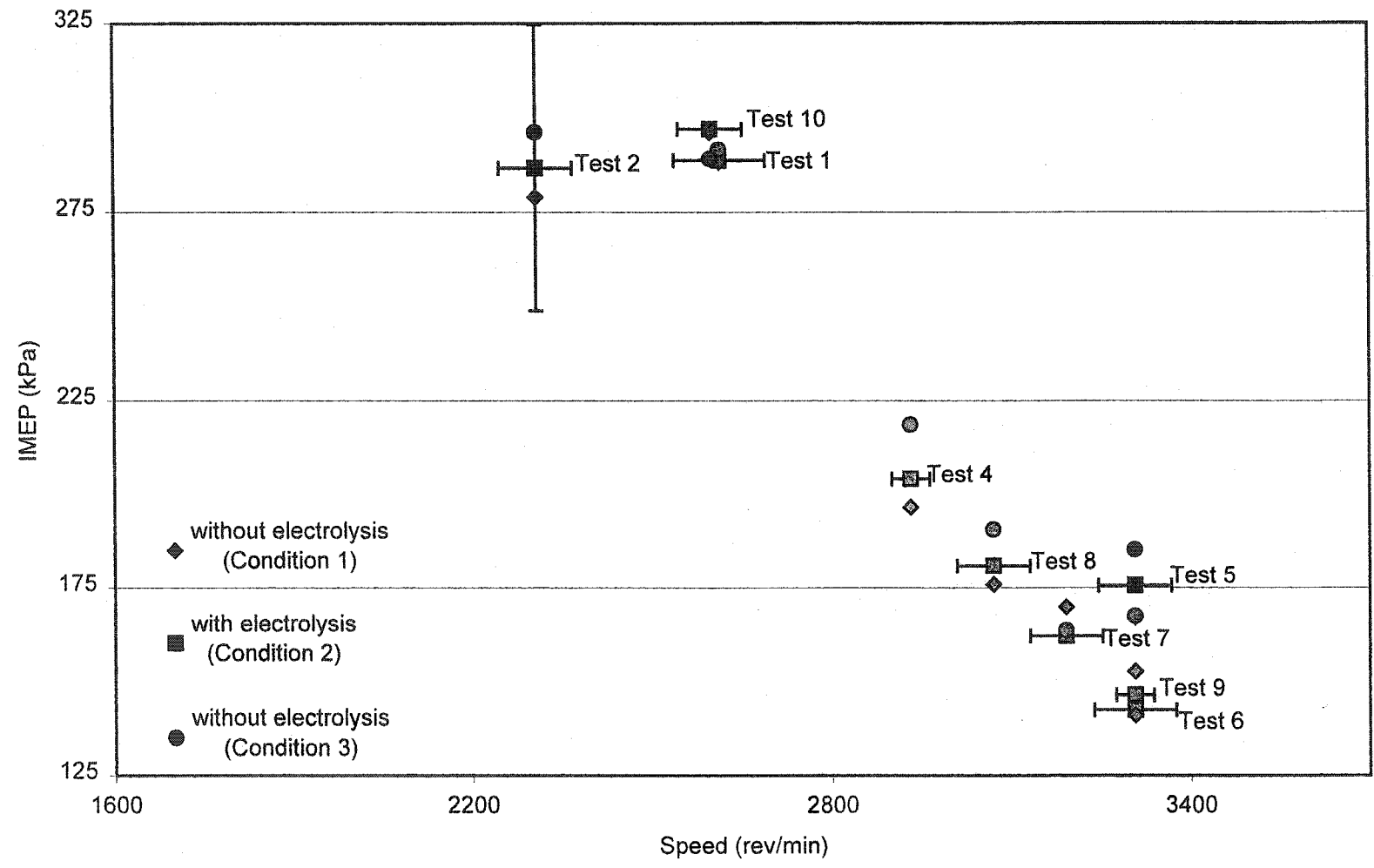


Figure 5.17: The effects of the addition of electrolysis products on imep

Table 5.4 imep results presented with fuel and H₂ flow rates, equivalence ratio and speed for each test.

Test	Condition	Speed		Fuel flow rate	H ₂ flow rate			Equivalence ratio (ϕ)	IMEP (kPa) <i>U_{imep}</i> =±38kPa
		rev/min	uncertainty (<i>u_{rpm}</i>)	L/s	L/s	% by mass	% by volume		
1	1	2620	78	0.083				0.78	288
	2			0.084	0.0056	0.12	6.7	0.79	289
	3			0.082				0.79	292
2	1	2310	62	0.080				0.82	279
	2			0.078	0.0055	0.12	7.0	0.82	287
	3			0.078				0.82	296
3	1	2000	25	0.073				0.81	Error in measurement
	2			0.072	0.0055	0.14	7.7	0.82	
	3			0.069				0.80	
4	1	2930	32	0.087				0.80	196
	2			0.086	0.0060	0.12	7.0	0.81	204
	3			0.086				0.82	219
5	1	3310	62	0.091				0.88	167
	2			0.092	0.006	0.11	6.0	0.90	176
	3			0.091				0.89	185
6	1	3310	70	0.085				0.74	153
	2			0.085	0.0056	0.12	6.6	0.75	142
	3			0.086				0.76	146
7	1	3190	62	0.084				0.80	170
	2			0.083	0.0051	0.11	6.2	0.78	162
	3			0.084				0.79	163
8	1	3050	62	0.086				0.73	176
	2			0.085	0.0053	0.11	6.2	0.73	181
	3			0.087				0.74	191
9	1	3300	32	0.085				0.69	141
	2			0.084	0.0053	0.11	6.3	0.70	146
	3			0.083				0.69	167
10	1	2600	55	0.090				0.82	296
	2			0.083	0.0058	0.12	7.0	0.77	297
	3			0.078				0.72	289
11	1	2300	55	0.083				0.72	Error in measurement
	2			0.081	0.0058	0.13	7.2	0.71	
	3			0.080				0.72	


Notes: 1) Condition 1 represents initial condition, engine run without electrolysis.

Condition 2 represents the addition of electrolysis products.

Condition 3 represents engine run without electrolysis products.

2) Oxygen added in a volume ratio of 1:2 (oxygen/hydrogen).

3) u_{rpm} represents the maximum uncertainty based on calculation in Appendix G.

4)  shading represents the maximum value for the test.

As discussed above, the engine speed, although set to run at a desired rpm by fixing the throttle setting and torque, did fluctuate within a given Condition. The uncertainty values, u_{rpm} , are calculated for each test based on the minimum and maximum fluctuation noted during testing. The x-directional error bars represent the u_{rpm} for each test. The uncertainty in imep, u_{imep} is ± 38 kPa, is an average of the uncertainty values for each section of area. Since the u_{imep} is assumed constant for the tests, only Test 2 provides an error bar representing u_{imep} in the y-direction centred around the result for the addition of the electrolysis products. Calculations for the uncertainty in speed and imep are described in Appendix G.

In general, the imep was greatest under Condition 3 with the following exceptions; Tests 6 and 7, where Condition 1 resulted in the greatest imep and Test 10 where the results for the addition of electrolysis products resulted in the greatest imep. The change in imep under each test was not significant, as the difference in maximum and minimum imep values was less than the uncertainty value for imep. Figure 5.18 is provided to show the differences in imep between Conditions 1 and 2 ($imep_1 - imep_2$) and Conditions 3 and 2 ($imep_3 - imep_2$) and clearly indicates that the decrease in imep with the addition of the electrolysis products was both positive and negative. Note all differences were less than the uncertainty in imep, 38kPa.

Similar to the torque results, the imep was more affected by the speed of the engine than the introduction of the electrolysis products. No correlation was found for imep and equivalence ratio.

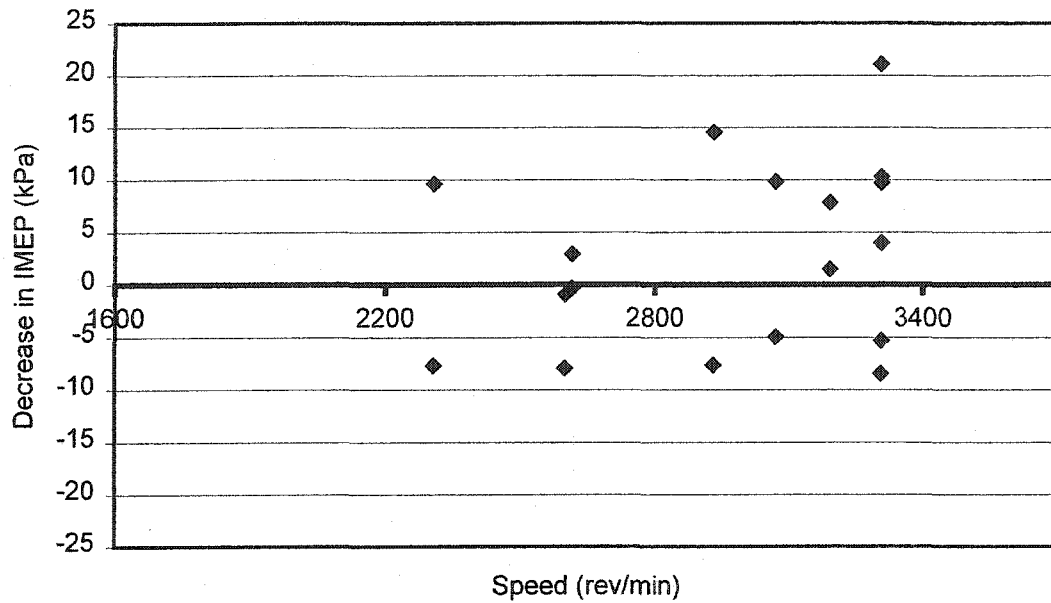


Figure 5.18 Decrease in imep for the addition of electrolysis products

5.3.3 Coefficient of Variation

The coefficient of variation, COV_{imep} , is an important measure of cyclic variability (see Section 4.4.4). The COV_{imep} is a function of the imep, therefore, as discussed in Section 5.3.2, Tests 3 and 11 were not included in this analysis due to errors in the measurement of pressure.

Each of the COV_{imep} results presented in Figures 5.18 and 5.19 and Table 5.5 is the average COV_{imep} for approximately 100 cycles. Figure 5.19 compares the COV_{imep} to the engine speed. As in the previous sections the x-directional error bars represent the u_{rpm} for each test. The calculation for the uncertainty in speed is described in Appendix G.

The COV_{imep} results provided in Figure 5.19 indicate that the COV_{imep} increases with the engine speed, with the exception of Test 5, which reported lower COV_{imep} results than Tests 7 and 8 (3192 and 3050 rpm, respectively). At slower engine speeds, higher loads, the combustion process is more repeatable reducing the COV_{imep} [Heywood, 1988].

Figure 5.20 provides a graphical relationship of COV_{imep} to the equivalence ratio. The equivalence ratio uncertainty, u_ϕ , ranges between 0.11 and 0.19. Due to the large uncertainty values, the values were not provided as x-directional error bars in Figure 5.20 but are included in Table 5.5. The calculation of u_ϕ is provided in Appendix G, Section G.5. The equivalence ratios for each test remained generally constant with the exception of Test 10, which had a reduction in equivalence ratio under each test condition. In general, the tests at lower equivalence ratios had higher COV_{imep} results, for example Test 9 had the lowest calculated equivalence ratio ($0.69 < \phi < 0.70$) but the highest COV_{imep} results. The minimum COV_{imep} results were reported for Test 2, which had one of the higher equivalence ratios ($\phi=0.82$). The differences in COV_{imep} between Conditions 1 and 2 ($COV_{imep1}-COV_{imep2}$) and Conditions 3 and 2 ($COV_{imep3}-COV_{imep2}$), shown in Figure 5.21, indicate that the decrease in COV_{imep} with the addition of the electrolysis products was both positive and negative.

Based on the results, the engine speed and equivalence ratio affected the COV_{imep} during testing. However, the addition of electrolysis products had no reliable effect on COV_{imep} .

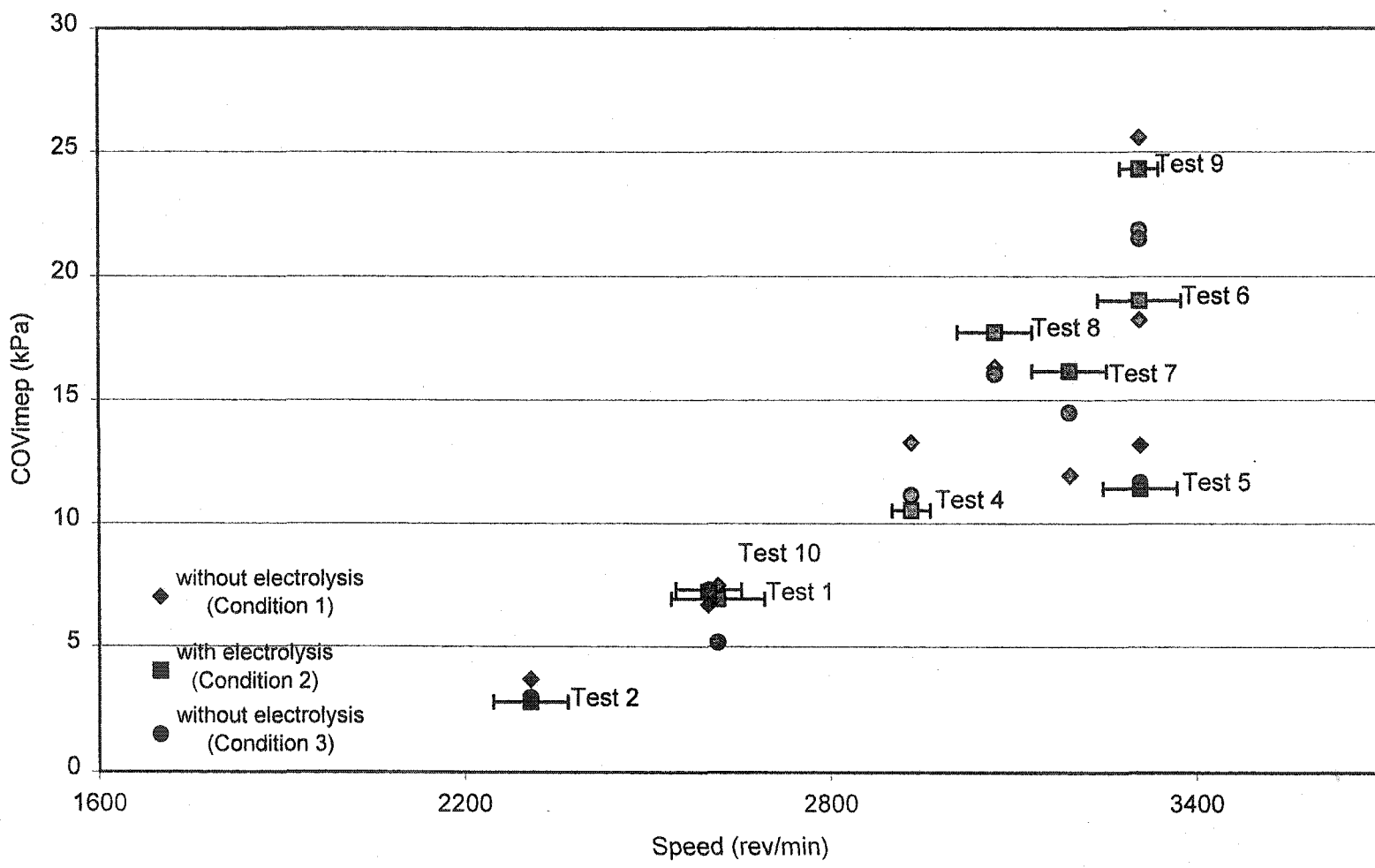


Figure 5.19 COV_{imep} versus engine speed

Table 5.5 COV_{imep} results presented with fuel and H₂ flow rates, equivalence ratio and speed for each test.

Test	Condition	Speed		Fuel flow rate	H ₂ flow rate			Equivalence ratio		COV _{imep} (%)
		rev/min	u_{rpm}	L/s	L/s	% by mass	% by volume	(ϕ)	$u_{(\phi)}$	
1	1	2620	78	0.083				0.78	0.144	7.5
	2			0.084	0.0056	0.12	6.7	0.79	0.149	6.9
	3			0.082				0.79	0.149	5.2
2	1	2310	62	0.080				0.82	0.165	3.7
	2			0.078	0.0055	0.12	7.0	0.82	0.168	2.8
	3			0.078				0.82	0.171	3.0
3	1	2000	25	0.073				0.81	0.178	Error in measurements
	2			0.072	0.0055	0.14	7.7	0.82	0.184	
	3			0.069				0.80	0.180	
4	1	2930	32	0.087				0.80	0.148	13.3
	2			0.086	0.0060	0.12	7.0	0.81	0.153	10.5
	3			0.086				0.82	0.152	11.1
5	1	3310	62	0.091				0.88	0.167	13.2
	2			0.092	0.006	0.11	6.0	0.90	0.173	11.4
	3			0.091				0.89	0.172	11.7
6	1	3310	70	0.085				0.74	0.129	18.2
	2			0.085	0.0056	0.12	6.6	0.75	0.131	19.0
	3			0.086				0.76	0.133	21.9
7	1	3190	62	0.084				0.80	0.148	11.9
	2			0.083	0.0051	0.11	6.2	0.78	0.144	16.1
	3			0.084				0.79	0.146	14.5
8	1	3050	62	0.086				0.73	0.123	16.3
	2			0.085	0.0053	0.11	6.2	0.73	0.124	17.7
	3			0.087				0.74	0.126	16.0
9	1	3300	32	0.085				0.69	0.112	25.6
	2			0.084	0.0053	0.11	6.3	0.70	0.115	24.1
	3			0.083				0.69	0.114	21.5
10	1	2600	55	0.090				0.82	0.148	6.7
	2			0.083	0.0058	0.12	7.0	0.77	0.142	7.2
	3			0.078				0.72	0.133	7.3
11	1	2300	55	0.083				0.72	0.122	Error in measurement
	2			0.081	0.0058	0.13	7.2	0.71	0.125	
	3			0.080				0.72	0.126	


Notes: 1) Condition 1 represents the initial condition, engine run without electrolysis.

Condition 2 represents the addition of electrolysis products.

Condition 3 represents engine run without electrolysis products.

2) Oxygen added in a volume ratio of 1:2 (oxygen/hydrogen).

3) u_{rpm} represents the maximum uncertainty based on calculation in Appendix G.

4)  shading represents the maximum value for the test.

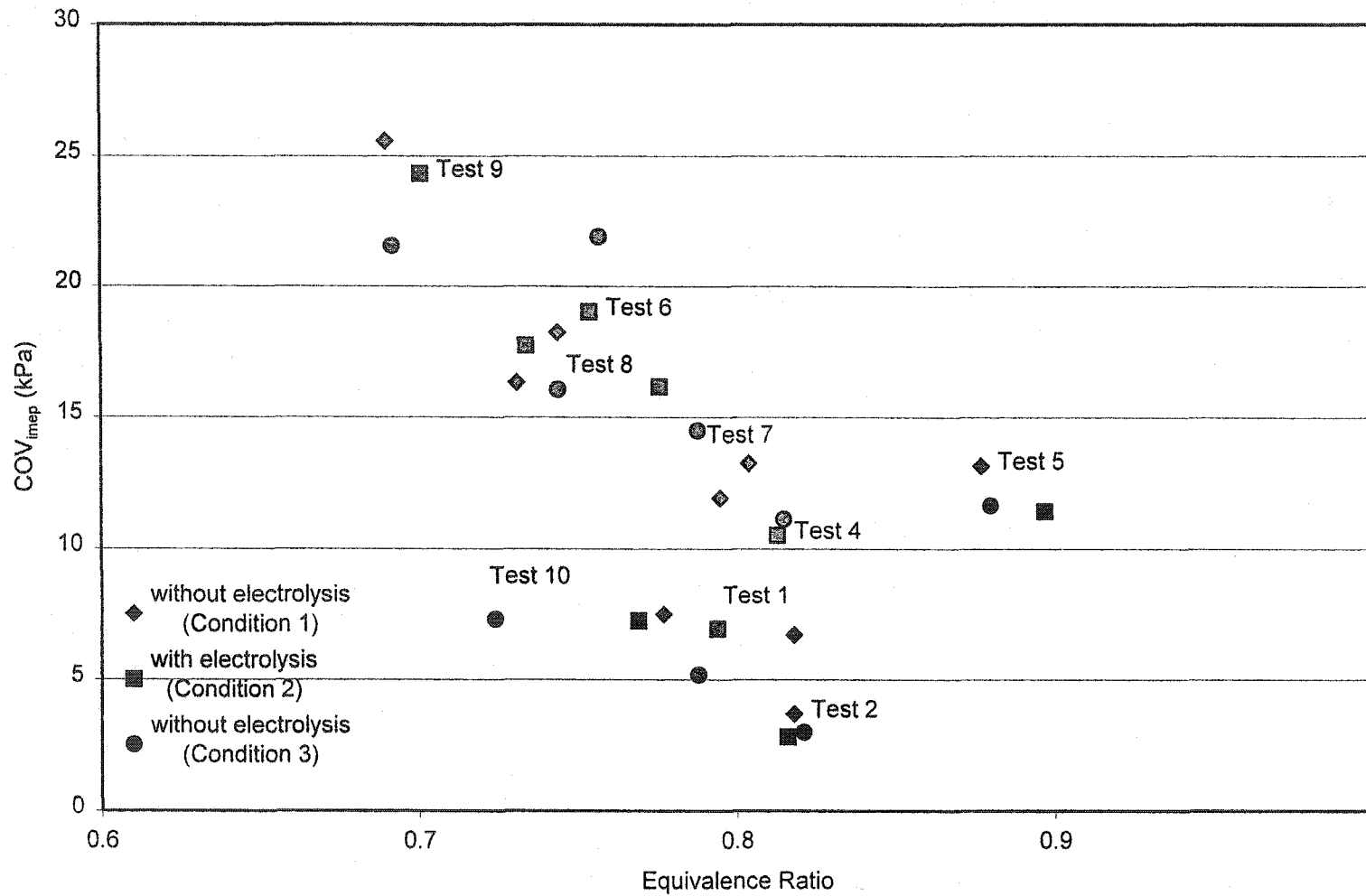


Figure 5.20 COV_{imep} versus equivalence ratio

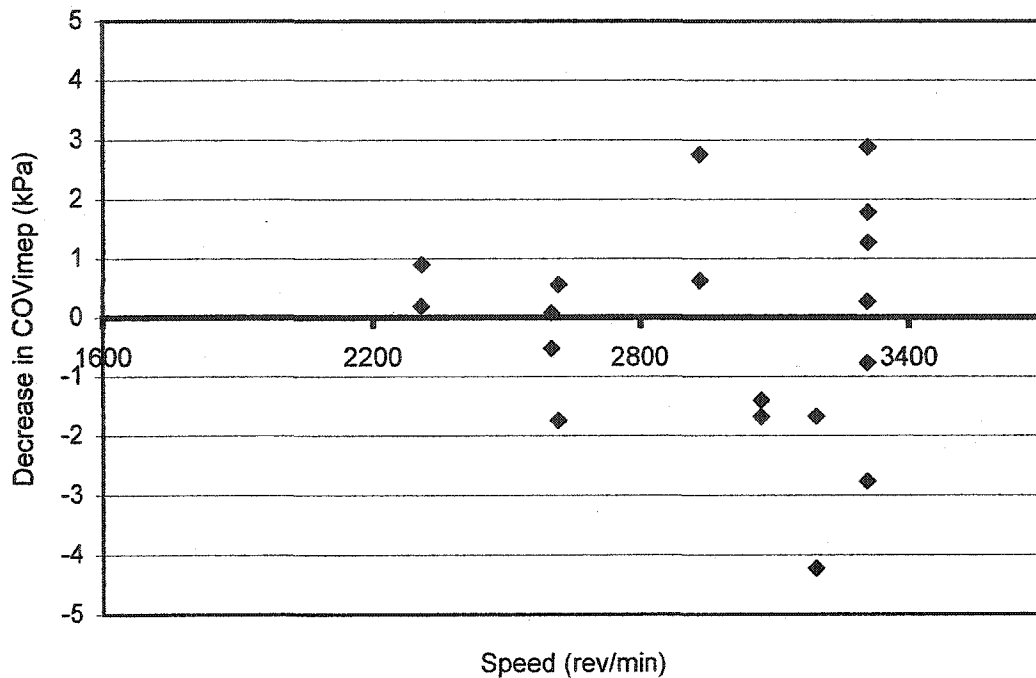


Figure 5.21 Decrease in COV_{imep} based on the addition of electrolysis products

5.3.4 Burn Duration

As described in Section 4.5, the burn duration analysis compares the pressure rise within a cylinder during a fired cycle to that in an unfired cycle. Examples of the relative pressure traces versus crank angle for the unfired and fired cycles are provided in Figure 5.22. The data used in Figure 5.22 was from Test 9 with engine speed equal to 3300 rpm. The uncertainty in the pressure data, u_p , is equal to ± 31 kPa; refer to Appendix G for uncertainty calculation details. A second method used to illustrate the difference between the unfired and fired cycles is $dP/dCAD$ versus crank angle degree as shown in Figure 5.23.

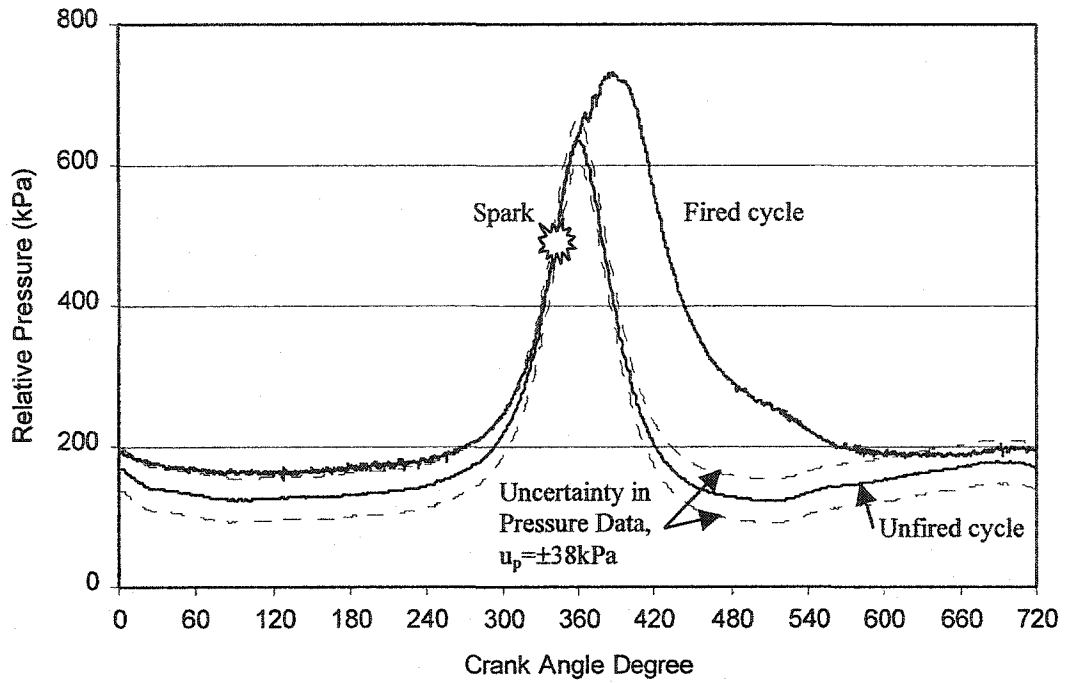


Figure 5.22 Relative pressure versus crank angle for fired and unfired cycle at 3300rpm

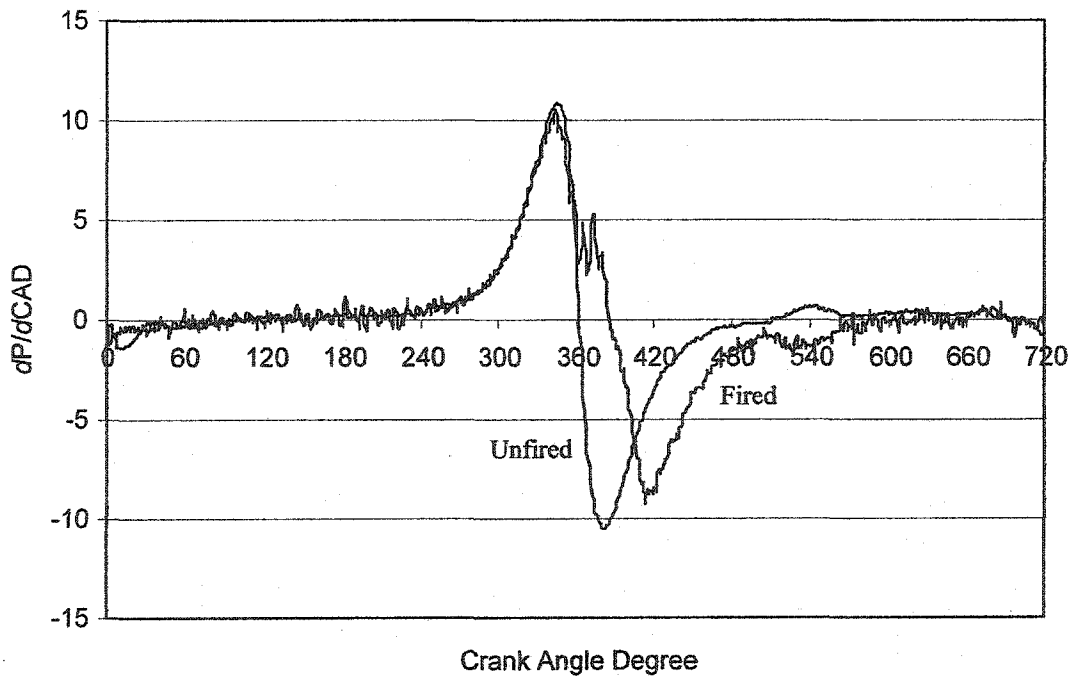


Figure 5.23 $dP/dCAD$ versus crank angle for fired and unfired cycle at 3300 rpm

The pressure traces in Figure 5.22 are shifted vertically, so the reference pressure was the same for both the fired and unfired cycles at the crank angle where the spark occurred. Figure 5.24 shows the mass fraction burned (mfb) curve obtained for 16 consecutive cycles calculated using the unfired cycle shown in Figure 5.22. Figure 5.24 provides a good representation of the cycle-to-cycle variation in the burn duration. The results provided in the following section are averaged burn duration values for approximately 100 cycles.

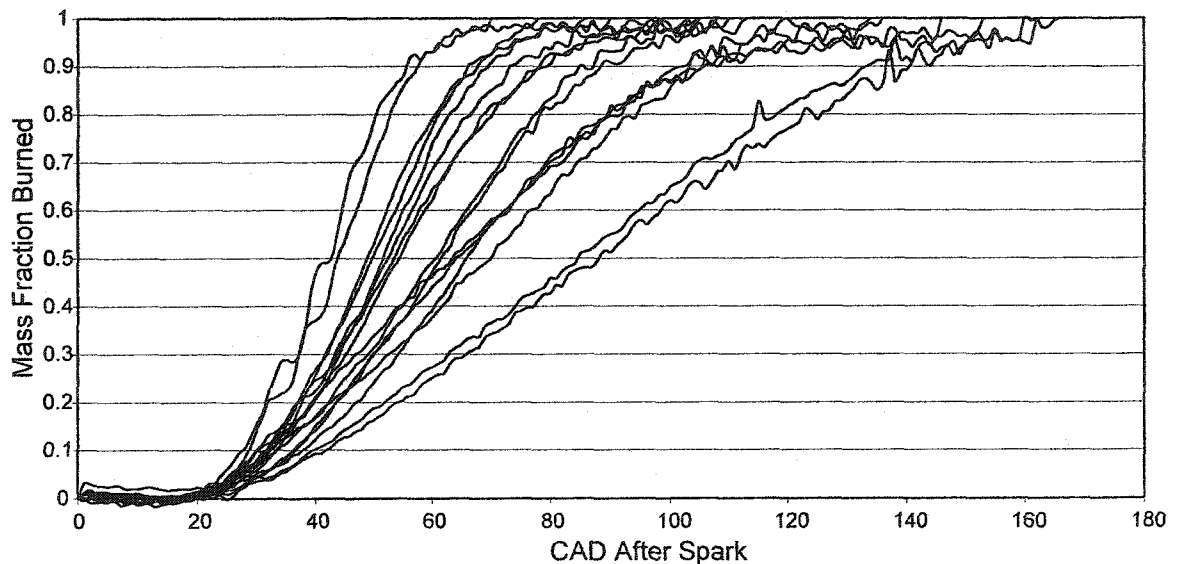


Figure 5.24 Mass fraction burned curves plotted for 16 consecutive cycles (Test 9, without electrolysis products)

The burn durations; 0 to 2%, 2 to 10%, 10 to 90%, and total burn duration were determined by the difference in CAD, corresponding to the required mass fraction burned (eg. 2 %, 10 %, 90 %, end of combustion). The burn duration is reported as the number of CAD required to burn the fraction of charge being considered. An example of this process is illustrated in Figure 5.25 where one of the middle cycles was selected to illustrate the process of determining the 10 to 90% burn duration. Based on the cycle selected below 10% of the mass is burned at approximately 30° after spark, and 90% of the mass is burned at 85° after spark. Therefore the 10 to 90% burn duration is equal to 55 CAD ($85^\circ - 30^\circ = 55^\circ$). This process was repeated for each burn duration; 0-2%, 2-

10%, 10-90% and total burn duration, for 100 cycles and then averaged. The results are presented in the following subsections.

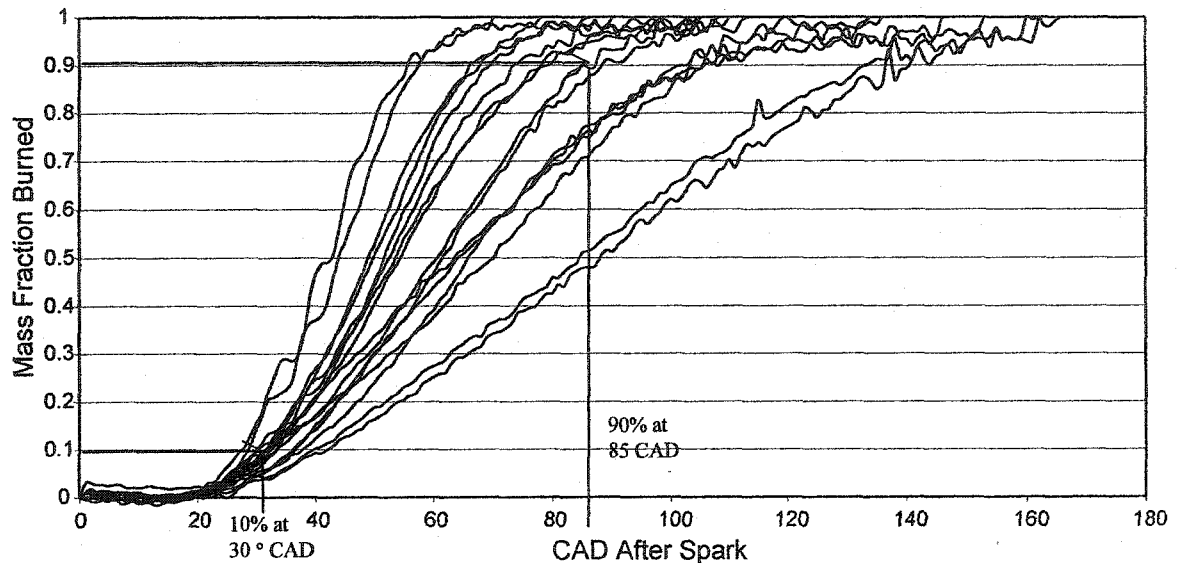


Figure 5.25 Illustration of the calculation of the 10 to 90 % burn duration

5.3.4.1 0 to 2 % Burn Duration

The initial spark and the early development of a flame kernel, is usually represented by the interval 0-2 % mfb, which is also referred to as the ignition delay period. The average number of CAD required for flame initiation for each test is provided in Table 5.6. Based on the results provided in Figure 5.26, engine speed did not influence the 0 to 2 % burn duration. Table 5.7 summarizes the effects of the addition of the electrolysis products by determining under which condition each test had a minimum and maximum average burn duration.

Table 5.6 0 – 2 % Burn duration results

Test	Condition	Speed		Fuel flow rate	H ₂ flow rate			Equivalence ratio	CAD (°)
		rev/min	u_{rpm}	L/s	L/s	% by mass	% by volume	(ϕ)	
1	1	2620	78	0.083				0.78	26
	2			0.084	0.0056	0.12	6.7	0.79	25
	3			0.082				0.79	24
2	1	2310	62	0.080				0.82	16
	2			0.078	0.0055	0.12	7.0	0.82	14
	3			0.078				0.82	14
3	1	2000	25	0.073				0.81	Error in measurement
	2			0.072	0.0055	0.14	7.7	0.82	
	3			0.069				0.80	
4	1	2930	32	0.087				0.80	23
	2			0.086	0.0060	0.12	7.0	0.81	23
	3			0.086				0.82	21
5	1	3310	62	0.091				0.88	16
	2			0.092	0.006	0.11	6.0	0.90	19
	3			0.091				0.89	19
6	1	3310	70	0.085				0.74	21
	2			0.085	0.0056	0.12	6.6	0.75	20
	3			0.086				0.76	18
7	1	3190	62	0.084				0.80	19
	2			0.083	0.0051	0.11	6.2	0.78	20
	3			0.084				0.79	20
8	1	3050	62	0.086				0.73	25
	2			0.085	0.0053	0.11	6.2	0.73	24
	3			0.087				0.74	23
9	1	3300	32	0.085				0.69	18
	2			0.084	0.0053	0.11	6.3	0.70	21
	3			0.083				0.69	20
10	1	2600	55	0.090				0.82	23
	2			0.083	0.0058	0.12	7.0	0.77	21
	3			0.078				0.72	23
11	1	2300	55	0.083				0.72	Error in measurement
	2			0.081	0.0058	0.13	7.2	0.71	
	3			0.080				0.72	


Notes: 1) Condition 1 represents the initial condition, engine run without electrolysis.

Condition 2 represents the addition of electrolysis products.

Condition 3 represents engine run without electrolysis products.

2) Oxygen added in a volume ratio of 1:2 (oxygen/hydrogen).

3) u_{rpm} represents the maximum uncertainty based on calculation in Appendix G.

4)  shading represents the maximum value for the test.

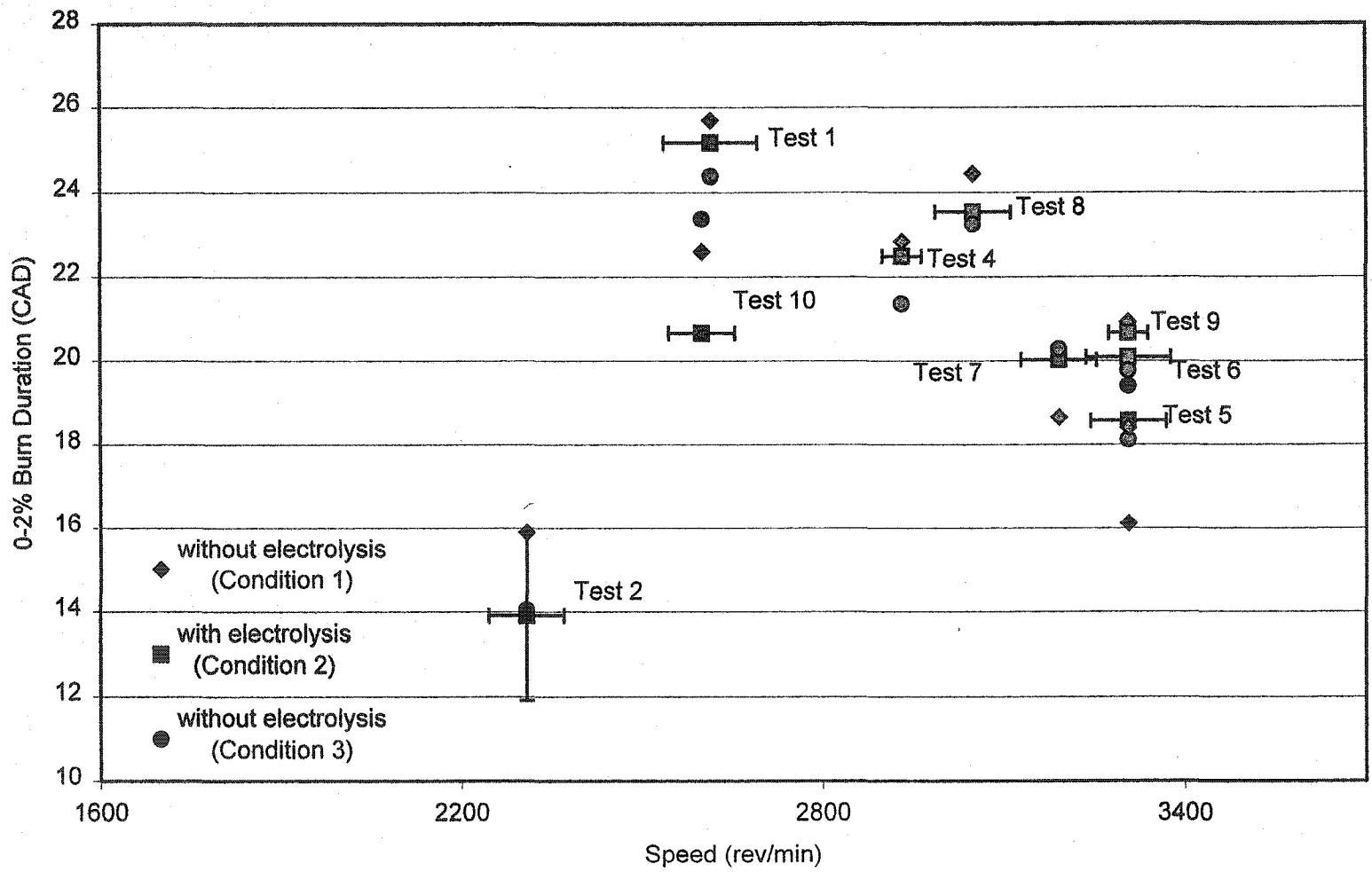


Figure 5.26 0 – 2% burn duration versus speed

Table 5.7 Summary of Test conditions resulting in minimum and maximum burn durations for that test

Test Condition	Tests in which the maximum burn duration occurred under this test condition	Tests in which the minimum burn duration occurred under this test condition
1. Without Electrolysis Products	1, 2, 4, 6, 8	5, 7, 9
2. With Electrolysis Products	9	2, 10
3. Without Electrolysis Products	5, 7, 10	1, 4, 6, 8

The burn duration decreased over the length of the test presumably due to the continuous warming of the engine beyond the initial warming up period. Tests 3 and 11 were not used as mentioned above because large errors were reported in the pressure measurement. From Table 5.7 it can be noted that addition of the electrolysis products did not consistently increase or decrease the 0 to 2% burn duration.

5.3.4.2 2 to 10 % Burn Duration

The average number of CAD required for the 2 to 10% burn duration for each test is provided in Table 5.8. The graphical representation of the results provided in Figure 5.27 indicates that the 2 to 10% burn duration increases with an increase in engine speed, with the exception of Test 2. An increase in engine speed produces higher flame speeds due to higher turbulence, swirl and swish, therefore the rate of combustion is increased in real time. However, with an increase in engine speed the number of CAD per unit time interval also increases [Pulkrabek, 1997]. The result indicate that the 2 to 10% burn duration was affected more by the increase in the number of CAD over time than any increase in combustion rate due to the higher engine speeds. Table 5.9 summarizes the conditions for each test that resulted in minimum and maximum average burn durations.

Table 5.8 2 – 10% Burn duration results

Test	Condition	Speed		Fuel flow rate	H ₂ flow rate			Equivalence ratio	CAD (°)
		rev/min	u_{rpm}	L/s	L/s	% by mass	% by volume	(ϕ)	
1	1	2620	78	0.083				0.78	5.2
	2			0.084	0.0056	0.12	6.7	0.79	7.6
	3			0.082				0.79	7.3
2	1	2310	62	0.080				0.82	16.7
	2			0.078	0.0055	0.12	7.0	0.82	17.9
	3			0.078				0.82	17.1
3	1	2000	25	0.073				0.81	Error in measurement
	2			0.072	0.0055	0.14	7.7	0.82	
	3			0.069				0.80	
4	1	2930	32	0.087				0.80	11.4
	2			0.086	0.0060	0.12	7.0	0.81	10.9
	3			0.086				0.82	10.4
5	1	3310	62	0.091				0.88	17.6
	2			0.092	0.006	0.11	6.0	0.90	13.6
	3			0.091				0.89	11.9
6	1	3310	70	0.085				0.74	15.2
	2			0.085	0.0056	0.12	6.6	0.75	16.9
	3			0.086				0.76	18.6
7	1	3190	62	0.084				0.80	16.2
	2			0.083	0.0051	0.11	6.2	0.78	15.1
	3			0.084				0.79	14.2
8	1	3050	62	0.086				0.73	11.5
	2			0.085	0.0053	0.11	6.2	0.73	11.4
	3			0.087				0.74	10.7
9	1	3300	32	0.085				0.69	18.7
	2			0.084	0.0053	0.11	6.3	0.70	16.5
	3			0.083				0.69	14.3
10	1	2600	55	0.090				0.82	6.9
	2			0.083	0.0058	0.12	7.0	0.77	8
	3			0.078				0.72	6.5
11	1	2300	55	0.083				0.72	Error in measurement
	2			0.081	0.0058	0.13	7.2	0.71	
	3			0.080				0.72	


Notes: 1) Condition 1 represents the initial condition, engine run without electrolysis.

Condition 2 represents the addition of electrolysis products.

Condition 3 represents engine run without electrolysis products.

2) Oxygen added in a volume ratio of 1:2 (oxygen/hydrogen).

3) u_{rpm} represents the maximum uncertainty based on calculation in Appendix G.

4)  shading represents the maximum value for the test.

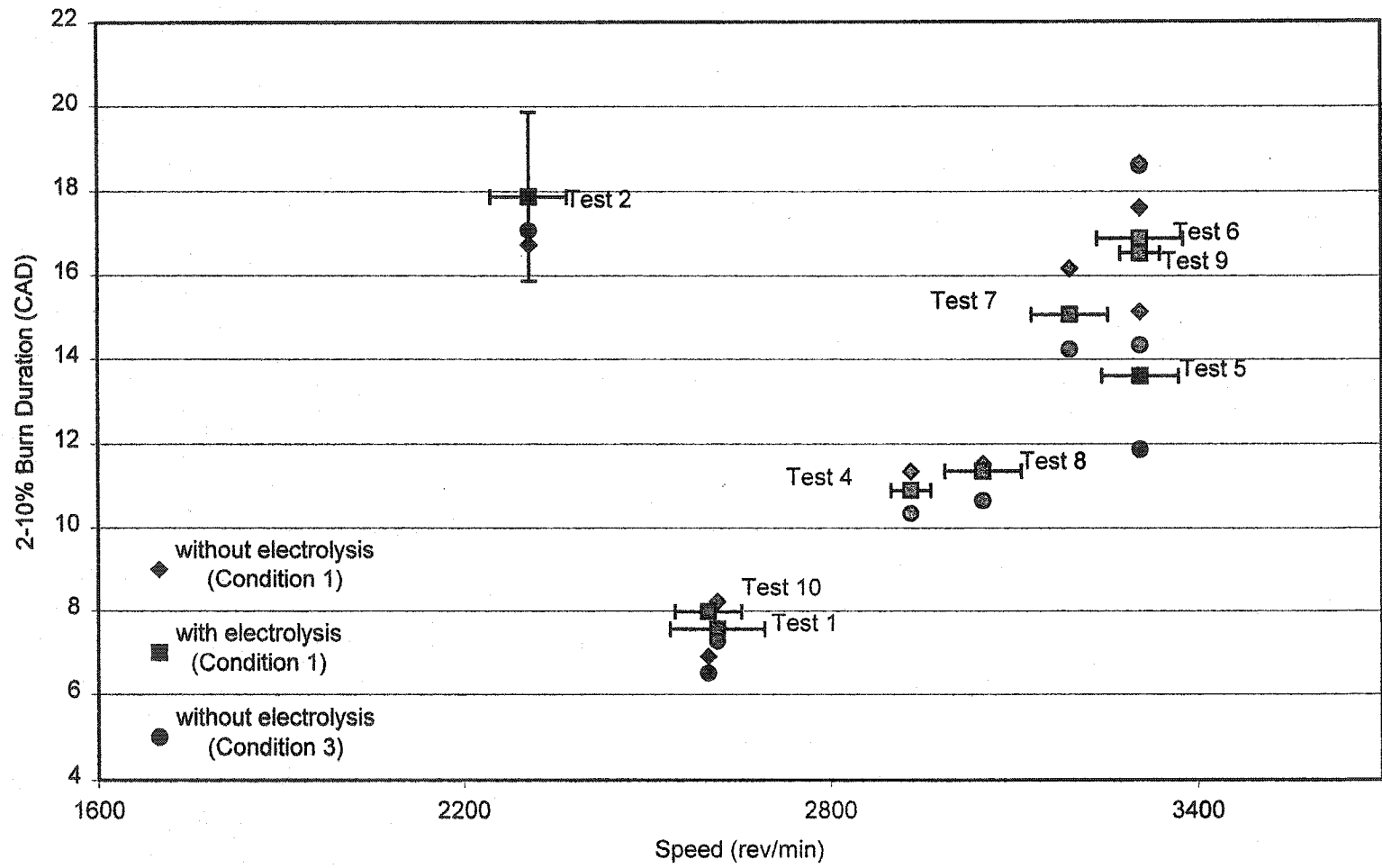


Figure 5.27 2-10% burn duration versus speed

Table 5.9 Summary of Test conditions resulting in minimum and maximum burn durations for that test

Test Conditions	Tests in which the maximum burn duration occurred under this test condition	Tests in which the minimum burn duration occurred under this test condition
1. Without Electrolysis Products	1, 4, 5, 7, 8, 9	2, 6
2. With Electrolysis Products	2, 10	
3. Without Electrolysis Products	6	1, 4, 5, 7, 8, 9, 10


The test condition where the electrolysis products had been removed generally had the lowest burn duration for the 2-10% burn duration phase with the highest burn durations occurring for the original test condition (before electrolysis). The addition of the electrolysis products generally produced burn durations within those of the other two test conditions. The average difference between Condition 1 and Condition 3 was approximately 2.5 CAD. The differences between Conditions 1 and 2 and Conditions 2 and 3 were generally similar indicating that the burn duration was changing over time due to the engine warming up beyond the initial warming up period. Also, the calculated uncertainty in the encoder is 1.6 CAD. Only in Test 4 was the decrease greater between Conditions 1 and 2 than between Conditions 2 and 3 with a decrease greater than the uncertainty of 1.6 CAD.

5.3.4.3 10 to 90% Burn Duration

The bulk of combustion takes place under this category in the interval 10% to 90% mfb. The 10% to 90% mfb is commonly referred to as the combustion duration or rapid burn stage. Table 5.10 documents the average number of CAD required for the rapid burn stage for each test. The graphical representation of the results provided in Figure 5.28 indicates that the 10 to 90% duration increases with an increase in engine speed. As explained earlier, even though the combustion rate is expected to increase with an increase in engine speed so does the number of CAD during combustion. Table 5.11 summarizes the conditions for each test that resulted in a minimum and maximum average burn duration.

Table 5.10 10–90% Burn duration results

Test	Condition	Speed		Fuel flow rate	H ₂ flow rate			Equivalence ratio	CAD (°)
		rev/min	u_{rpm}	L/s	L/s	% by mass	% by volume	(ϕ)	
1	1	2620	78	0.083				0.78	37
	2			0.084	0.0056	0.12	6.7	0.79	34
	3			0.082				0.79	34
2	1	2310	62	0.080				0.82	26
	2			0.078	0.0055	0.12	7.0	0.82	25
	3			0.078				0.82	24
3	1	2000	25	0.073				0.81	Error in measurement
	2			0.072	0.0055	0.14	7.7	0.82	
	3			0.069				0.80	
4	1	2930	32	0.087				0.80	55
	2			0.086	0.0060	0.12	7.0	0.81	48
	3			0.086				0.82	46
5	1	3310	62	0.091				0.88	57
	2			0.092	0.006	0.11	6.0	0.90	52
	3			0.091				0.89	48
6	1	3310	70	0.085				0.74	67
	2			0.085	0.0056	0.12	6.6	0.75	73
	3			0.086				0.76	72
7	1	3190	62	0.084				0.80	60
	2			0.083	0.0051	0.11	6.2	0.78	60
	3			0.084				0.79	61
8	1	3050	62	0.086				0.73	63
	2			0.085	0.0053	0.11	6.2	0.73	60
	3			0.087				0.74	56
9	1	3300	32	0.085				0.69	69
	2			0.084	0.0053	0.11	6.3	0.70	66
	3			0.083				0.69	56
10	1	2600	55	0.090				0.82	33
	2			0.083	0.0058	0.12	7.0	0.77	31
	3			0.078				0.72	32
11	1	2300	55	0.083				0.72	Error in measurement
	2			0.081	0.0058	0.13	7.2	0.71	
	3			0.080				0.72	

- Notes: 1) Condition 1 represents the initial condition, engine run without electrolysis.
 Condition 2 represents the addition of electrolysis products.
 Condition 3 represents engine run without electrolysis products.
 2) Oxygen added in a volume ratio of 1:2 (oxygen/hydrogen).
 3) u_{rpm} represents the maximum uncertainty based on calculation in Appendix G.
 4)  shading represents the maximum value for the test.

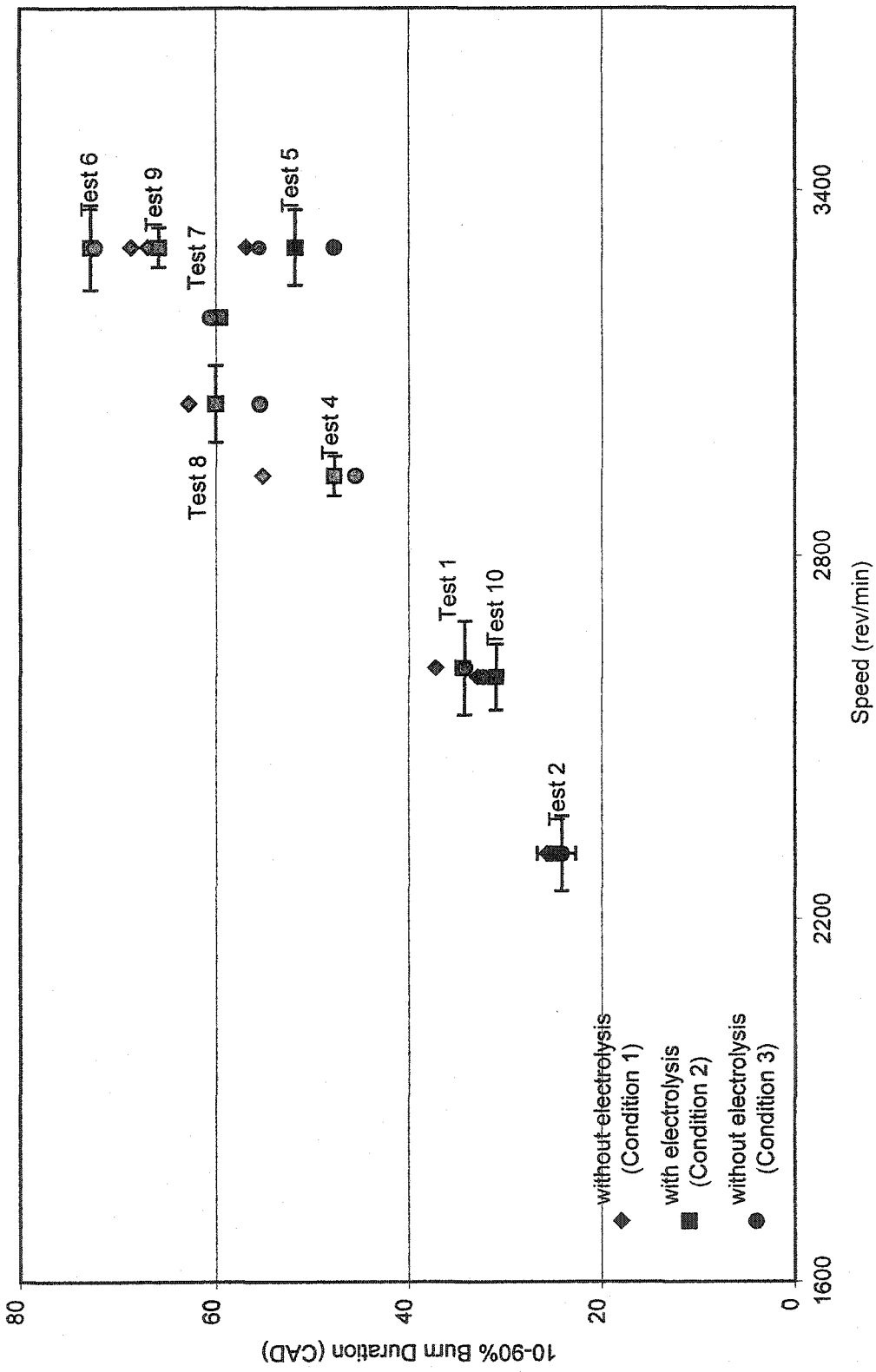


Figure 5.28 10 – 90% burn duration versus speed

Table 5.11 Summary of Test conditions resulting in minimum and maximum burn durations for that test

Test Condition	Tests in which the maximum burn duration occurred under this test condition	Tests in which the minimum burn duration occurred under this test condition
1. Without Electrolysis Products	1, 2, 4, 5, 8, 9, 10	6
2. With Electrolysis Products	6	7, 10
3. Without Electrolysis Products	7	1, 2, 4, 5, 8, 9

Similar to the results in the 2-10% burn duration, the original test condition, operating without electrolysis products, had the longest burn duration. The minimum burn durations generally occurred in Condition 3. Only Tests 6 and 7, do not comply with these generalized statements. The average difference between Conditions 1 and 3 was approximately 4 CAD, which was also the average difference between Conditions 2 and 3, indicating that the change in burn duration was affected by the engine run time with no indication that the electrolysis products had a significant effect.

5.3.4.4 Location of Peak Burn Rate

The peak burn rate was calculated for each cycle by determining the slope of the mfb curve at each CAD. The slope was determined using a running average of the 5 CAD before and the 5 CAD after the CAD desired. A burn rate curve was developed, with slope versus CAD after spark. The peak on this curve represents the peak burn rate, which corresponds to the inflection point on the burn duration curve.

Table 5.12 documents the CAD where the peak burn rate occurred for each test. The graphical representation of the results provided in Figure 5.29 indicates that the peak burn rate increases with an increase in engine speed. As explained in Section 5.3.4.2, the combustion rate is expected to increase with an increase in engine speed, however, so does the number of CAD during combustion per unit time. Table 5.13 summarizes the conditions for each test that resulted in a minimum and maximum CAD at peak burn rate.

Table 5.12 Location of Peak Burn Rate

Test	Condition	Speed		Fuel flow rate	H ₂ flow rate			Equivalence ratio	CAD (°)
		rev/min	u_{rpm}	L/s	L/s	% by mass	% by volume	(ϕ)	
1	1	2620	78	0.083				0.78	53
	2			0.084	0.0056	0.12	6.7	0.79	52
	3			0.082				0.79	50
2	1	2310	62	0.080				0.82	47
	2			0.078	0.0055	0.12	7.0	0.82	46
	3			0.078				0.82	45
3	1	2000	25	0.073				0.81	Error in measurement
	2			0.072	0.0055	0.14	7.7	0.82	
	3			0.069				0.80	
4	1	2930	32	0.087				0.80	59
	2			0.086	0.0060	0.12	7.0	0.81	57
	3			0.086				0.82	57
5	1	3310	62	0.091				0.88	60
	2			0.092	0.006	0.11	6.0	0.90	57
	3			0.091				0.89	56
6	1	3310	70	0.085				0.74	69
	2			0.085	0.0056	0.12	6.6	0.75	73
	3			0.086				0.76	69
7	1	3190	62	0.084				0.80	66
	2			0.083	0.0051	0.11	6.2	0.78	65
	3			0.084				0.79	64
8	1	3050	62	0.086				0.73	64
	2			0.085	0.0053	0.11	6.2	0.73	63
	3			0.087				0.74	60
9	1	3300	32	0.085				0.69	71
	2			0.084	0.0053	0.11	6.3	0.70	71
	3			0.083				0.69	63
10	1	2600	55	0.090				0.82	48
	2			0.083	0.0058	0.12	7.0	0.77	47
	3			0.078				0.72	48
11	1	2300	55	0.083				0.72	Error in measurement
	2			0.081	0.0058	0.13	7.2	0.71	
	3			0.080				0.72	


Notes: 1) Condition 1 represents the initial condition, engine run without electrolysis.

Condition 2 represents the addition of electrolysis products.

Condition 3 represents engine run without electrolysis products.

2) Oxygen added in a volume ratio of 1:2 (oxygen/hydrogen).

3) u_{rpm} represents the maximum uncertainty based on calculation in Appendix G.

4)  shading represents the maximum value for the test.

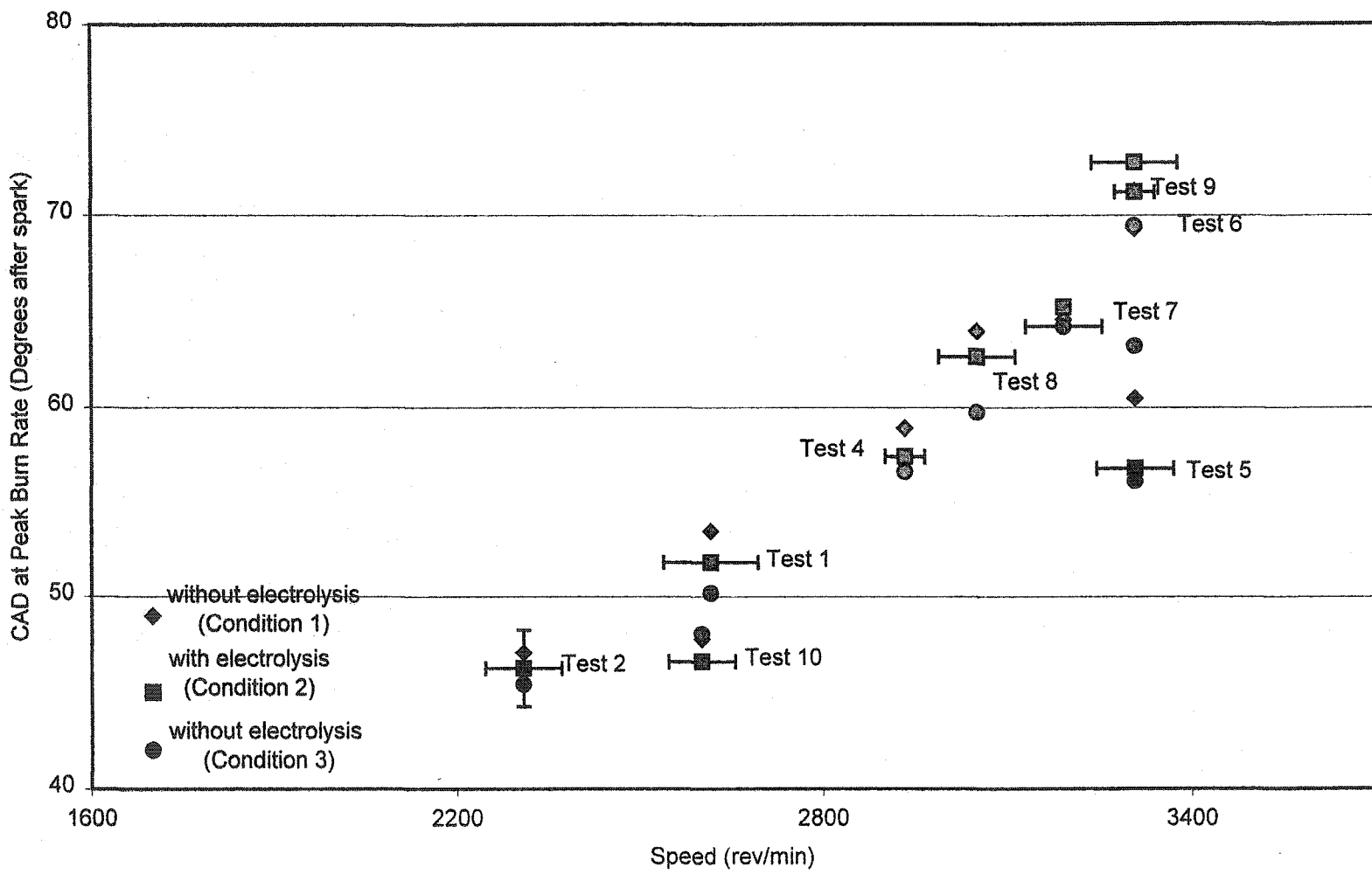


Figure 5.29 Location of Peak Burn Rate versus speed

Table 5.13 Summary of Test conditions resulting in minimum and maximum CAD at peak burn rate

Test Condition	Tests in which the maximum CAD corresponding to the peak burn rate occurred under this test condition	Tests in which the minimum CAD corresponding to the peak burn rate occurred under this test condition
1. Without Electrolysis Products	1, 2, 4, 5, 8, 9	6
2. With Electrolysis Products	6, 7	
3. Without Electrolysis Products	10	1, 2, 4, 5, 7, 8, 9, 10

The summary in Table 5.13 generally shows similar trends as the percent burn duration results with the peak burn rate occurring at a minimum CAD for Condition 3 and at a maximum CAD for Condition 1. The average difference between Conditions 1 and 2 was less than 1 CAD (uncertainty in encoder is 1.6 CAD), while the average difference between Conditions 2 and 3 was 2.7 CAD, indicating that the change in burn duration was affected by the engine run time with no indication that the electrolysis products had a significant effect.

5.3.5 Emissions

Initially exhaust gases were analysed using an IMR [St. Petersburg, Florida] 2800P gas analyser, which measured exhaust and room temperatures, as well as concentrations of CO, NO, and O₂ on a dry basis in ppm. During Test 7 the IMR's NO and CO electrochemical sensors and the T-gas temperature sensor failed. Therefore, starting with Test 8 a new ENERAC model 3000EV [Westbury, New York] gas analyser was used. This provided an opportunity to try the new unit and compare the emission results to those reported from the older IMR unit.

5.3.5.1 Carbon Monoxide


CO emissions were reported by both the IMR 2800P and the ENERAC 3000EV units at 1 minute time intervals. Emissions data was collected for over ten minutes. The data was averaged for each condition, with average CO emissions presented in Table 5.14 and

Figure 5.30. In general, the average CO emissions increased over the duration of the tests, with the exception of Tests 10 and 11. Tests 10 and 11 showed no trend in data. Test 10 reported maximum CO emissions with the addition of the electrolysis products and Test 11 reporting maximum CO emission for the original test condition, before the electrolysis products were added. The differences in CO between Conditions 1 and 2 ($[CO]_1 - [CO]_2$) and Conditions 3 and 2 ($[CO]_3 - [CO]_2$), shown in Figure 5.31, indicate that the decrease in CO with the addition of the electrolysis products was both positive and negative indicating that the addition of the electrolysis products had no consistent effect on CO emissions from the engine. The engine speed had no apparent effect on the CO emissions.

The emission results from Test 5 are noticeably higher than the other tests, although there was no radical difference in the engine operating conditions. The sensors failed during Test 7 and may have contributed to the higher results reported in Test 5, however, it would be expected that similar results would have been reported for Test 6, which is not the case.

Table 5.14 Carbon Monoxide Emissions Results

Test (unit used)	Condition	Speed		Fuel flow rate	H ₂ flow rate			Equivalence ratio	CO (ppm)
		rev/m in	u_{rpm}	L/s	L/s	% by mass	% by volume	(ϕ)	
1 (IMR)	1	2620	78	0.083				0.78	3586
	2			0.084	0.0056	0.12	6.7	0.79	4612
	3			0.082				0.79	5388
2 (IMR)	1	2310	62	0.080				0.82	8166
	2			0.078	0.0055	0.12	7.0	0.82	10572
	3			0.078				0.82	12009
3 (IMR)	1	2000	25	0.073				0.81	10024
	2			0.072	0.0055	0.14	7.7	0.82	12905
	3			0.069				0.80	15560
4 (IMR)	1	2930	32	0.087				0.80	8345
	2			0.086	0.0060	0.12	7.0	0.81	11538
	3			0.086				0.82	11875
5 (IMR)	1	3310	62	0.091				0.88	28923
	2			0.092	0.0060	0.11	6.0	0.90	37363
	3			0.091				0.89	48690
6 (IMR)	1	3310	70	0.085				0.74	1247
	2			0.085	0.0056	0.12	6.6	0.75	1468
	3			0.086				0.76	1675
7 (IMR)	1	3190	62	0.084				0.80	IMR - sensor defect
	2			0.083	0.0051	0.11	6.2	0.78	
	3			0.084				0.79	
8 (ENERAC)	1	3050	62	0.086				0.73	No CO emissions from ENERAC
	2			0.085	0.0053	0.11	6.2	0.73	
	3			0.087				0.74	
9 (ENERAC)	1	3300	32	0.085				0.69	833
	2			0.084	0.0053	0.11	6.3	0.70	1167
	3			0.083				0.69	1436
10 (ENERAC)	1	2600	55	0.090				0.82	2781
	2			0.083	0.0058	0.12	7.0	0.77	3838
	3			0.078				0.72	3791
11 (ENERAC)	1	2300	55	0.083				0.72	5281
	2			0.081	0.0058	0.13	7.2	0.71	4078
	3			0.080				0.72	4192

- Notes: 1) Condition 1 represents the initial condition, engine run without electrolysis.
 Condition 2 represents the addition of electrolysis products.
 Condition 3 represents engine run without electrolysis products.
 2) Oxygen added in a volume ratio of 1:2 (oxygen/hydrogen).
 3) u_{rpm} represents the maximum uncertainty based on calculation in Appendix G.
 4)  shading represents the maximum value for the Test.

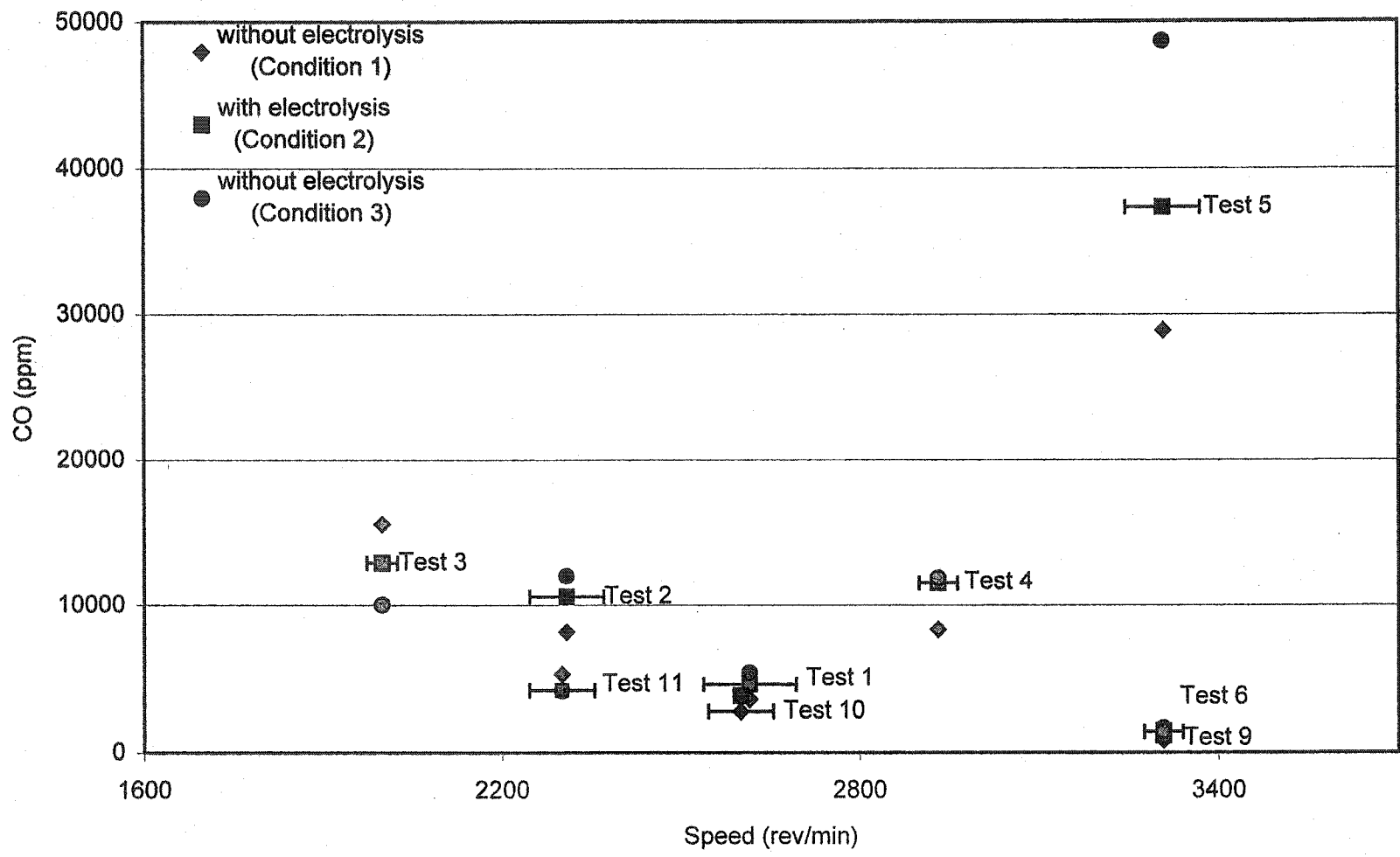


Figure 5.30 Carbon Monoxide Emissions with Engine Speed

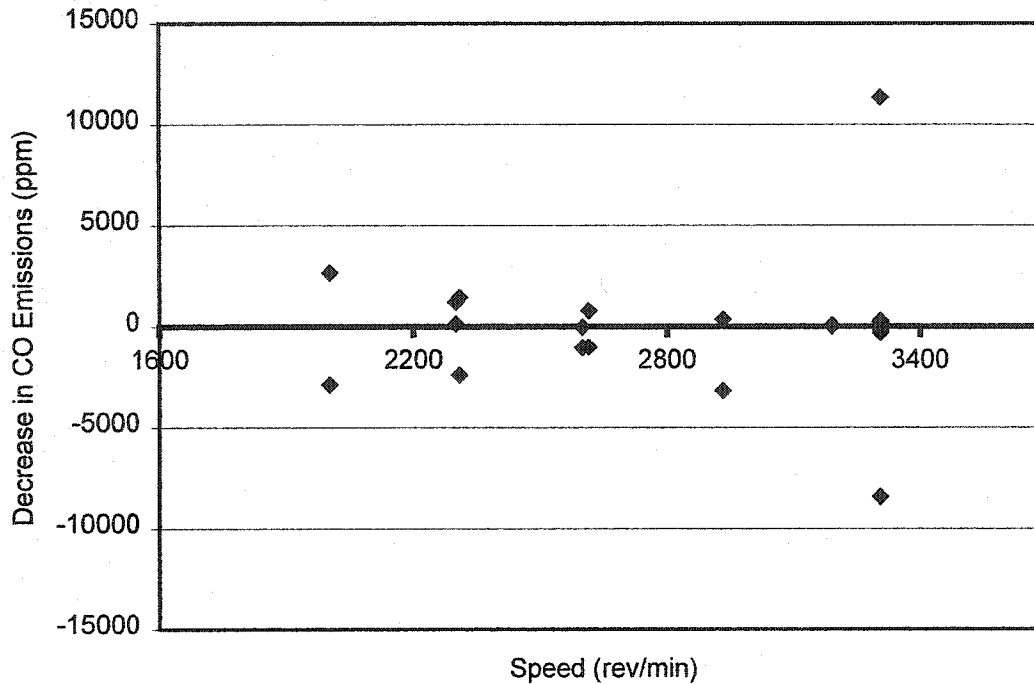


Figure 5.31 Decrease in carbon monoxide emissions from the addition of electrolysis products

Figure 5.32 shows the influence of equivalence ratio on the CO emissions. The CO emissions are a compilation of the data from both the IMR and ENERAC units. The results from the units overlap with no apparent discrepancy between the CO emissions measured by the two units. Both sets of CO emissions show that the CO emissions increase with an increase in equivalence ratio, with the greatest CO emissions occurring in Test 5 ($\phi = 0.89$, 48690 ppm CO) and the lowest CO emissions occurring in Test 9 ($\phi = 0.69$, 833 ppm CO). This trend was also observed in the STANJAN and CHEMKIN simulations.

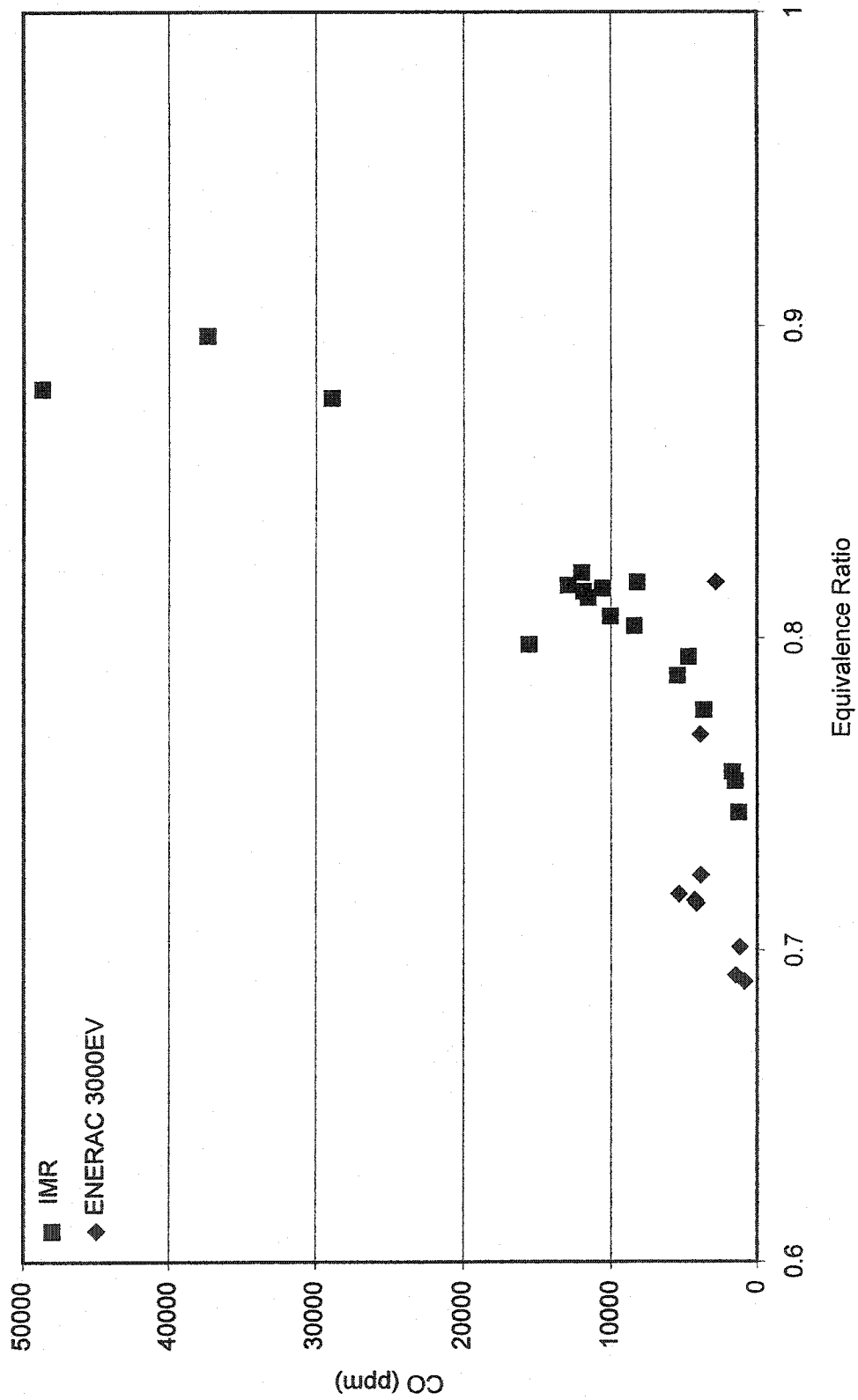


Figure 5.32 Carbon Monoxide Emissions versus Equivalence Ratio


5.3.5.2 Nitrogen Oxide

NO emissions were reported by both the IMR 2800P and the ENERAC 3000EV units at 1 minute time intervals, similar to CO emissions. The data was averaged for each condition, with average NO emissions presented in Table 5.15 and Figure 5.33. In general, the NO emissions increased over the duration of each test, with the exception of Tests 3 and 10, which reported higher NO emissions during the addition of the electrolysis products and Test 7, which reported a minimum reading of NO during the addition of the electrolysis products. The differences in NO between Conditions 1 and 2 ($[\text{NO}]_1 - [\text{NO}]_2$) and Conditions 3 and 2 ($[\text{NO}]_3 - [\text{NO}]_2$), shown in Figure 5.34, indicate that the decrease in NO with the addition of the electrolysis products was both positive and negative indicating that the addition of the electrolysis products had no consistent effect on NO emissions from the engine.

As shown in Figure 5.33, the NO emissions decreased with an increase in engine speed (reduction in load). NO emissions are greatly influenced by the residual gas fraction (burned gas mixture), which in SI engines ranges from 20 percent at light loads to 7 percent at higher loads [Heywood, 1988]. The residual gas fraction acts as a diluent in the unburned mixture, lowering the absolute temperature reached after combustion, which decreases the formation of NO. Therefore, NO emissions are expected to decrease with a reduction in load. Based on the engine-dynamometer set-up the engine speed is controlled by adjusting the load. The load is decreased as the engine speed increases.

Table 5.15 Nitrogen Oxide Emissions Results

Test (unit used)	Condition	Speed		Fuel flow rate	H ₂ flow rate			Equivalence ratio	NO (ppm)
		rev/m in	u_{rpm}	L/s	L/s	% by mass	% by volume	(ϕ)	
1 (IMR)	1	2620	78	0.083				0.78	1732
	2			0.084	0.0056	0.12	6.7	0.79	2050
	3			0.082				0.79	2343
2 (IMR)	1	2310	62	0.080				0.82	2747
	2			0.078	0.0055	0.12	7.0	0.82	3238
	3			0.078				0.82	3427
3 (IMR)	1	2000	25	0.073				0.81	3498
	2			0.072	0.0055	0.14	7.7	0.82	3742
	3			0.069				0.80	3650
4 (IMR)	1	2930	32	0.087				0.80	995
	2			0.086	0.0060	0.12	7.0	0.81	1028
	3			0.086				0.82	1030
5 (IMR)	1	3310	62	0.091				0.88	498
	2			0.092	0.006	0.11	6.0	0.90	501
	3			0.091				0.89	544
6 (IMR)	1	3310	70	0.085				0.74	454
	2			0.085	0.0056	0.12	6.6	0.75	498
	3			0.086				0.76	533
7 (IMR)	1	3190	62	0.084				0.80	189
	2			0.083	0.0051	0.11	6.2	0.78	180
	3			0.084				0.79	251
8 (ENERAC)	1	3050	62	0.086				0.73	583
	2			0.085	0.0053	0.11	6.2	0.73	642
	3			0.087				0.74	673
9 (ENERAC)	1	3300	32	0.085				0.69	165
	2			0.084	0.0053	0.11	6.3	0.70	248
	3			0.083				0.69	306
10 (ENERAC)	1	2600	55	0.090				0.82	1575
	2			0.083	0.0058	0.12	7.0	0.77	1608
	3			0.078				0.72	1599
11 (ENERAC)	1	2300	55	0.083				0.72	1458
	2			0.081	0.0058	0.13	7.2	0.71	1820
	3			0.080				0.72	1852

- Notes: 1) Condition 1 represents the initial condition, engine run without electrolysis.
 Condition 2 represents the addition of electrolysis products.
 Condition 3 represents engine run without electrolysis products.
 2) Oxygen added in a volume ratio of 1:2 (oxygen/hydrogen).
 3) u_{rpm} represents the maximum uncertainty based on calculation in Appendix G.
 4)  shading represents the maximum value for the Test.

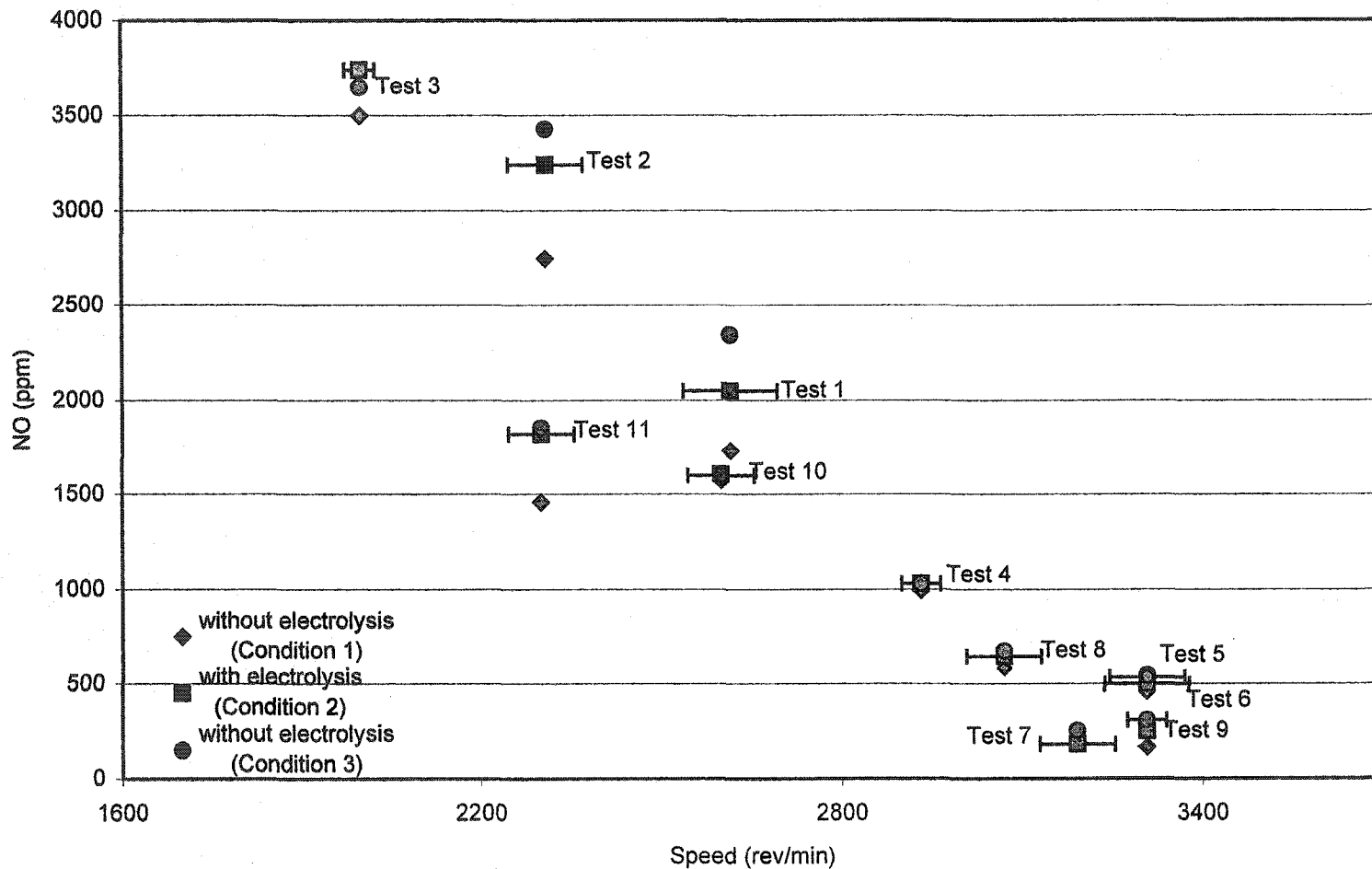


Figure 5.33 Nitrogen oxide emissions with engine speed

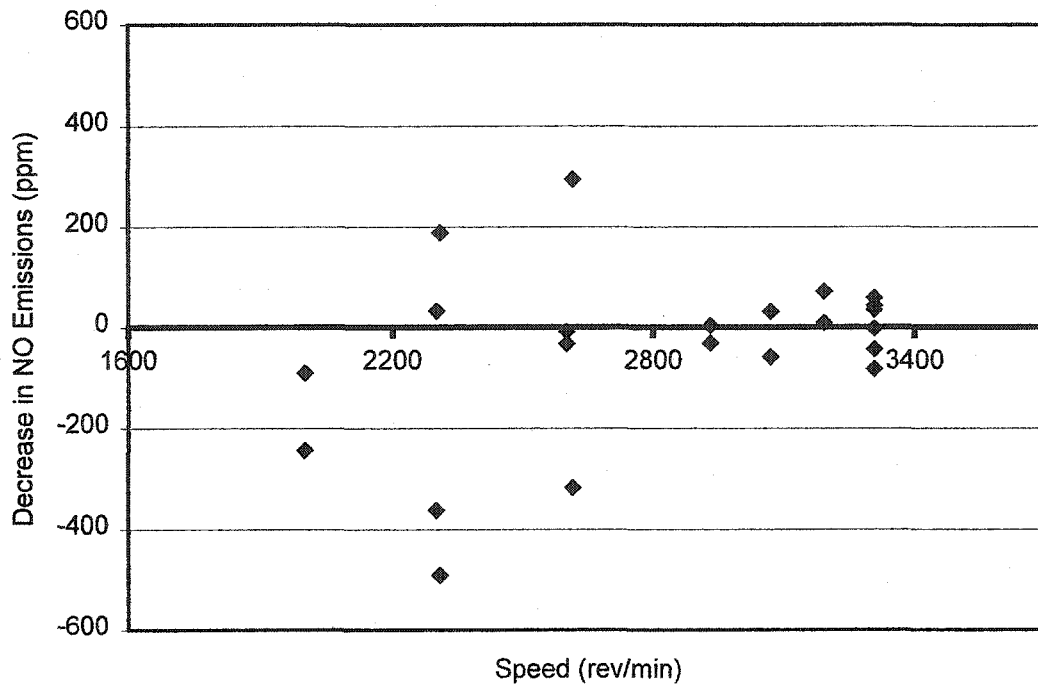


Figure 5.34 Decrease in nitrogen oxide emissions from the addition of electrolysis products

The effect of equivalence ratio on the NO emissions is not conclusive based on Figure 5.35. The NO emissions are a compilation of the data from both the IMR and ENERAC units, with the IMR generally reporting the higher NO values for equivalence ratios around 0.82. Test 5, which had equivalence ratios greater than 0.82, should show an increase in NO emissions, however, the results reported significantly lower NO emissions. The peak in NO concentrations is typically just on the lean side of stoichiometric ($\phi = 0.9$) [Stone, 1999]. Test 9, which had the lowest calculated equivalence ratios also had the lowest NO emissions results. Test 7, which had a higher equivalence ratio than Test 9, also reported NO emissions around the same level, however, the results from Test 7 are questionable as sensor errors were reported during this test.

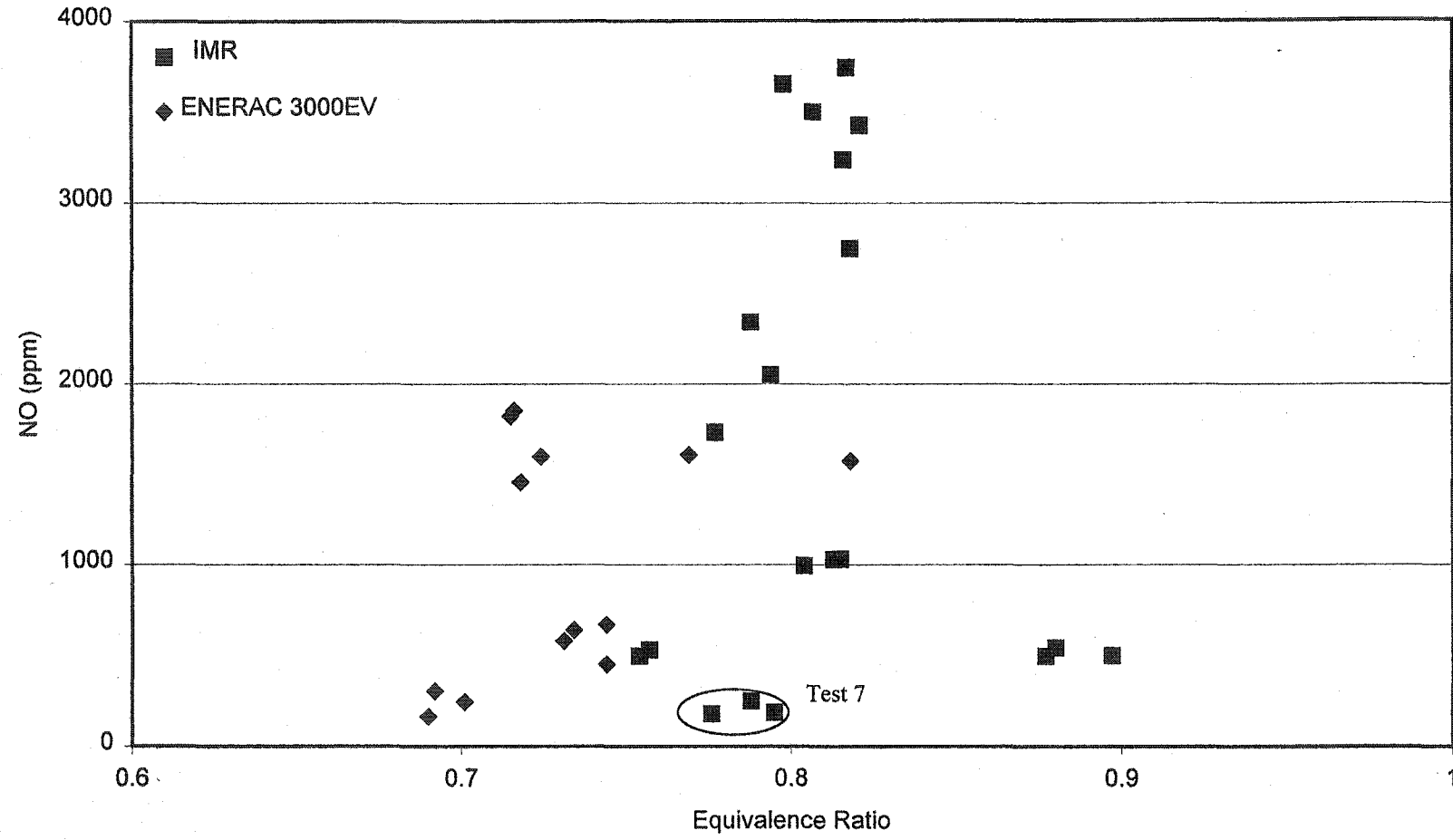


Figure 5.35 Nitrogen oxide emissions versus equivalence ratios. Test 7 results are expected to be erroneous due to a malfunction of the NO sensor in the IMR unit

5.3.5.3 Hydrocarbons

The unburned hydrocarbon (HC) emissions were measured with the ENERAC 3000EV unit for Tests 8 through 11. The HC emissions are reported as propane according to the US EPA's Method 25B. The accuracy of the ENERAC unit for hydrocarbon emissions is $\pm 5\%$ of the reading, shown in Appendix G. The HC emissions were reported by the unit at 1 minute time intervals. Emissions data was collected for over ten minutes. The data was averaged for each cycle, with average HC emissions presented in Table 5.16 and Figure 5.36.

Table 5.16 Hydrocarbon Emissions Results

Test (unit used)	Condition	Speed		Fuel flow rate	H ₂ flow rate			Equivalence ratio	HC (as propane) (ppm)
		rev/m in	u_{rpm}	L/s	L/s	% by mass	% by volume	(ϕ)	
8 (ENERAC)	1	3050	62	0.086				0.73	30
	2			0.085	0.0053	0.11	6.2	0.73	32
	3			0.087				0.74	34
9 (ENERAC)	1	3300	32	0.085				0.69	11
	2			0.084	0.0053	0.11	6.3	0.70	11
	3			0.083				0.69	14
10 (ENERAC)	1	2600	55	0.090				0.82	52
	2			0.083	0.0058	0.12	7.0	0.77	50
	3			0.078				0.72	50
11 (ENERAC)	1	2300	55	0.083				0.72	135
	2			0.081	0.0058	0.13	7.2	0.71	122
	3			0.080				0.72	120


Notes: 1) Condition 1 represents the initial condition, engine run without electrolysis.

Condition 2 represents the addition of electrolysis products.

Condition 3 represents engine run without electrolysis products.

2) Oxygen added in a volume ratio of 1:2 (oxygen/hydrogen).

3) u_{rpm} represents the maximum uncertainty based on calculation in Appendix G.

4)  shading represents the maximum value for the Test.

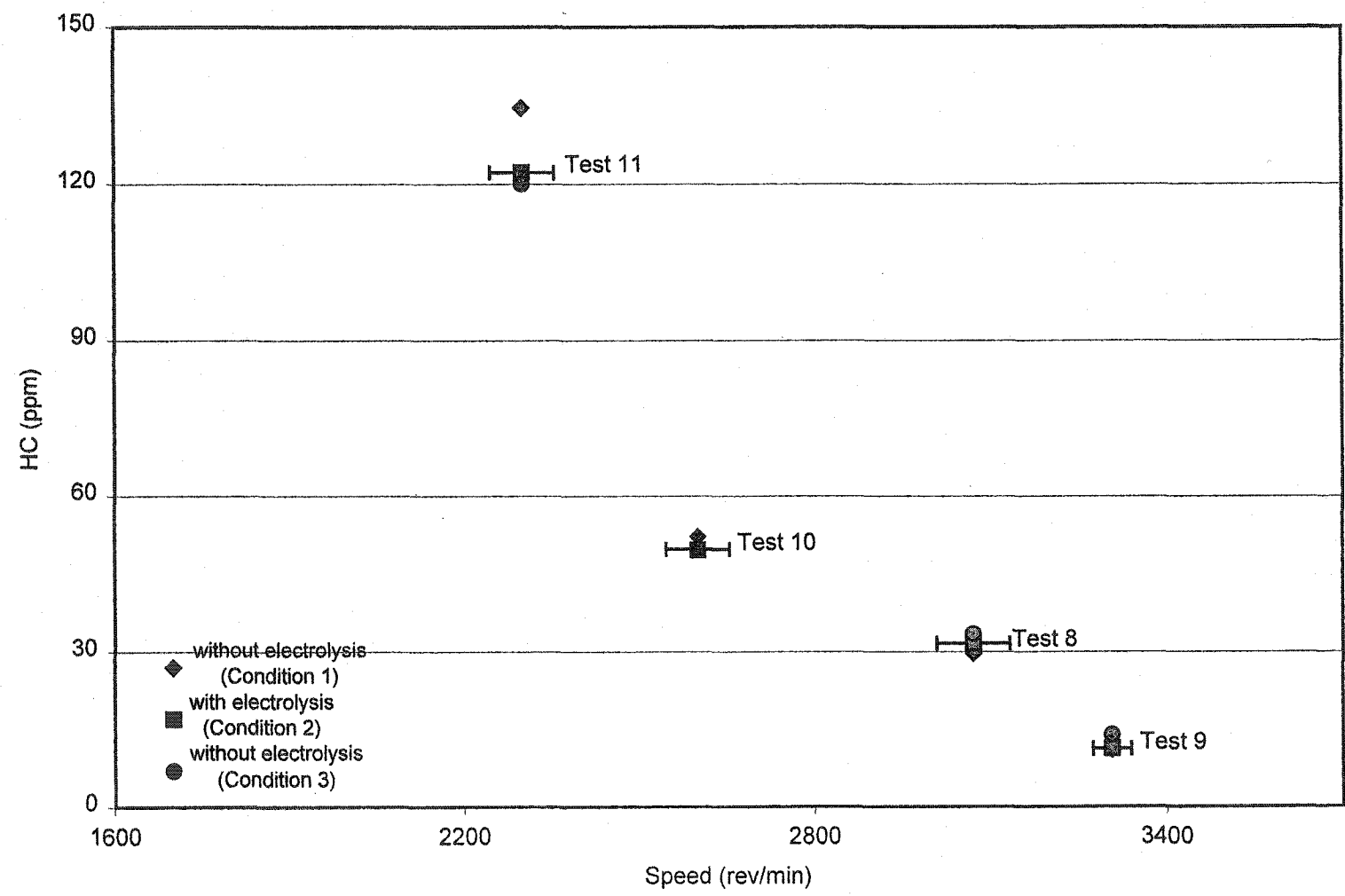


Figure 5.36 Hydrocarbon emissions versus speed

Figure 5.36 showed an effect of engine speed on HC emissions with a reduction in HC emissions with an increase in engine speed. Speed and load likely affect several of the complex mechanisms that lead to the formation of unburned hydrocarbons, but it is unclear exactly how. It is known however, that with oxygen present, an increase in engine speed will increase the oxidation of unburned hydrocarbons both in the cylinder and in the exhaust system [Heywood, 1988].

Tests 8 and 9 showed an increase in HC emissions over the duration of the test, while Tests 10 and 11 had the greatest HC emissions for the original test condition. No evident effect was produced by the introduction of the electrolysis products as shown in Figure 5.37 by the differences in HC emissions between Conditions 1 and 2 ($[HC]_1 - [HC]_2$) and Conditions 3 and 2 ($[HC]_3 - [HC]_2$).

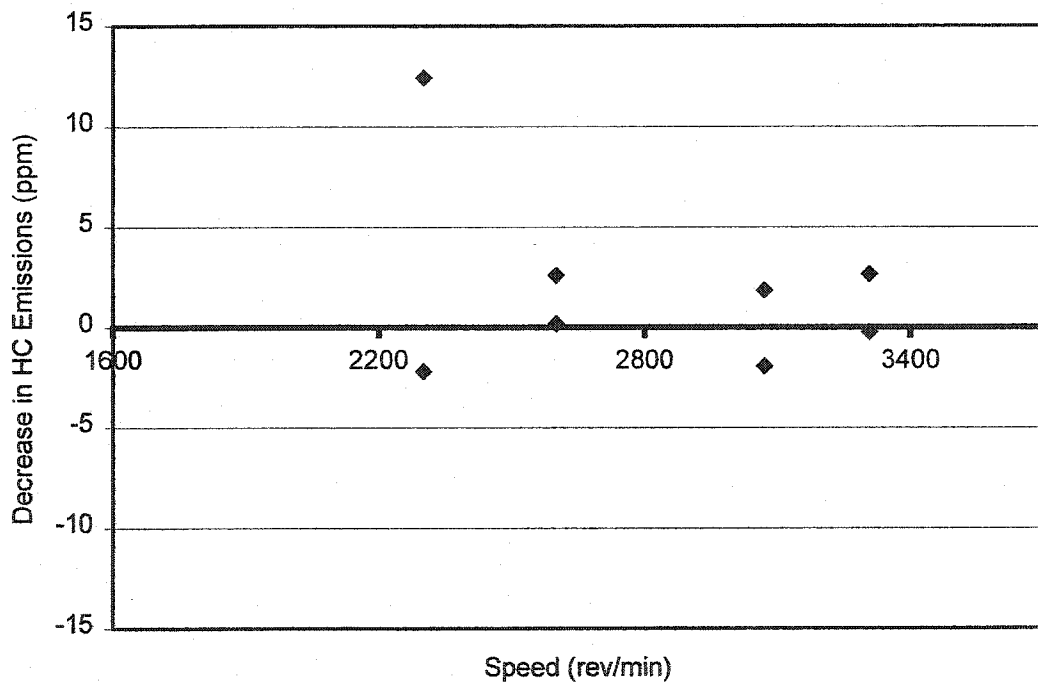


Figure 5.37 Decrease in hydrocarbon emissions due to the addition of electrolysis products

In general, HC emissions increase with an increase in equivalence ratio except at the lean burn limit [Schafer and van Basshuysen, 1995]. This trend is seen in Figure 5.38 with the exception of the high HC emissions reported near $\phi=0.72$ (Test 11).

5.4 ELECTROLYSIS UNIT POWER REQUIREMENTS

The electrolysis unit provided by Global Tech [Aurora, Ontario] was used in the engine testing. The electrolysis unit was found to produce on average 496 mL/min electrolysis products (Appendix E) in a 2:1 hydrogen/oxygen ratio (331 mL/min H₂ and 165 mL/min O₂). Based on manufacturer's specifications the unit requires 169 W (169 J/s) to operate. For this calculation it is assumed that power for the electrolysis unit can be generated by an equivalent amount of engine power (ie. the alternator is 100% efficient). An increase in brake power was observed during Tests 6 and 7 only. A comparison of power requirements for these two tests are summarized in Table 5.17.

Table 5.17 Comparison of Power Requirements and Power Gain

Test	Engine Brake Power Gain (J/s)	Electrolysis Power Requirement (J/s)	Difference in Power (J/s)
6	112	169	-57
7	53	169	-116

The electrolysis power requirement of 169 J/s is greater than the power gain reported for Tests 6 and 7. These two tests were the only tests to show a power increase with the addition of the electrolysis products. Even if the results produced in these two tests were seen for all tests and the assumption of alternator efficiency is valid, the use of the electrolysis unit (at the current rate of production of electrolysis products and power requirement) would lead to an overall decrease in power that would be supplied from the engine to operate a car. No emissions improvement was found for the addition of the electrolysis products in Test 6. The emissions results for Test 7 are questionable due to the sensors failing during the test.

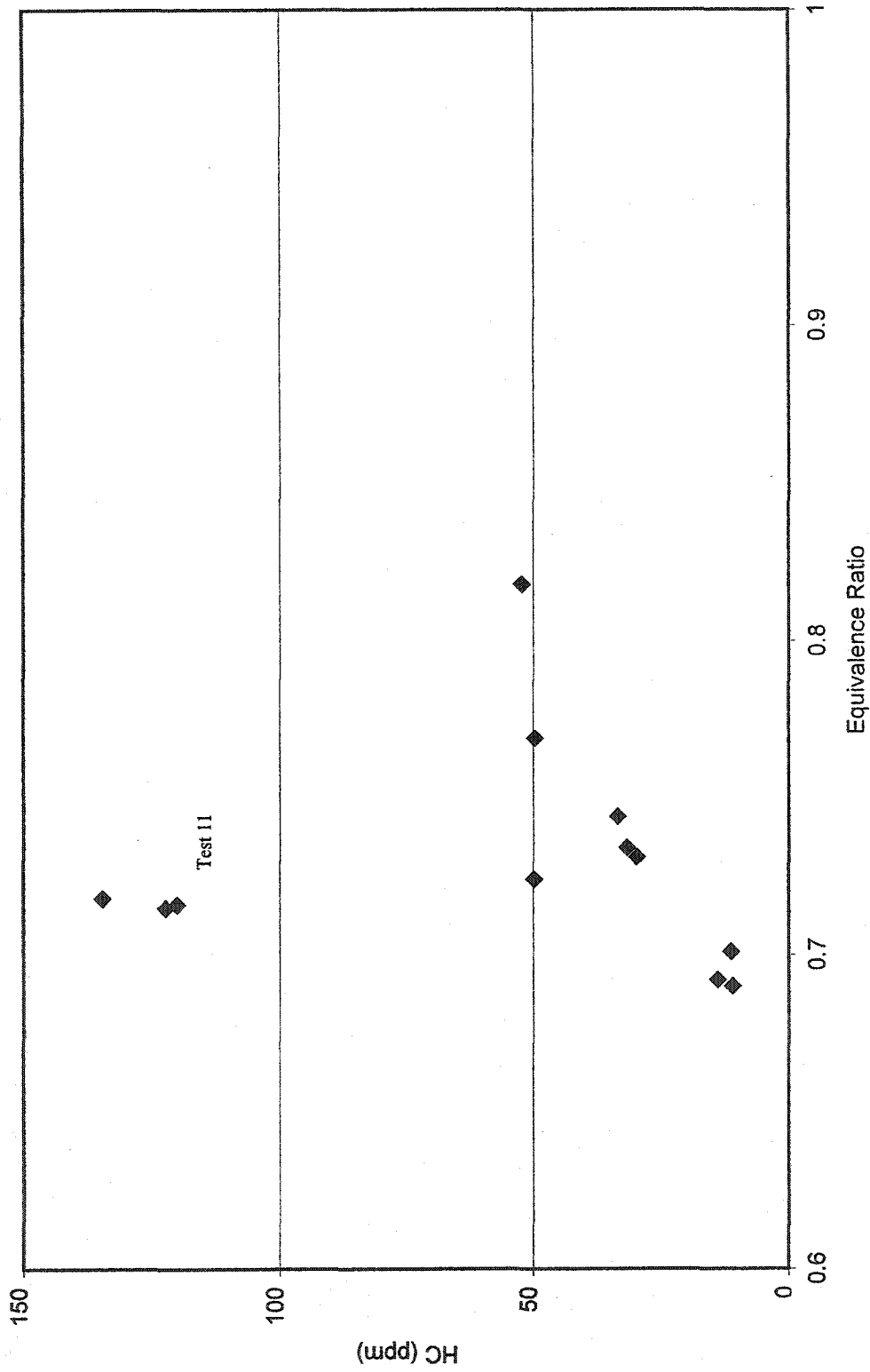


Figure 5.38 Hydrocarbon emissions versus equivalence ratio.

5.5 SUMMARY

Based on the results provided above from the simulations and engine testing sections, it is apparent that even though the electrolysis unit is producing hydrogen and oxygen at an approximate 2:1 ratio, the production rate of the unit is too low to observe any effect. The test matrix for the simulation was developed to predict the effects of the addition of electrolysis products ($H_2=0.15\%$). These results were compared to the results for the engine testing, where the electrolysis products on average provided H_2 at 0.12% by mass of fuel. As recommended by the electrolysis unit supplier the shortest possible length of hose was used between the electrolysis unit and the engine intake.

5.5.1 Work

Work was predicted through simulations completed by STANJAN and ESP. The percent difference in the predicted work was calculated from the addition of the electrolysis products ($H_2=0.15\%$) and without the addition. These differences are reported in Table 5.18 with the percent differences of the imep results averaged for all engine tests.

Table 5.18 Comparison of Work Results for the Addition of Electrolysis Products

STANJAN	ESP	Engine Testing		
$(H_2=0.15\%$ by mass)		$(H_2\approx 0.12\%$ by mass)		
Comparison for electrolysis products	Comparison for electrolysis products	Average, Condition 2 – Condition 1	Average, Condition 3 – Condition 2	Comparison to the average values for conditions without electrolysis
Expressed as Percent Difference				
+0.2 %	+ 0.1 – 0.2 %	+ 0.7 %	- 4.0 %	-1.7 %

Note: + indicates an increase and - indicates a decrease.

The engine testing shows an overall decrease of 1.73% in work due to the addition of electrolysis products, while the simulations predict an increase of approximately 0.2%. The simulation results are calculated based on ideal operating conditions; conditions

during testing are almost never ideal. The maximum imep during engine testing was 297 kPa. A 0.2% increase (as predicted by STANJAN and ESP) would translate to an increase of 0.60 kPa (297×0.002). This anticipated increase is significantly less than the uncertainty of the imep measurement (± 38 kPa). Therefore, a noticeable increase during engine testing would only occur if the electrolysis products mixture contained something other than hydrogen and oxygen.

5.5.2 Emissions

The emission results from the simulations involving STANJAN and CHEMKIN are compared to the results from the engine testing in the following subsections. The unburned hydrocarbon results are not compared here as the mole fractions calculated by STANJAN and CHEMKIN are very small ($< 10^{-30}$).

5.5.2.1 Carbon Monoxide

The percent differences are calculated using the mole fractions determined in STANJAN and CHEMKIN and compared to the percent differences calculated from the reported emissions results (ppm) from the engine testing. For the simulations the results are provided for equivalence ratios equal to 0.7, 0.8 and 0.9 as this is the range of equivalence ratios calculated during the engine testing. Based on the results provided in Table 5.19, the simulations predict a small increase in CO emissions with the addition of the electrolysis products. STANJAN reported an average increase of 1.7% and CHEMKIN reported an increase of 13% over the range of equivalence ratios between 0.7 and 0.9. Measured CO emissions showed an overall increase of 2.3% with the addition of electrolysis products when compared to the two conditions without electrolysis addition during the engine testing. However, it is important to note that during the engine testing the CO emissions generally increased throughout the length of the test.

Table 5.19 Comparison of simulation results and engine testing results for the addition of electrolysis products (CO emissions)

Equivalence Ratio	STANJAN	CHEMKIN	Engine Testing		
	(H ₂ =0.15% by mass)		(H ₂ ≈0.12% by mass)		
	Comparison for electrolysis products	Comparison for electrolysis products	Average, Condition 2 – Condition 1	Average, Condition 3 – Condition 2	Comparison to the average values for conditions without electrolysis
ϕ	Expressed as Percent Difference				
0.7	+2.6 %	-11.3%	+21.0%	-12.4%	+2.3%
0.8	+1.5 %	+42.8%			
0.9	+0.9%	+8.1%			

Note: + indicates an increase and - indicates a decrease.

5.5.2.2 Nitrogen Oxide

Nitrogen Oxide results are compared by the same method as the carbon monoxide results. These results are provided in Table 5.20. The simulations predicted an increase in NO emissions with the addition of the electrolysis products. STANJAN reported an average increase of 0.4% and CHEMKIN reported an increase of 21% over range of equivalence ratios between 0.7 and 0.9. NO emissions showed an overall increase of 2.7% with the addition of electrolysis products when compared to the two conditions without electrolysis addition during the engine testing. As with the CO emissions, the NO emissions generally increased over the duration of the engine testing.

Table 5.20 Comparison of simulation results and engine testing results for the addition of electrolysis products (NO emissions)

Equivalence Ratio	STANJAN	CHEMKIN	Engine Testing		
	(H ₂ =0.15% by mass)		(H ₂ ≈0.12% by mass)		
	Comparison for electrolysis products	Comparison for electrolysis products	Average, Condition 2 – Condition 1	Average, Condition 3 – Condition 2	Comparison to the average values for conditions without electrolysis
ϕ	Expressed as Percent Difference				
0.7	+1.2 %	-9.2%	+13.1%	-5.8%	+2.7%
0.8	+0.1 %	+49%			
0.9	+0.0%	+23%			

Note: + indicates an increase and - indicates a decrease.

6 CONCLUSIONS AND RECOMMENDATIONS

6.1 CONCLUSIONS

The Global Tech electrolysis unit produces hydrogen and oxygen in a 2:1 ratio at a rate of approximately 500 L/min. This mixture was confirmed, and no other by-products were detected during the chemical analysis.

Eleven engine tests results showed that the addition of the electrolysis products at an average flow rate of 500 mL/min did not have a noticeable effect on the engine performance. An increase in torque was noted for the addition of the electrolysis products in only three tests. The remaining tests showed a decrease in torque.

Similar to the torque results, the imep was affected by the speed of the engine with no consistent effect due to the introduction of the electrolysis products. Simulations predict an increase of approximately 0.2% due to the addition of electrolysis products, which would represent an increase of 0.6 kPa (for the maximum imep result, 298 kPa). This anticipated increase is significantly less than the uncertainty of the imep measurement of ± 38 kPa.

The engine speed and equivalence ratio affected the COV_{imep} during testing with no evidence that the addition of the electrolysis products had any effect on COV_{imep} . The results presented for the burn durations 2–10% and 10–90% showed that the burn duration increases with an increase in engine speed. Generally, Condition 3 had the fastest burn (shortest burn duration) and Condition 1 had the longest burn duration. The equivalence ratio did not have a measurable effect on the burn duration.

In general, the average CO emissions increased over the length of each test, with no noticeable increase related to the introduction of the electrolysis products. As expected, the CO emissions increased with an increase in equivalence ratio, while the engine's speed had no noticeable effect on CO emissions. Also as expected, STANJAN and

CHEMKIN simulations predict that with an increase in equivalence ratio the CO emissions will increase. The simulations also predict a small increase in CO emissions with the addition of the electrolysis products ($H_2=0.15\%$).

Similar to CO emissions, the NO emissions generally increased over the length of each test, without an effect from the electrolysis addition. It was also noted that the NO emissions decreased with a reduction in load. The load was applied to control the engine speed, the greater the engine speed the less load applied to the engine. The load was not adjusted between Conditions. The effects of the equivalence ratio on NO emissions were not evident based on these test results, however, STANJAN predicts peak NO concentrations to occur at an equivalence ratio of 0.8, while CHEMKIN predicts the peak NO concentrations to occur around stoichiometric conditions. STANJAN and CHEMKIN both predict a small increase in NO emissions with the addition of the electrolysis products.

The hydrocarbon emissions are more affected by engine speed than the equivalence ratio with no noticeable effect due to the addition of the electrolysis products.

The engine testing results showed an increase in power in only two out of nine tests in which imep was measured. Even in these two tests, the increase in power was less than that required to run the electrolysis unit. Therefore, the use of the electrolysis unit on an SI engine would not lead to increased fuel economy or decreased emissions as claimed based on the current engine and operating conditions tested.

6.2 RECOMMENDATIONS

For future extension of this work, the following recommendations are provided:

- ❖ The principles behind the use of electrolysis products with iso-octane in spark ignition engines is promising as is seen in the simulation results for the addition of electrolysis products, where $H_2 = 5\%$ by mass. Therefore, a more efficient

electrolysis unit which can produce a higher rate of hydrogen and oxygen with lower power requirements should be developed.

- ❖ The Briggs & Stratton Vanguard 20 HP Engine is a two cylinder engine. The effects of the second cylinder were seen in the cylinder used to record the pressure data, especially at lower engine speeds. These effects lead to large errors in the imep and COV in Tests 3 and 11. Investment into a one cylinder research engine would be beneficial in future spark ignition engine testing. Alternatively monitor both cylinders.
- ❖ Results such as burn duration showed a change over the length of the test (approximately one hour) with no apparent effects due to the addition of electrolysis products. An increase in engine temperature may have influenced the results. With a new liquid cooled engine, the tests could be completed over a longer period without overheating and the electrolysis products could be introduced a second time for further comparisons.
- ❖ The accuracy of the airflow in the current experiment had the largest impact on the uncertainty in the equivalence ratio calculation. A more accurate means to measure the air flow should be investigated.
- ❖ Several attempts were made to run CHEMKIN simulations with the more detailed Curran [Curran, 2002] mechanism. However, due to computer limitations, CHEMKIN was unable to perform the analysis. A study comparing the detailed Curran's mechanism to the mechanism used in this study could determine if the simplified mechanism is sufficient to model the effects of iso-octane combustion.
- ❖ The electrolysis unit provided by Global Tech is marketed to diesel truck operators. Diesel engines run leaner than spark ignition engines, therefore, it is recommended that the electrolysis products be tested on a diesel engine.

7 REFERENCES

Al-Baghdadi, Maher Abdul-Resul Sadiq and Al-Janabi, Haroun Abdul-Kadim Shahad "Improvement of performance and reduction of pollutant emission of a four stroke spark ignition engine fueled with hydrogen-gasoline fuel mixture", *Energy Conversion & Management*, 41, pp 77-91, 2000.

Alltech Associates Inc, "Chrom 1441" [Online] <http://www.alltechweb.com/chromaccess/chromview.asp?refno=1441&details=yes>, 2003

Apostolescu, N. and Chiriac R.. "A Study of Combustion of Hydrogen-Enriched Gasoline in a Spark Ignition Engine" *SAE Paper* 960603, 1996.

Bade Shrestha, S.O. and Karim, G.A. "Hydrogen as an Additive to Methane for Spark Ignition Engine Applications," *International Journal of Hydrogen Energy*, 24, pp 577-586, 1999.

Bain, A., Barclay, J.A., Bose, T.K., Edeskuty, F.J., Fairlie, M.J., Hansel, J.G., Hay, D.R., Swain, M.R. *Sourcebook for Hydrogen Applications*, Hydrogen Research Institute and National Renewable Energy Laboratory, 1998.

Briggs & Stratton, *Vanguard Repair Manual*, Milwaukee, Wisconsin, 1998.

Borman, G.L. and Ragland, K.W. *Combustion Engineering*, McGraw-Hill , Boston, 1998.

Cooper, C.D., and Alley, F.C. *Air Pollution Control A Design Approach*, 2nd Edition, Waveland Press, Inc., Illinois, 1994.

Crosse, J., "Hydrogen: which way will the world go?" *Ricardo Quarterly Review*, Summer 2003.

Curran, H.J., Gaffuri, P., Pitz, W.J., and Westbrook, C.K., "A Comprehensive Modeling Study of iso-Octane Oxidation", *Combustion and Flame*, 129, pp 253-280, 2002.

Curran, H.J. "Iso-octane Mechanism" [Online at] <http://www-cms.llnl.gov/combustion/combustion2.html>, 2002.

D'Andrea, T. "The Addition of Hydrogen and Oxygen to a Gasoline-Fuelled SI Engine to Enhance Combustion and Reduce Emissions", M.A.Sc. Thesis, University of Windsor, 2003.

Das, L.M. "Safety Aspects of a Hydrogen-Fuelled Engine System Development", *International Journal of Hydrogen Energy*, 16 (9), pp 619-624, 1991.

Dügler, Z. and Özçelik, K.R. "Fuel economy improvement by on board electrolytic hydrogen production", *International Journal of Hydrogen Energy*, 25, pp 895-897, 2000.

ENERAC 3000E Instruction Manual Rev. 4, Westbury, NY, 2000.

Engelhardt, V., *The Electrolysis of Water, Processes and Applications*, The Chemical Publishing Company, Easton, PA., 1904.

Environment Canada – The Green Lane [Online]. <http://www.ec.gc.ca/emission/1-1e.html> [2001]

Environment Canada – The Green Lane [Online] <http://www.ec.gc.ca/emission/2-6e.html> [1998].

Figliola, R.S., and Beasley, D.E. *Theory and Design for Mechanical Measurements*, 3rd Edition, John Wiley & Sons, Inc, New York, 2000.

Fox, R. and McDonald, A.T., *Introduction to Fluid Mechanics*, 5th edition, John Wiley & Sons, New York, NY, 1973.

Fulton, J., Lynch, F., and Marmaro, R., “Hydrogen for Reducing Emissions from Alternative Fuel Vehicles”, *SAE Paper 931813*, 1993.

Gardiner, W.C. *Combustion Chemistry* Springer-Verlag, NY, 1984.

Global Tech Environmental Products, [Online] <http://www.globaltech.ca/> [<November 2003].

Go-Power, *D-100 Series Portable Dynamometer Installations, Operating and Service Manual*, Go-Power Systems, Carrollton, Texas, 1992.

Hacohen, Y. and Sher, E. “Fuel Consumption and Emission of SI Engine Fueled with H₂-Enriched Gasoline”, *SAE Paper 899403*, 1989.

Heywood, J.B. *Internal Combustion Engine Fundamentals*, McGraw-Hill, Inc., New York, 1988.

Houseman, J. and Hoehn, F.W., “A Two-Charge Engine Concept: Hydrogen Enrichment” *SAE Paper 741169*, 1974.

IMR. *IMR 2800P Gas Analyzer Operating Manual*, IMR Environmental Equipment International Inc., St. Petersburg, Florida.

Kee, R.J., Rupley, F.M., Miller, J.A., Coltrin, M.E., Grcar, J.F., Meeks, E., Moffat, H.K., Lutz, A.E., Dixon-Lewis, G., Smooke, M.D., Warnatz, J., Evans, G.H., Larson, R.S., Mitchel, R.E., Petzold, L.R., Reynolds, W.C., Caracotsios, M., Stewart, E., Glarborg, P., Wang, C., Adigun, O., *CHEMKIN Collection, Release 3.6*, Reaction Design San Diego, CA (2001).

Klopfenstein, R.Jr. "Air Velocity and flow measurements using a Pitot tube" *ISA Transactions*, 37(4), pp 257-263, 1998.

Lumley, J.L., *Engines An Introduction*, Cambridge University Press, New York, 1999.

Milton, B.E. and Keck, J.C. "Laminar Burning Velocities in Stoichiometric Hydrogen and Hydrogen-Hydrocarbon Gas Mixtures", *Combustion and Flame*, 58, pp 13-22, 1984.

Omega Engineering, *User's Guide HHF10 Hygro-thermo Anemometer*, Omega Engineering, Stamford, CT, 1996.

OSHA, *CFR Title 29, Code of Federal Regulations, Parts 1900 to 1910*, Occupational Health and Safety Administration, US Government Printing Office, Washington, 1993.

PCB. *In-Line Charge Amplifier Series 422E Operating Manual*, PCB Piezotronics Inc., Depew, NY, 1999.

Peters, N., Abschlußbericht zum DFG Forschungsvorhaben Pe 241/9-2, [Online] at <http://www.itm.rwth-aachen.de>, RWTH-Aachen, Institut für Technische Mechanik, D-52056 Aachen, Germany, 2002.

Pulkrabek, W.W. *Engineering Fundamentals of the Internal Combustion Engine*, Prentice-Hall, Inc., New Jersey, 1997.

Rauckis, M.J. and McLean, W.J. "The Effect of Hydrogen Addition on Ignition Delays and Flame Propagation in Spark Ignition Engines," *Combustion Science and Technology*, Vol. 19, pp. 207-216, 1979.

Reaction Design Inc., "Chemkin version 3.7.1" [Online] at <http://www.reactiondesign.com>, 2002.

Reynolds, W.C. *The Element Potential Method for Chemical Equilibrium Analysis: Implementation in the Interactive Program STANJAN, Version 3*, Department of Mechanical Engineering, Stanford University, January 1986.

Reynolds, W.C. "ESP Software" [Online] at <http://esp.stanford.edu>, 2001.

Reynolds, W.C. (2002) personal communication, Stanford University, California.

Schäfer, F., and van Basshuysen, R., *Reduced Emissions and Fuel Consumption in Automobile Engines*, Springer-Verlag/Wien, New York, 1995.

Sher, E. and Hacoen, Y. "Ignition Delay and Combustion Duration in H₂-Enriched Gasoline SI Engines", *Combustion Science and Technology*, 65, pp 263-275, 1989.

Smith, G.P., Golden, D.M., Frenklach, M., Moriarty, N.W., Eiteneer, B., Goldenberg, M., Bowman, C.T., Hanson, R.K., Song, S., Gardiner, W.C., Lissianski, V. V. and Qin, Z., "GRI –Mech 3.0" [Online] at http://www.me.berkeley.edu/gri_mech/, 1999.

Sobiesiak, A., Uykur, C., Ting, D.S.K., and Henshaw, P. "Hydrogen/Oxygen Additives Influence on Premixed Iso-Octane/Air Flame", *SAE Paper 2002-01-1710*, 2000.

Statistics Canada. 2000. *Canadian Vehicle Survey*, Catalogue no. 53-223-XIE. Statistics Canada and Transport Canada, Ottawa.

Stebar, R.F. and Parks, F.B., "Emission Control with Lean Operation Using Hydrogen-Supplemented Fuel", *SAE Paper 740187*, 1974.

Stewart, Sandra. (2003) personal communication, Mandel Scientific Co, Ontario.

Stone, Richard. *Introduction to Internal Combustion Engines*, 3rd Edition", SAE, 1999.

Strehlow, R.A. *Combustion Fundamentals*, McGraw-Hill, NY, 1984.

Tabaczynski, R.J., Ferguson, C.L. and Radhakrishnan, K. "A Turbulent Entrainment Model for Spark Ignition Engine Combustion", *SAE Paper 770647*, 1977.

Turns, Stephen R. *An Introduction to Combustion, Concepts and Applications*, 2nd Edition, McGraw Hill Higher Education, Boston, 2000.

US Environmental Protection Agency, EPA Home [Online] at http://www.epa.gov/wtc/pm10/pm_fact_sheet.html, 2003.

Varde, K.S. "Combustion Characteristics of Small Spark Ignition Engines Using Hydrogen Supplemented Fuel Mixtures", *SAE Paper 810921*, 1981.

Wendt, H. and Plzak, V. "Hydrogen production by water electrolysis", *Kerntechnik*, 56(1), 1991.

Yu, G., Law, C.K., and Wu, C.K. "Laminar Flame Speeds of Hydrocarbon + Air Mixtures with Hydrogen Addition", *Combustion and Flame*, 63, pp. 339-347, 1986.

APPENDIX A

STANJAN Procedures

The procedures detailed below were used to model an idealized fuel-air Otto cycle. In order to model the Otto cycle five steps (A, B, C, D, and E) are required to determine the state conditions (1 – 5) as illustrated in Figure A.1.

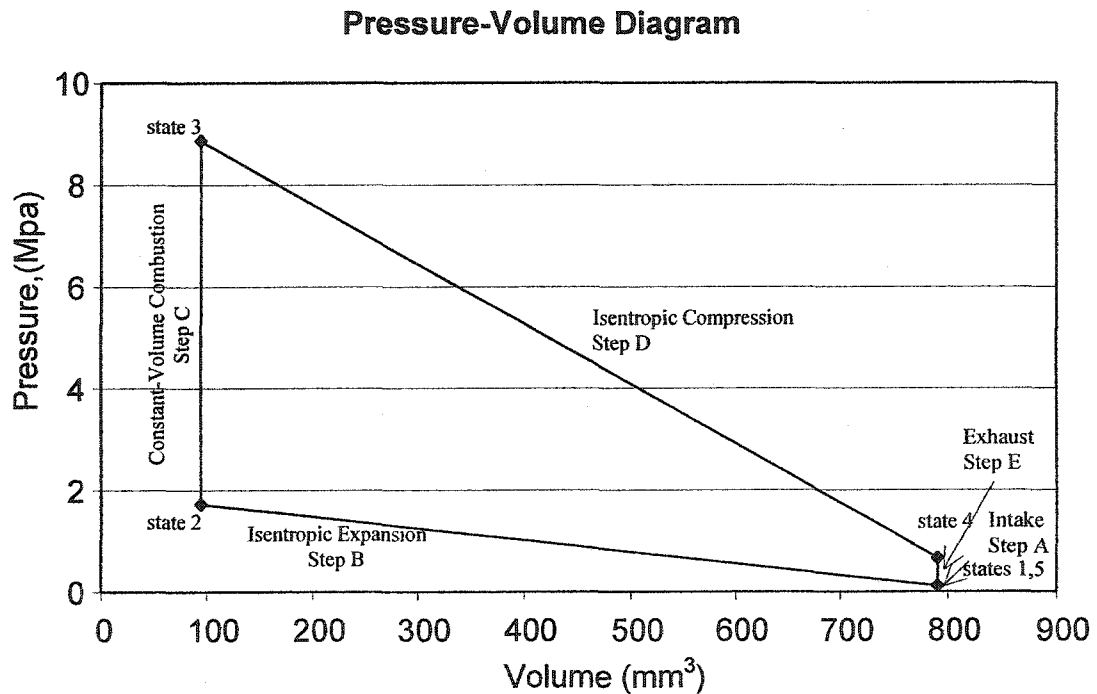
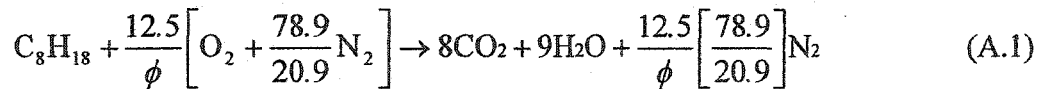


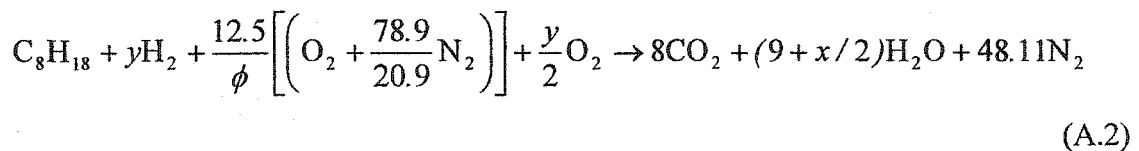
Figure A.1 Idealized Otto cycle used in STANJAN

STEP A

The fuel-air mixture in the cylinder is determined by the stoichiometric equation and entered into the Stanjan program as the reactants. The standard stoichiometric equation for the complete combustion of iso-octane and air is:



In this study the equivalence ratio, ϕ , was varied between 0.7 and 1.2. These procedures were used to model the effects that the addition of hydrogen and oxygen may have on the system. The procedures outlined below are for one percent hydrogen addition by mass of fuel at equivalence ratio equal to 1. Step A requires the input of the reactant mol concentrations. The mol concentrations for this example are determined by



where: $y = \frac{114(\%/100)}{(2.016 \times (1 - \%/100))}$ and % is the desired percent hydrogen addition

Therefore the mol concentrations are

$$C_8H_{18} = 1 \quad O_2 = 12.79 \quad N_2 = 48.11 \quad H_2 = 0.58$$

STANJAN Prompts	User Input	Description and Explanation
Do you want to be instructed?	N	By entering Y a description of the Stanjan calculation method will be given.
Select a species data file or <return> if no file is desired. Species data file?	ICENG.sud	The datafile ICENG.sud includes the thermodynamic properties for iso-octane (C_8H_{18}) and products of incomplete combustion such as, NO, NO_2 , etc. This datafile was downloaded from http://filebox.vt.edu/eng/mech/me4204/stanjan.htm
Is this the file you wanted?	Y	
Do you want to select REACTANTS or PRODUCTS (r/p)?	R	
Type the species in phase 1, separated by commas or blanks; <return>=done	IC8H18 O2 N2 H2	Stanjan can accommodate for mixtures in different phases. For our purpose we assume that the reactants are in the gaseous phase only.
Type the species in phase 2, separated by commas or blanks; <return>=done	<return>	If additional reactants were present in the liquid or solid phase they could be entered here.

Do you want to CHECK the ATOMS in the molecules?	Y	By choosing Yes, the mol concentrations can be added by the user.
Enter the mols of each SPECIES in phase 1 after its name: IC ₈ H ₁₈ :	1	
O ₂ :	12.79	
N ₂ :	48.11	
H ₂ :	0.58	
Do you want to CHANGE the SETUP?	N	If reactants were entered incorrectly, Stanjan allows for corrections to be made. Stanjan also provides a warning if obvious errors were made.
Enter P (atm):	1	Stanjan allows for initial system conditions to be inputted. Assume ambient room temperature and pressure for the beginning of the cycle.
Enter T (K):	300	
Do you want the SOUND SPEED?	N	
Do you want to SAVE the run OUTPUT in a file?	Y	Save file!
Save file name?	Type desired file name	
Is this an existing file?	N	
Do you want to MONITOR the run (probably not)?	N	Monitoring the run is not necessary and takes extra time. If the program reports an error it may be handy to monitor further attempts to run under similar conditions.
Do you want to see the JANNAF data used?	Y <enter> <enter>	The results will appear on the screen providing an opportunity to review inputs and outputs before continuing on to next step. At this time record the volume result, as it will be required in Steps 4 and 5. Press enter a second time to show results. Press enter again to begin Step B. Below are the results as saved for Step A.

JANNAF table data for the reactants

species	molal mass g/mol	enth. form kcal/mol	S0 cal/mol-K	H-H0 kcal/mol
phase 1: Gas species: T = 300.0 K				
IC ₈ H ₁₈	114.22400	-53.570	101.494	.079
O ₂	31.99879	.000	49.047	.013
N ₂	28.01340	.000	45.813	.013
H ₂	2.01600	.000	31.251	.013

Computed properties

atoms	population
C	8.00000000E+00
H	1.93400000E+01
O	2.56600000E+01
N	9.65600000E+01

Reactants at P = 1.000E+00 atmospheres

species	molal mass	mol fraction in the phase	mol fraction in mixture	mass fraction in mixture	mols*
phase 1: molal mass = 29.924 kg/kmol T = 300.00 K					
IC ₈ H ₁₈		.15929E-01	.15929E-01	.60803E-01	1.00000E+00

O2	.20436E+00	.20436E+00	.21854E+00	1.28300E+01
N2	.76903E+00	.76903E+00	.71994E+00	4.82800E+01
H2	.10672E-01	.10672E-01	.71900E-03	6.70000E-01

Calculations made using frozen composition.

* Species mols for the atom populations in mols.

Mixture properties: molal mass = 29.924 kg/kmol
P = 1.0133E+05 Pa V = 8.2265E-01 m**3/kg
U = -.2007E+06 J/kg H = -.1173E+06 J/kg S = .6778E+04 J/kg-K

Made 0 (T,P) iterations; 0 equilibrium iterations; v 3.89 IBM-PC

STEP B

Step B models the isentropic compression of the gaseous reactants. In this study a compression ratio, r_c of 8.5 was used because that is the compression ratio of the Briggs & Stratton engine used.

$$r_c = \frac{V_1}{V_2} = 8.5 \quad (\text{A.3})$$

STANJAN Prompts	User Input	Description and Explanation
Do you want to CHANGE the SETUP?	N	Entering NO here will allow the same reactants and conditions to be saved for the next step.
Want to mix reactants from last run?	Y	
Enter run option:	15	Option 15 "Specified V, S same as last run". This option allows for the isentropic compression over a known compression ratio.
Enter V (m**3/kg):	0.0968	V_2 is calculated by V_1/r_c . V_1 is determined in Step A. $V_2 = 0.82265 / 8.5 = 0.0968$
Enter estimated T(K):	300	Temperature and pressure entered here will be used as an initial estimate. A good estimate is not always necessary. As seen in this example, estimated temperature and pressure are 300K and 1 atm, respectively, for all steps. However, if the program fails to converge, try rerunning with more accurate estimates.
Enter estimated P(atm):	1	
Do you want the SOUND SPEED?	N	
Do you want to SAVE the run OUTPUT in a file?	Y	Save file!
Save file name?	Type desired file name	
Is this an existing file?	N	
Do you want to MONITOR the run (probably not)?	N	
Do you want to see the JANNAF data used?	Y <enter> <enter>	Below are the results as saved for Step B.

JANNAF table data for the reactants

species	molal mass g/mol	enth. form kcal/mol	S0 cal/mol-K	H-H0 kcal/mol
phase 1; Gas species: T = 609.9 K				
IC8H18	114.22400	-53.570	146.326	20.313
O2	31.99879	.000	54.224	2.286
N2	28.01340	.000	50.803	2.196
H2	2.01600	.000	36.197	2.175

Computed properties

atoms	population
C	8.00000000E+00
H	1.93400000E+01
O	2.56600000E+01
N	9.65600000E+01

Reactants at P = 1.728E+01 atmospheres

species	mol fraction in the phase	mol fraction in mixture	mass fraction in mixture	mols*
phase 1: molal mass = 29.924 kg/kmol T = 609.87 K				
IC8H18	.15929E-01	.15929E-01	.60803E-01	1.00000E+00
O2	.20436E+00	.20436E+00	.21854E+00	1.28300E+01
N2	.76903E+00	.76903E+00	.71994E+00	4.82800E+01
H2	.10672E-01	.10672E-01	.71900E-03	6.70000E-01

Calculations made using frozen composition.

* Species mols for the atom populations in mols.

Mixture properties: molal mass = 29.924 kg/kmol
P = 1.7506E+06 Pa V = 9.6800E-02 m**3/kg
U = .6119E+05 J/kg H = .2306E+06 J/kg S = .6778E+04 J/kg-K

Made 19 (T,P) iterations; 0 equilibrium iterations; v 3.89 IBM-PC

STEP C

The combustion reaction is modeled in Step C with an assumption that the reaction is taking place at adiabatic constant volume conditions. By setting volume and enthalpy equal to that at state 2, the adiabatic flame temperature can be computed as well as the products of combustion.

The user predicts the combustion products. In this case the products of complete combustion include: CO₂, H₂O, N₂. However, one of the main objectives of running STANJAN was to determine the equilibrium concentrations of the products of incomplete combustion such as: NO₂, NO, O₂, C₈H₁₈, HO, O, H₂, CO, and H.

STANJAN Prompts	User Input	Description and Explanation
Do you want to CHANGE the SETUP?	Y	
Change option?	2	Option 2 "Select DIFFERENT SPECIES (same data file)" allows you to choose the anticipated products from the iceng.sud file.
Do you want to select REACTANTS or PRODUCTS (r/p)?	P	
Type the species in phase 1, separated by commas or blanks; <return>=done	CO ₂ H ₂ O N ₂ NO ₂ NO O ₂ IC ₈ H ₁₈ HO O H ₂ CO H	As noted in Step A, Stanjan can accommodate for mixtures in different phases. For our purposes we assume that the reactants are in the gaseous phase only. Additional products can be included if applicable.
Type the species in phase 2, separated by commas or blanks; <return>=done	<enter>	If additional reactants were present in the liquid or solid phase they could be entered here.
Do you want to CHECK the ATOMS in the molecules?	N	
Do you want to CHANGE the SETUP?	N	If products were entered incorrectly, Stanjan allows for corrections to be made. Stanjan also provides a warning if obvious errors were made.
Enter run option:	12	Option 12 "V and U same as last run". This will give us adiabatic, constant volume combustion.
Enter estimated T(K):	300	
Enter estimated P(atm):	1	
Do you want the SOUND SPEED?	N	
Do you want to SAVE the run OUTPUT in a file?	Y	Save file!
SAVE file name?	Type desired filename	
Is this an existing file?	N	
Do you want to MONITOR the run (probably not)?	N	
Do you want to see the JANNAF data used?	Y <enter> <enter>	The temperature calculated by Step C is assumed to be the adiabatic flame temperature. Below are the results as saved for Step C.

JANNAF table data for the products at T = 2868.80 K

species	molal mass g/mol	enth. form kcal/mol	S0 cal/mol-K	H-H0 kcal/mol
phase 1; Gas species:				
CO2	44.00995	-94.054	79.184	34.586
H2O	18.01601	-57.798	67.828	28.463
N2	28.01340	.000	63.369	21.005
NO2	46.00800	7.910	84.182	32.683
NO	30.00800	21.580	68.448	21.526
O2	31.99879	.000	67.547	22.197
IC8H18	114.22400	-53.570	300.992	249.505
HO	17.00740	9.432	60.964	20.262
O	16.00000	59.559	49.872	12.866
H2	2.01600	.000	48.071	20.065
CO	28.01054	-26.420	64.973	21.192
H	1.00797	52.100	38.640	12.771

Computed properties

Independent atom	population	element potential
C	8.00000000E+00	-1.7692E+01
H	1.93400000E+01	-1.0790E+01
O	2.56600000E+01	-1.5232E+01
N	9.65600000E+01	-1.2038E+01

Products at T = 2868.80 K P = 8.678E+01 atmospheres

species	mol fraction in the phase	mol fraction in mixture	mass fraction in mixture	mols*
phase 1: molal mass = 28.022 kg/kmol				
CO2	.96361E-01	.96361E-01	.15134E+00	6.46027E+00
H2O	.13590E+00	.13590E+00	.87373E-01	9.11086E+00
N2	.71622E+00	.71622E+00	.71601E+00	4.80170E+01
NO2	.81114E-05	.81114E-05	.13318E-04	5.43804E-04
NO	.78373E-02	.78373E-02	.83929E-02	5.25427E-01
O2	.79966E-02	.79966E-02	.91316E-02	5.36109E-01
IC8H18	.12643E-96	.12643E-96	.51536E-96	8.47596E-96
HO	.66370E-02	.66370E-02	.40283E-02	4.44961E-01
O	.67387E-03	.67387E-03	.38477E-03	4.51777E-02
H2	.46437E-02	.46437E-02	.33409E-03	3.11322E-01
CO	.22967E-01	.22967E-01	.22958E-01	1.53973E+00
H	.75589E-03	.75589E-03	.27190E-04	5.06764E-02

* Species mols for the atom populations in mols.

Mixture properties: molal mass = 28.022 kg/kmol

T = 2868.80 K P = 8.7934E+06 Pa V = 9.6800E-02 m**3/kg

U = .6119E+05 J/kg H = .9124E+06 J/kg S = .8742E+04 J/kg-K

WARNING! The thermochemical data for IC8H18 are extrapolated above 1000 K.

Made 28 (T,P) iterations; 310 equilibrium iterations; v 3.89 IBM-PC

STEP D

The isentropic expansion of the products is modeled by Step D. It is assumed that the volume after the isentropic expansion is equal to the volume determined through the modeling in Step A and is provided in the data output file as V.

STANJAN Prompts	User Input	Description and Explanation
Do you want to CHANGE the SETUP?	N	For Step D we would like to continue with the products inputted in Step C.
Enter run option:	15	Option 15 "Specified V,S same as last run". As in Step B option 15 allows for the isentropic expansion to the original volume.
Enter V (m**3/kg):	0.82265	Enter V ₁ as determined in Step A.
Enter estimated T (K):	300	
Enter estimated P (atm):	1	
Do you want the SOUND SPEED:	N	
Do you want to SAVE the run OUTPUT in a file?	Y	Save file!
SAVE file name?	Type desired filename	

Is this an existing file?	N	
Do you want to MONITOR the run (probably not)?	N	
Do you want to see the JANNAF data used?	Y <enter> <enter>	Below are the results as saved for Step D.

JANNAF table data for the products at T = 1874.08 K

species	molal mass g/mol	enth. form kcal/mol	S0 cal/mol-K	H-H0 kcal/mol
phase 1; Gas species:				
CO2	44.00995	-94.054	72.968	20.046
H2O	18.01601	-57.798	62.447	15.848
N2	28.01340	.000	59.664	12.338
NO2	46.00800	7.910	78.398	19.161
NO	30.00800	21.580	64.686	12.761
O2	31.99879	.000	63.626	13.016
IC8H18	114.22400	-53.570	257.148	147.072
HO	17.00740	9.432	57.354	11.812
O	16.00000	59.559	47.751	7.909
H2	2.01600	.000	44.475	11.626
CO	28.01054	-26.420	61.245	12.473
H	1.00797	52.100	36.525	7.829

Computed properties

Independent atom	population	element potential
C	8.00000000E+00	-2.2378E+01
H	1.93400000E+01	-1.2753E+01
O	2.56600000E+01	-1.7225E+01
N	9.65600000E+01	-1.2571E+01

Products at T = 1874.08 K P = 6.566E+00 atmospheres

species	mol fraction in the phase	mol fraction in mixture	mass fraction in mixture	mols*
phase 1: molal mass = 28.468 kg/kmol				
CO2	.12024E+00	.12024E+00	.18589E+00	7.93482E+00
H2O	.14616E+00	.14616E+00	.92495E-01	9.64489E+00
N2	.73150E+00	.73150E+00	.71982E+00	4.82722E+01
NO2	.54738E-07	.54738E-07	.88463E-07	3.61215E-06
NO	.23687E-03	.23687E-03	.24968E-03	1.56308E-02
O2	.40582E-03	.40582E-03	.45615E-03	2.67799E-02
IC8H18	.10954-132	.10954-132	.43949-132	7.22829-132
HO	.16624E-03	.16624E-03	.99313E-04	1.09700E-02
O	.18611E-05	.18611E-05	.10460E-05	1.22812E-04
H2	.29518E-03	.29518E-03	.20903E-04	1.94788E-02
CO	.98777E-03	.98777E-03	.97190E-03	6.51835E-02
H	.43457E-05	.43457E-05	.15387E-06	2.86772E-04

* Species mols for the atom populations in mols.

Mixture properties: molal mass = 28.468 kg/kmol
T = 1874.08 K P = 6.6533E+05 Pa V = 8.2265E-01 m**3/kg
U = -.1429E+07 J/kg H = -.8815E+06 J/kg S = .8742E+04 J/kg-K
WARNING! The thermochemical data for IC8H18 are extrapolated above 1000 K.

Made 13 (T,P) iterations; 141 equilibrium iterations; v 3.89 IBM-PC

STEP E

The final step is to model the blowdown/exhaust process. The blowdown/exhaust step assumes that the volume has returned to the original volume (Step D) and then the products have returned to the pressure to the original 1 atm.

STANJAN Prompts	User Input	Description and Explanation
Do you want to CHANGE the SETUP?	N	
Enter run option:	4	Select option 4 "Specified P and V". By specifying the original pressure and volume we can get back to original conditions.
Enter P (atm):	1	
Enter V (m**3/kg):	0.82265	
Enter estimated T (K):	300	
Do you want the SOUND SPEED?	N	
Do you want to SAVE the run output in a file?	Y	Save file!
SAVE file name?	Type desired filename	
Is this an existing file?	N	
Do you want to MONITOR the run (probably not)?	N	
Do you want to see the JANNAF data used?	Y <enter> <enter>	Below are the results as saved for Step E. These results can be used to determine if the original parameters such as temperature were correct.

JANNAF table data for the products at T = 285.60 K

species	molal mass g/mol	enth. form kcal/mol	S0 cal/mol-K	H-H0 kcal/mol
phase 1; Gas species:				
CO2	44.00995	-94.054	50.689	-.111
H2O	18.01601	-57.798	44.755	-.101
N2	28.01340	.000	45.466	-.087
NO2	46.00800	7.910	56.960	-.111
NO	30.00800	21.580	50.035	-.090
O2	31.99879	.000	48.697	-.088
IC8H18	114.22400	-53.570	98.882	-.653
HO	17.00740	9.432	43.566	-.090
O	16.00000	59.559	38.239	-.066
H2	2.01600	.000	30.910	-.086
CO	28.01054	-26.420	46.910	-.087
H	1.00797	52.100	27.175	-.063

Computed properties

Independent atom	population	element potential
C	8.00000000E+00	8.7460E+00
H	1.93400000E+01	-1.2659E+01
O	2.56600000E+01	-1.0114E+02
N	9.65600000E+01	-1.1673E+01

Products at T = 285.60 K P = 1.000E+00 atmospheres

species	mol fraction in the phase	mol fraction in mixture	mass fraction in mixture	mols*
phase 1: molal mass = 28.487 kg/kmol				
CO2	.12128E+00	.12128E+00	.18737E+00	7.99821E+00
H2O	.14654E+00	.14654E+00	.92674E-01	9.66358E+00
N2	.73211E+00	.73211E+00	.71994E+00	4.82800E+01
NO2	.36281E-86	.36281E-86	.58596E-86	2.39263E-85
NO	.31269E-54	.31269E-54	.32938E-54	2.06205E-53
O2	.72232E-77	.72232E-77	.81136E-77	4.76342E-76
IC8H18	.33902E-05	.33902E-05	.13594E-04	2.23571E-04
HO	.88987E-47	.88987E-47	.53127E-47	5.86834E-46
O	.80326E-81	.80326E-81	.45116E-81	5.29720E-80
H2	.66883E-04	.66883E-04	.47333E-05	4.41072E-03
CO	.25648E-09	.25648E-09	.25219E-09	1.69139E-08
H	.41717E-39	.41717E-39	.14761E-40	2.75112E-38

* Species mols for the atom populations in mols.

Mixture properties: molal mass = 28.487 kg/kmol

T = 285.60 K P = 1.0133E+05 Pa V = 8.2265E-01 m³/kg

U = -.3016E+07 J/kg H = -.2933E+07 J/kg S = .6979E+04 J/kg-K

WARNING! The thermochemical data for IC8H18 are extrapolated below 298 K.

Made 5 (T,P) iterations; 196 equilibrium iterations; v 3.89 IBM-PC

Examples of Calculations based on STANJAN Results

WORK

The total work performed by the combustion process is calculated using the internal energies determined in Steps 1 through 4.

Internal Energy results for Steps 1 – 4.

$$u_1 = -200.7 \text{ kJ/kg}$$

$$u_2 = u_3 = 61.19 \text{ kJ/kg}$$

$$u_4 = -1429 \text{ kJ/kg}$$

(Remember: Steps 2 and 3 the enthalpy is equal to produce adiabatic conditions)

$$w_{1,2} = u_1 - u_2 = -200.7 - 61.19 = -261.89 \text{ kJ/kg}$$

$$w_{3,4} = u_3 - u_4 = 61.19 - (-1429) = 1490.19 \text{ kJ/kg}$$

$$w_T = w_{1,2} + w_{3,4} = -261.89 + 1490.19 = 1228.3 \text{ kJ/kg}$$

APPENDIX B

CHEMKIN

The four files used for the CHEMKIN simulations are provided on a CD:

- 1) Premix input file
- 2) Chemical mechanism
- 3) Transport file
- 4) Thermodynamics file

CHEMKIN Equations

The priority differential equations used for determining flame propagation under steady state and constant pressure are described below.

Continuity Equations

$$\dot{M} = \rho u A \quad (\text{B.1})$$

Energy Equation

$$\dot{M} \frac{dT}{dx} - \frac{1}{c_p} \frac{d}{dx} \left(\lambda A \frac{dT}{dx} \right) + \frac{A}{c_p} \sum_{k=1}^K \rho Y_k V_k c_{pk} \frac{dT}{dx} + \frac{A}{c_p} \sum_{k=1}^K \dot{w}_k h_k W_k = 0 \quad (\text{B.2})$$

Species Equation

$$\dot{M} \frac{dY_k}{dx} + \frac{d}{dx} (\rho A Y_k V_k) - A \dot{w}_k W_k = 0 \quad (\text{B.3})$$

Equation of State

$$\rho = \frac{p\bar{W}}{RT} \quad (\text{B.4})$$

where, \dot{M} = mass flow rate (which is independent of x)

T = temperature

Y_k = mass fraction of the k th species

p = pressure

W_k = molecular weight of the k th species

\bar{W} = mean molecular weight of the mixture

R = universal gas constant

λ = thermal conductivity of the mixture

c_p = constant-pressure heat capacity of the mixture

c_{pk} = constant pressure heat capacity of the k th species

$\dot{\omega}_k$ = molar rate of production by chemical reaction of the k th species per unit volume

h_k = specific enthalpy of the k th species

V_k = diffusion velocity of the k th species

A = cross sectional area

Elementary Reaction Kinetics (CHEMKIN interpreter/chemical mechanism)

The CHEMKIN interpreter uses the modified Arrhenius equation,

$$k_f = AT^\beta \exp\left(\frac{-E_A}{RT}\right) \quad (\text{B.5})$$

that presumes that each equation proceeds according to the law of mass action.

Transport Equations (TRANSPORT program/viscosity, diffusion)

The TRANSPORT program uses a matrix of equations to determine the ordinary multicomponent diffusion coefficient, D_{kj} , species thermal coefficients, and thermal conductivities.

$$V_k = v_k + \omega_k \quad (\text{B.6})$$

$$v_k = \frac{1}{X_k \bar{W}} \sum_{j \neq k}^K W_j D_{k,j} d_j \quad (\text{B.7})$$

$$d_j = \nabla X_k + (X_k - Y_k) \frac{1}{p} \nabla p \quad (\text{B.8})$$

$$\omega_k = -\frac{D_k^T}{\rho Y_k T} \nabla T \quad (\text{B.9})$$

where; V_k = diffusion velocity of the k th species

v_k = ordinary diffusion velocity of the k th species

ω_k = thermal diffusion velocity of the k th species

X_k = mole fraction of the k th species

\bar{W} = mean molecular weight of the mixture

W_j = molecular weight of the j th species

$D_{k,j}$ = multicomponent diffusion coefficient of the species k in species j

Y_k = mass fraction of the k th species

p = pressure

D_k^T = thermal diffusion coefficient of the k th species

This complex system of equations is solved by making finite difference approximations to determine a system of algebraic equations. The algebraic equations are then solved using a combination of the modified Newton algorithm and time integration [Kee *et al*, 2001].

APPENDIX C

GC Calibration and Calculations

Chemical analysis was performed on the electrolysis products using a Varian Chrompack CP-3800 gas chromatograph (Walnut Creek, California) with thermal conductivity detector (TCD). A Hayesep A Packed Column (Alltech, Deerfield, IL) was selected for analysis of hydrogen, oxygen, and nitrogen. The Hayesep A 120/140 column is a 1/8 inch diameter, 40 foot column. The calibration and sampling were conducted using the operating conditions listed in Table C.1

Table C.1 Summary of operating conditions

Carrier Gas	Helium at 18 mL/min
Head Pressure	73 psi
Oven temperature	30 °C
Injection temperature	120 °C
Detector	TCD at 220 °C
Filament temperature	140 °C
Syringe temperature	50 °C
Sample temperature	50 °C
Sample Size	100 µL

The column was attached to the injection port and preconditioned overnight at 30°C with helium carrier gas.

A chromatograph similar to the one provided in Figure C.1 was used to calibrate the column using ambient air and pure hydrogen and oxygen. A data file is produced from the chromatograph, which reports the total area count for each peak. Based on these results a ratio of area counts/mass can be determined and used to calculate unknown quantities of gases. These calculations are based on the ideal gas law, an example is provided below.

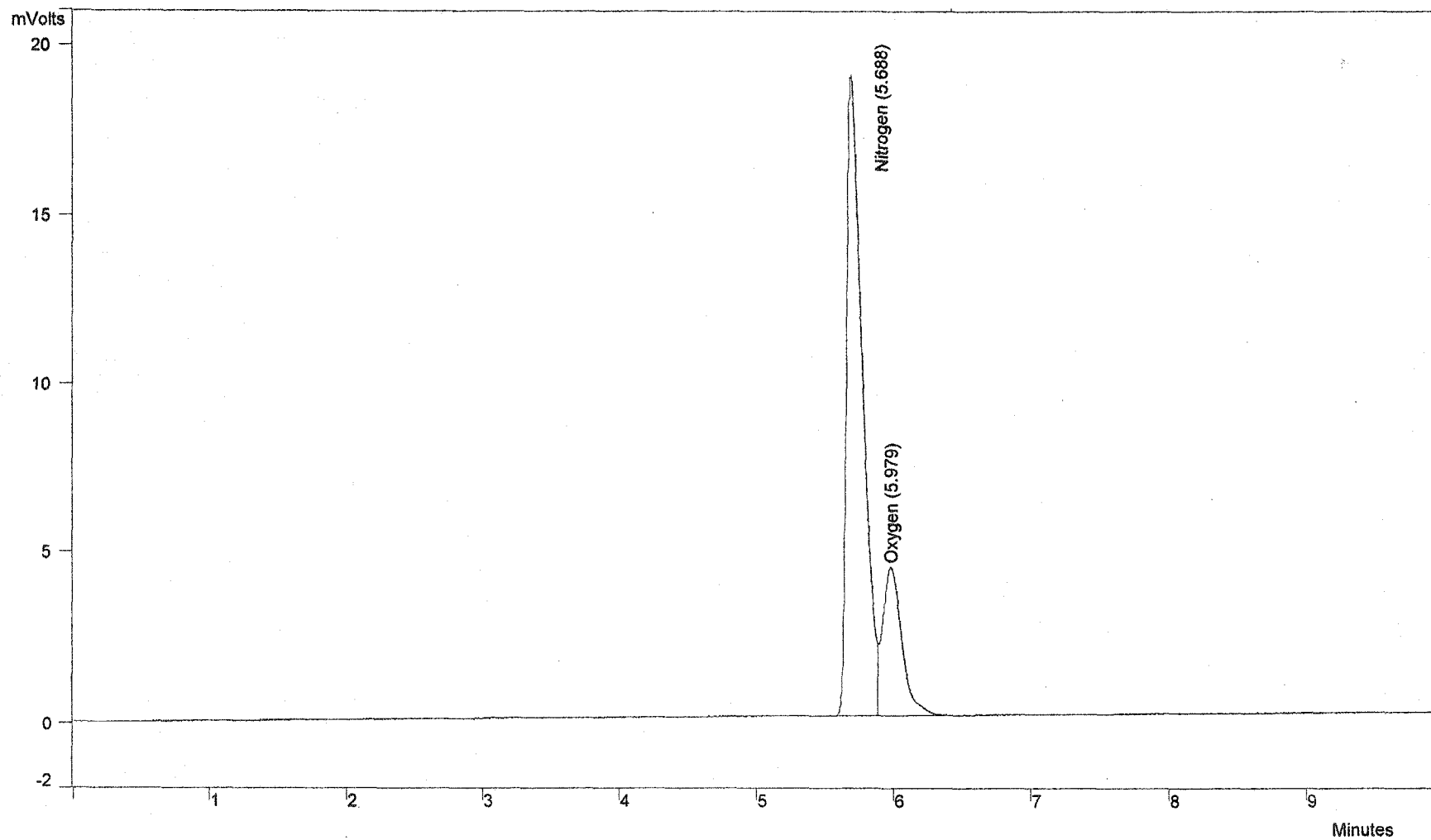


Figure C.1 Sample of chromatograph produced for ambient air samples used during calibration

C.1 Calibration using ambient air samples

$$m_{N_2} = V \times \left(\frac{\% N_2 \text{ by vol. in air}}{100} \right) \times \frac{MW_{N_2}}{(T + 273.15) \times R}$$

$$m_{O_2} = V \times \left(\frac{\% O_2 \text{ by vol. in air}}{100} \right) \times \frac{MW_{O_2}}{(T + 273.15) \times R}$$

where: m_{N_2} = mass of nitrogen, μg

m_{O_2} = mass of oxygen, μg

V = volume of sample, μL

MW_{N_2} = molecular weight of nitrogen = 28 g/g·mol

MW_{O_2} = molecular weight of oxygen = 32 g/g·mol

T = operating temperature = 50 °C

R = gas constant = 0.08205 L·atm/mol·K

$\% N_2 \text{ by vol. in air} = 78.08 \%$

$\% O_2 \text{ by vol. in air} = 20.95$

The area count given in the calibration chromatograph was then divided by the known mass of N_2 and O_2 injected into the column to determine the area count/mass ratio, R_{AN_2} , which was used later for calculating the mass of an unknown sample.

$$R_{AN_2} = \frac{AC_{N_2}}{m_{N_2}}$$

$$R_{AO_2} = \frac{AC_{O_2}}{m_{O_2}}$$

where: R_{AN_2} = area count/mass ratio for nitrogen

R_{AO_2} = area count/mass ratio for oxygen

AC_{N_2} = area count for hydrogen

AC_{O_2} = area count for oxygen

C.2 Calibration using pure hydrogen and pure oxygen samples

A vial was purged for 5 minutes using pure hydrogen (99.995% pure) and another was purged with pure oxygen (99.995% pure). The purging time was long enough to assume that all air had been purged from the vial. Unfortunately, the calibration chromatographs reported peaks of nitrogen and oxygen in the pure hydrogen sample and nitrogen in the pure oxygen sample. The source of this air is unknown, but it could have originated either from inadequate purging, or during the injection when the needle was filled repeatedly, resulting in air entering the vial. The procedure used to account for the air in the pure hydrogen sample is outlined in the equations below.

The masses of nitrogen and oxygen found in the pure hydrogen sample can be determined by using the equation for the ratio of area counts/mass.

$$m_{N_2} = \frac{AC_{N_2}}{R_{AN_2}} \qquad m_{O_2} = \frac{AC_{O_2}}{R_{AO_2}}$$

The O_2 was predicted using the theoretical N_2/O_2 ratio of 3.264.

If the two equations provided to calculate the mass of oxygen do not provide similar results, it is an indication that gases other than ambient air contaminated the hydrogen sample. The masses of oxygen in the hydrogen sample calculated by the two methods differed by less than 5 %.

The volume of air was then calculated by:

$$V_{air} = \frac{m_{N_2} \times R \times (T + 273.15)}{MW_{N_2}} + \frac{m_{O_2} \times R \times (T + 273.15)}{MW_{O_2}}$$

Therefore the volume of hydrogen injected can be calculated by subtracting the calculated volume of air from the sample volume.

$$V_{H_2} = V - V_{air}$$

The ideal gas law is used to calculate the mass of hydrogen.

$$m_{H_2} = \frac{V_{H_2} \times MW_{H_2}}{(T + 273.15)(R)}$$

where: m_{H_2} = mass of hydrogen, μg

V = volume of sample, μL

MW_{H_2} = molecular weight of nitrogen = 2.02 g/g·mol

T = operating temperature = 50 °C

R = gas constant = 0.08205 L·atm/mol·K

The mass calculated based on the pure hydrogen sample was then used to determine the area count/mass ratio for hydrogen. This ratio was used to determine unknown quantities of hydrogen in electrolysis products.

$$R_{AH_2} = \frac{AC_{H_2}}{m_{H_2}}$$

Pure oxygen samples were used in the calibration as well. The calculations were completed similar to the hydrogen sample calculations with the assumption that nitrogen present was from contamination of ambient air, therefore, the volume of oxygen calculated had to be adjusted to account for this ambient air.

$$V_{O_2} = V - V_{air}$$

The area count/mass ratios determined during calibration are as follows.

$$R_{AN_2} = 922.84 \quad R_{AO_2} = 824.58 \quad R_{AH_2} = 198.64$$

C.3 Determination of the composition of electrolysis products

Once the calibration was completed using ambient air, pure hydrogen and pure oxygen, the area count/mass ratios, R_A , were used to calculate unknown quantities of hydrogen and oxygen in the electrolysis products.

The samples were collected in a 20 mL vial using two syringes, one syringe was attached to the electrolysis outlet tube, pierced the rubber vial septum and went to the bottom of the vial. The second syringe was used as an exhaust, and simply pierced the rubber septum. The electrolysis unit was allowed to purge the vial for 25 minutes at a flow rate of 480 mL/min. This is equivalent to 600 vial volumes. Two different volumes were injected into the GC from the same vial for analysis.

The masses of hydrogen, oxygen and any nitrogen present were calculated using the ratios determined during calibration.

$$m_{H_2} = \frac{AC_{H_2}}{R_{AH_2}} \quad m_{N_2} = \frac{AC_{N_2}}{R_{AN_2}} \quad m_{O_2} = \frac{AC_{O_2}}{R_{AO_2}}$$

The area counts reported in the data files in for two different sample volumes are provided in Table C.2 along with the masses calculated from the equations above.

Table C.2 Calculated masses of hydrogen, nitrogen and oxygen from the electrolysis products sample

V(μ L)	Area Counts			Calculated mass (μ g)		
	H ₂	N ₂	O ₂	H ₂	N ₂	O ₂
100	1021	1869	30014	5.14	2.03	36.40
200	1657	8430	62874	8.34	9.13	76.25

As with the pure hydrogen and oxygen samples used during calibration, the chromatographs developed for the electrolysis products show a peak in nitrogen as well as the expected hydrogen and oxygen peaks. The chromatograph produced for Sample 1 is provided as an example in Figure C.2. No other peaks were observed. Similar to the calibration curves it was assumed that the peak in nitrogen was due to contamination of the sample by ambient air either by inadequate purging of the vial or by the injection process. Therefore, it is expected that extra oxygen from the ambient air is also included in the sample. To account for the ambient air, the theoretical ratio of N_2/O_2 was used to calculate the “extra” oxygen. This extra oxygen was then subtracted from the total mass of oxygen as shown in Table C.3. The volume of nitrogen was higher in the second sample, which is likely a result of the introduction of air during the first or second injection process.

$$m_{O_2 \text{ from air}} = m_{N_2} \times \text{mass ratio } O_2 / N_2$$

Table C.3 Calculation to determine contribution of O_2 from electrolysis products

Sample Volume	Mass O_2 calculated from chromatograph	Predicted mass of O_2 from air	Mass of O_2 from electrolysis products
(μL)	μg	μg	μg
100	36.399	0.620	35.779
200	76.250	2.798	73.451

Based on the ideal gas law the volumes of the hydrogen and oxygen are calculated in Table C.4.

Table C.4 Calculated volumes of hydrogen and oxygen from electrolysis products

Sample Volume	V_{H_2}	$V_{\text{elec}O_2}$	$H_2:O_2$
(μL)	μL	μL	
100	67.47	29.65	2.3
200	109.49	60.86	1.8

Therefore, it was determined that the average ratio of $H_2:O_2$ is 2:1 Based on the calculations completed above, a remainder of the sample volume was unaccounted for.

This unaccounted-for volume is calculated in Table C.5. As noted above, no other peaks were observed in the chromatograph. It was determined that the samples contained ambient air, therefore the unaccounted volume may be due to impurities in the air, which could not be determined with the Hayesep A column.

Table C.5 Calculation to determine % of sample unaccounted

Sample Volume	V_{air}	% V_{air} in sample	V_{total}		Unaccounted Volume	% unaccounted
			$V_{\text{air}}+V_{\text{H}_2}+V_{\text{O}_2}$	$V_{\text{H}_2}+V_{\text{O}_2}$		
(μL)	μL	%	μL	μL	$V-V_{\text{total}}$	%
100	2.43	2.4	99.54	97.11	0.46	0.5
200	10.96	5.5	181.32	170.35	18.68	11.0

The percent air and the percent unaccounted for increased in the second sample. The same vial was used for both runs. The first sample was used because of the high percent unaccounted for in the second sample.

Overall, hydrogen and oxygen were produced in approximately a 2:1 ratio as expected during electrolysis. Also, it is important to note that no other electrolysis products were observed, although highly reactive electrolysis products (eg. ozone) would likely be destroyed during chromatography [Stewart, 2003].

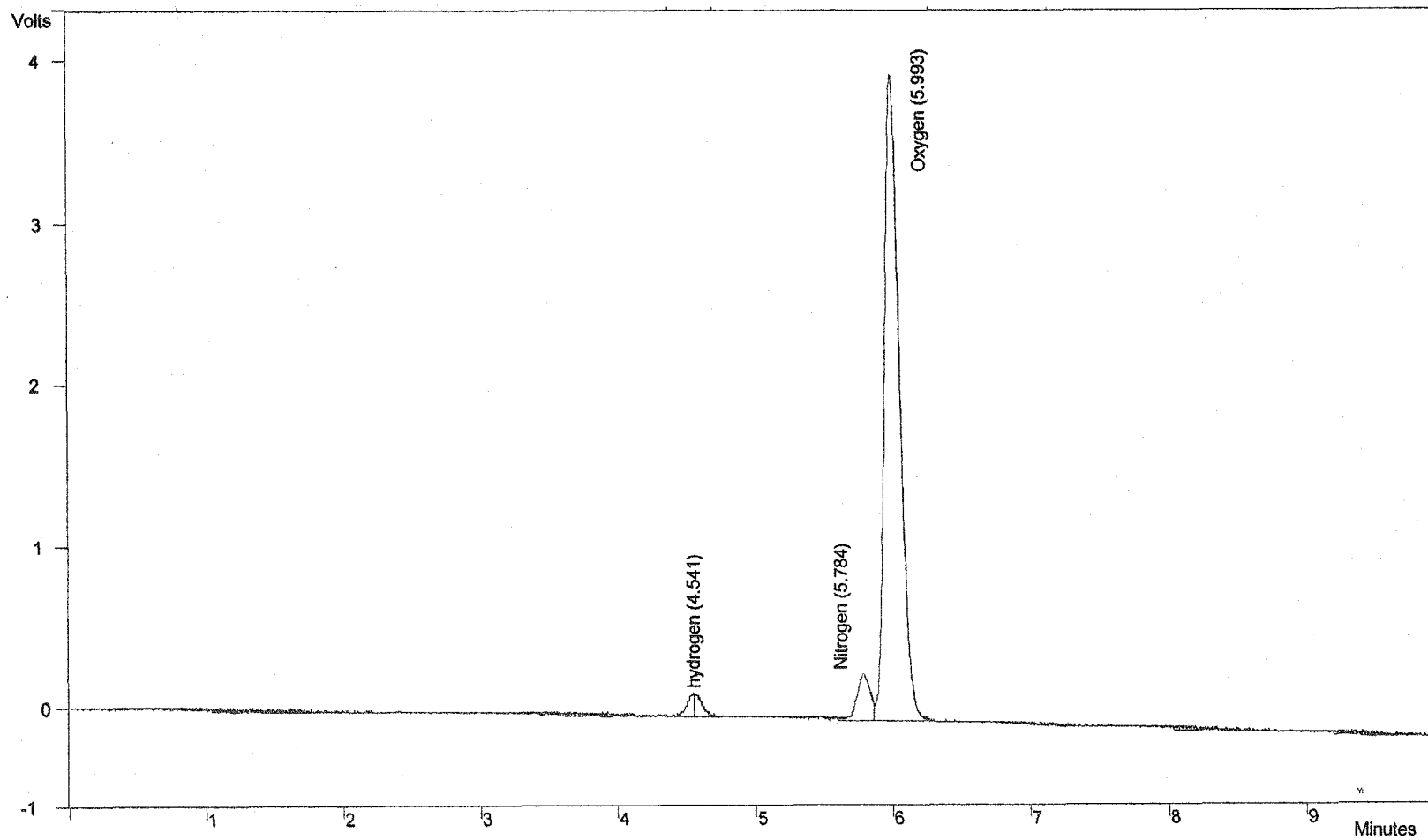


Figure C.2 Sample chromatograph produced from Varian Chrompack CP-3800 gas chromatograph with thermal conductivity detector (TCD)

APPENDIX D

LabVIEW Code

The LabVIEW software [Omega, Stamford, Connecticut] was used to collect pressure and crank angle measurements. Three channels were used on the data acquisition board. Two channels were used to collect the top dead centre (TDC) signal and every crank angle degree (CAD) from the encoder. The third channel was used to collect the pressure signal from the pressure transducer. The LabVIEW interface, as shown in Figure D.1, continuously displays the signals received from the three channels on a graph. The user enters the rpm and begins the program with the data saved to a user defined file name.

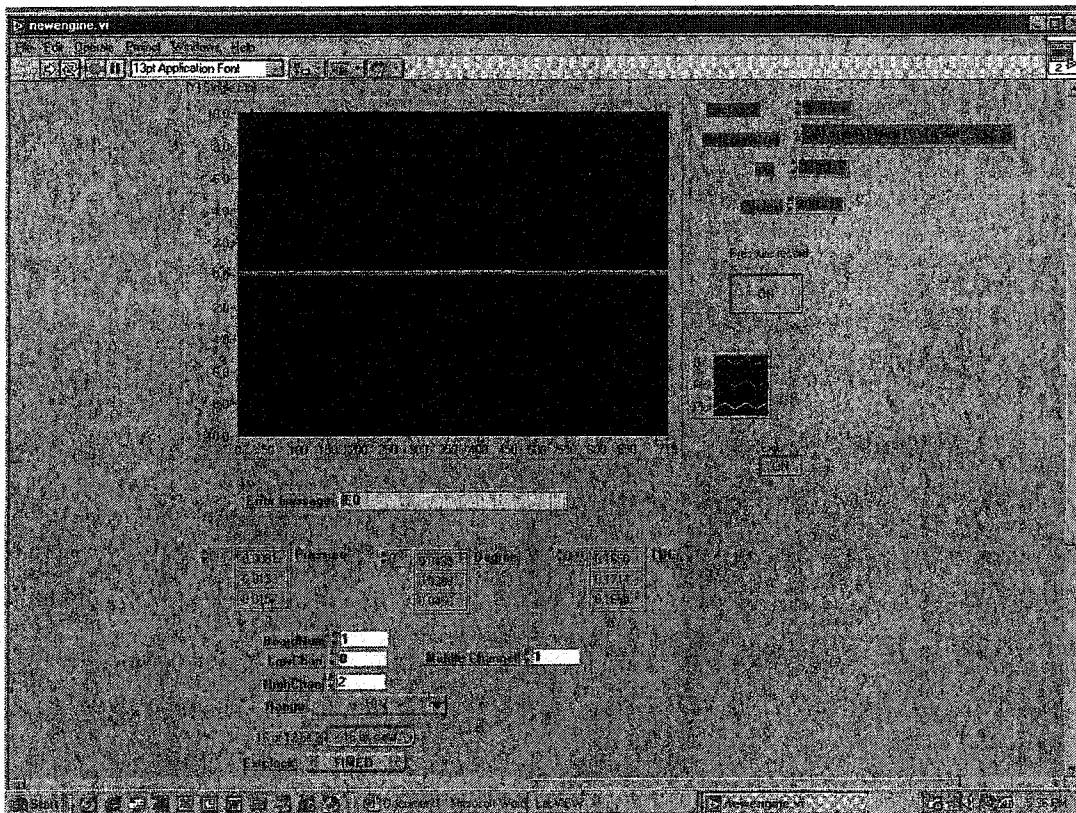


Figure D.1: LabView User Interphase

LabView displays a schematic diagram that shows how the program collects the signals from the three channels on the data acquisition board, (Figure D.2) and sends the data from the three channels to a file (Figure D.3).

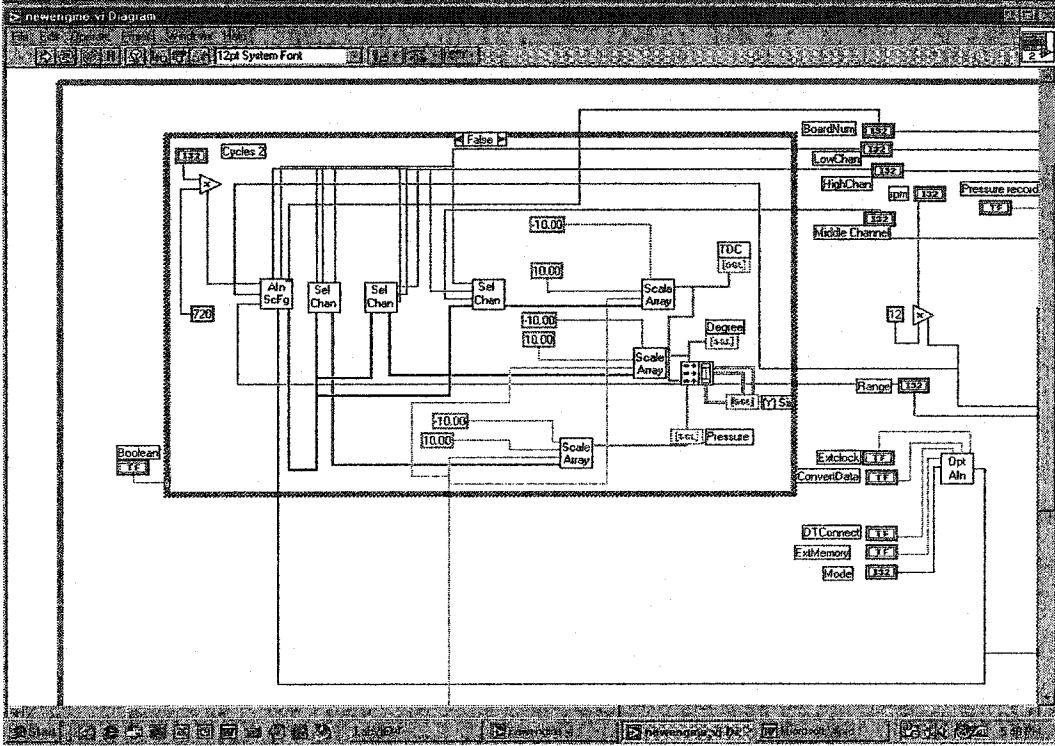


Figure D.2: LabView code for collecting signals from the three channels

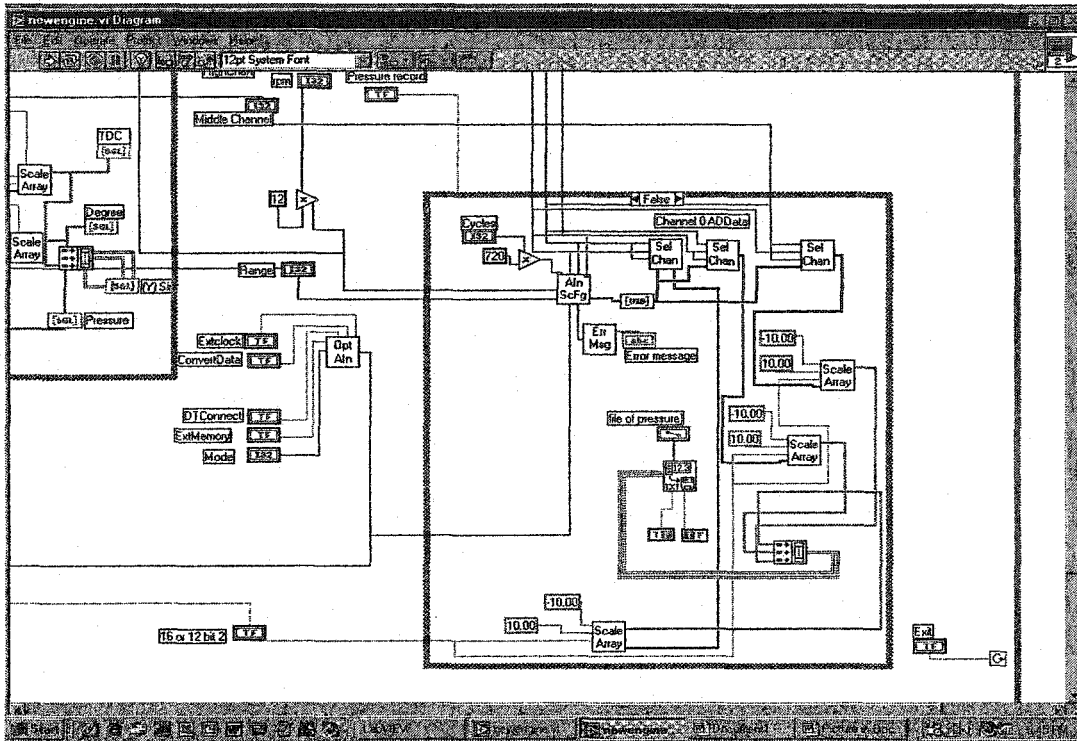


Figure D.3: LabVIEW code that sends data to the designated file

APPENDIX E

Electrolysis Flow Rate Measurements

The electrolysis unit required approximately 20 minutes before a steady flow was produced. To assure that the electrolysis unit was producing a steady flow of products and to determine the flow rate a mini-Buck Calibrator (A.P. Buck, Orlando, Florida) was used before the electrolysis products were introduced to the engine. As a gaseous flow is passed through the mini-Buck Calibrator a bubble is formed and moves up a clear tube of known volume. There are two sensors set at a known distance apart that measure the time required for the bubble to move between the two sensors. Using the known volume and the time measured the mini-Buck can calculate the volumetric flow rate.

Figure E.1 provides the electrolysis flow rate measurements over time. The mini-Buck has a detection limiting of 0.1 L/min, any flows under 0.1 L/min are reported as 0 L/min. The first reading greater than 0 L/min was obtained at approximately 15 minutes and at approximately 20 minutes the electrolysis products were generally considered to have reached a steady state. To verify this, during each engine test the flow rate of electrolysis products was measured several times to predetermine if a steady flow rate was achieved. The flow rate was measured again after the engine tests. The averaged results before and after the engine tests are provided in Table E.1.

Most tests completed had a flow rate difference of less than five percent before and after testing. Only tests 4, 10 and 11 had percent differences greater than five percent but were below 10 percent. The largest difference was noted in Test 11, with a difference in flow rate of 0.047 L/min (0.0313 L/min H₂ and 0.0157 L/min O₂).

Electrolysis Flow Rate versus Time

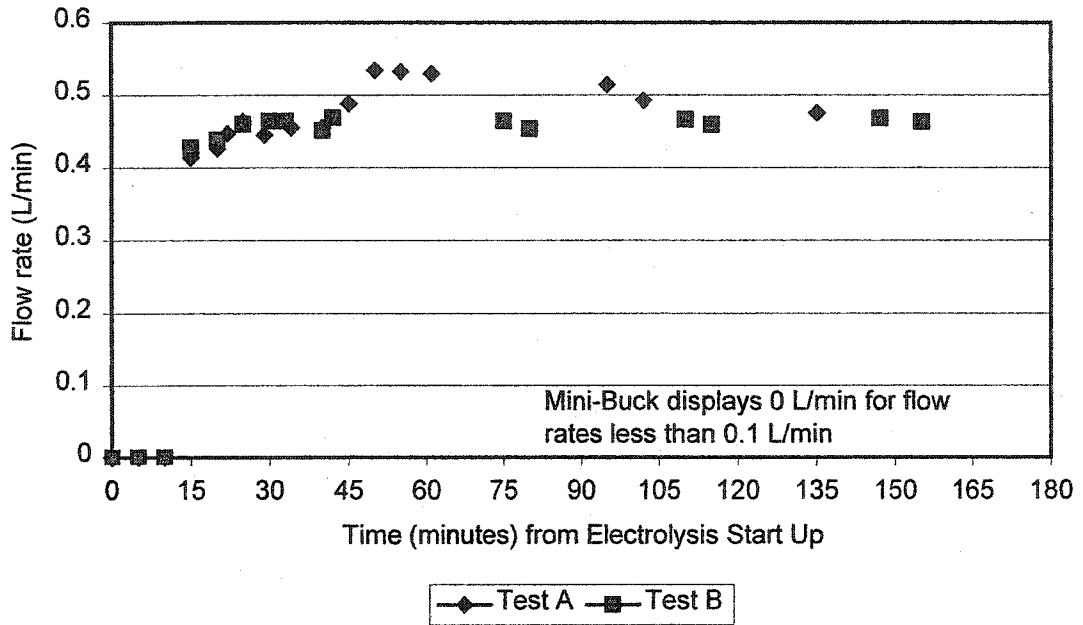


Figure E.1 Flow Rate of Electrolysis Products versus Time

Table E.1 Electrolysis products flow rate comparison for engine tests

Test	Before Introduction to Engine L/min	After Introduction to Engine L/min	% difference %
1	0.493	0.509	3.19
2	0.478	0.492	2.89
3	0.491	0.507	3.21
4	0.520	0.556	6.69
5	0.488	0.505	3.42
6	0.500	0.504	0.80
7	0.497	0.504	1.40
8	0.459	0.466	2.00
9	0.476	0.475	0.21
10	0.462	0.490	5.88
11	0.547	0.500	8.97

APPENDIX F

Air Flow Measurements

Engine tests were run at varying speeds (1600 to 3000 rpm) for one quarter and one half throttle settings. In collaboration with Ramiz Ahemad, a velocity profile was estimated based on discrete velocity measurements. Manometer readings were recorded and tabulated according to the Equal-Area method and compared against the anemometer readings. The Equal-Area method uses velocities measured at points along the diameter of a pipe, which corresponds to the centre of equally-sized elements (areas) across the duct. The volumetric flow rate is estimated from the average of these measured velocities multiplied by the cross-sectional area of the whole duct [Fox and McDonald, 1973].

Initial manometer readings were taken with the pitot-static tube traversing a 7.62 cm (3") ABS pipe directly above the anemometer. The velocity within this pipe was too low to register a difference in pressure in the manometer. To increase the velocity, a 5.08 cm (2 in) ABS pipe was fitted upstream of the 7.62 cm (3") ABS pipe which houses the anemometer (Figure 4.4). This reduction in diameter provided a sufficient increase in the velocity allowing for accurate manometer readings. The ports for the pitot-tube were located 9.5 diameters upstream from the 7.62 cm to 5.08 cm ABS pipe expansion area and 26 diameters downstream from the opening of the air intake to minimize the effects of the change in cross-sectional area. Six readings were taken along the diameter of the 5.08 cm ABS pipe at distances reported in Table F.1 [EPA Method 1].

Table F.1 Location of Pitot Tube Measurements for Equal Area Method

Method for pitot static tube traverse	Distance from inner wall (mm)					
	Position 1	Position 2	Position 3	Position 4	Position 5	Position 6
% stack diameter	4.4	14.6	29.6	70.4	85.4	95.6
Distance from wall of 5.08 cm pipe	2.2	7.5	15.0	35.7	43.3	48.6

The velocity was calculated for each location using the following equations [Klopfenstein, 1998]:

$$V(\text{m/sec}) = 44.72 \sqrt{\frac{h_{dynamic}}{\rho}}$$

where: ρ = air density = 1.1634 kg/m³ (@ STP)

$$h_{dynamic} = 1.962 * 0.001P(\text{mm}_{\text{H}_2\text{O}})$$

$$P(\text{mm}_{\text{H}_2\text{O}}) = (P\text{mm}_{\text{m.fluid}}) * 0.827$$

The calculated velocities for each of the six locations were averaged and used to calculate the flow rate through the 5.08 cm ABS pipe.

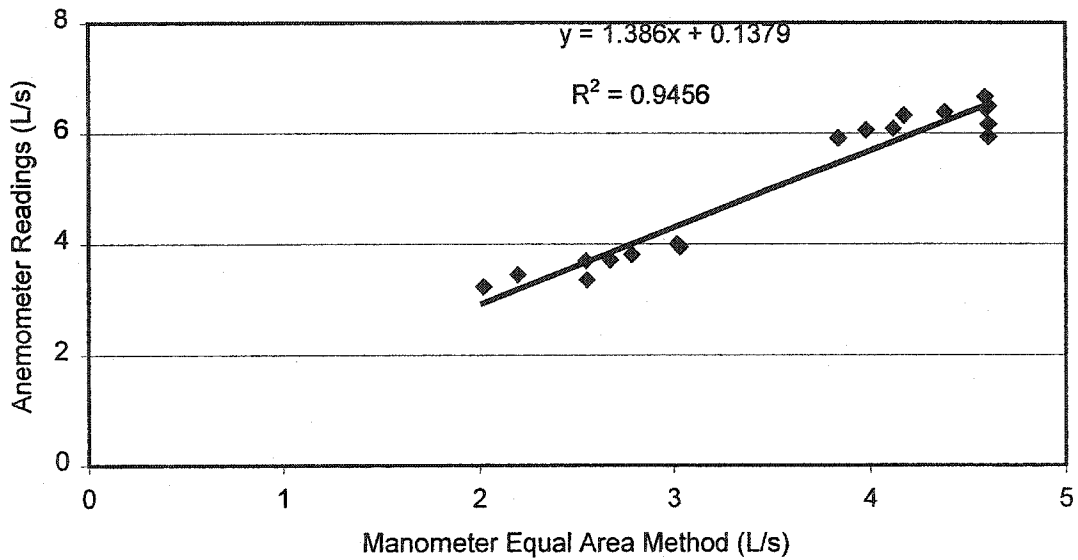
$$Q_{m.air} (\text{m}^3/\text{sec}) = \pi r^2 V_{av}$$

where: $Q_{m.air}$ = the flow rate calculated by manometer readings

$$\pi r^2 = \text{cross-sectional area of duct} = 0.00203 \text{ m}^2$$

The volumetric flow rates estimated using the anemometer velocity readings and the manometer readings were plotted to determine if a relationship existed between the two readings. The graph is provided in Figure F.1. As shown in Figure F.1, a linear relationship was found for flow rates between 4.24 and 9.9 L/s (9 and 21 cfm) with an R² value of 0.95. Based on the strength of this relationship the engine tests were completed using the anemometer only. The anemometer readings were then corrected using the linear relationship, $y=1.386x+0.1379$ (or $y=1.386x + 0.619$ when using cfm), where x is the corrected flow rate and y is equal to the reported anemometer reading.

Anemometer Flow Rates versus Manometer Equal Area Method (a)



Anemometer Flow Rates versus Manometer Equal Area Method (b)

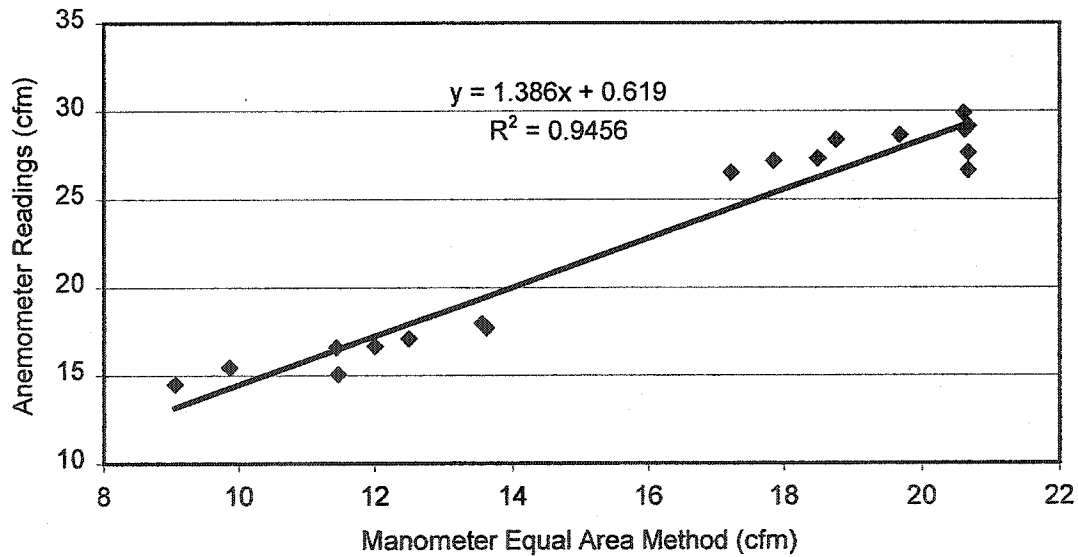


Figure F.1 Flow Rate Comparison for Anemometer and Manometer Readings a) flow rates in L/s; b) flow rates in ft³/min.

APPENDIX G

Uncertainty Analysis

G.1 Speed

The uncertainty in engine rotational speed is function of the instrumentation errors (u_I) and fluctuation in speed (u_R) reported by the user.

The total uncertainty is calculated by:

$$u_{rpm} = \sqrt{(u_R)^2 + (u_I)^2}$$

where:

u_R = maximum of either 1) the average rpm minus minimum observed rpm or 2) the maximum observed rpm minus the average rpm. The average rpm is assumed to be the desired rpm.

$$u_I = \pm 10 \text{ rev/min}$$

Table G.1 Speed uncertainty calculations for each engine test completed

Test	Average (desired) rpm	Minimum documented rpm	Maximum documented rpm	Uncertainty calculated for min. rpm	Uncertainty calculated for max. rpm	u_R	u_I	u_{rpm}
1	2615	2538	2692	77	77	77	10	78
2	2308	2246	2315	62	8	62	10	62
3	2000	1977	2023	23	23	23	10	25
4	3000	2985	3031	15	31	31	10	32
5	3308	3277	3369	31	62	62	10	62
6	3308	3285	3377	23	69	69	10	70
7	3192	3169	3254	23	62	62	10	62
8	3077	3077	3138	0	62	62	10	62
9	3308	3277	3331	31	23	31	10	32
10	2615	2600	2669	15	54	54	10	55
11	2308	2300	2362	8	54	54	10	55

G.2 Torque

This uncertainty in torque was based on the GoPower (Carrollton, Texas) D-100 water brake dynamometer manufacture's specification.

$$u_{torque} = \pm 0.3 \text{ lb} \cdot \text{ft} \times 1.356 (\text{N} \cdot \text{m} / \text{lb} \cdot \text{ft}) = \pm 0.41 \text{ N} \cdot \text{m}$$

G.3 Indicated Mean Effective Pressure

The process used for the calculation of imep is described in detail in Section 4.4.3. The imep is a function of the work produced in one cycle. The work is calculated by determining the area within the p - V diagram as represented by the integral;

$$W = \oint p \times dV$$

The trapezoidal method was used to calculate the area for specified sections of the curve.

$$A = 1/2 PV$$

Based on these two equations the uncertainty in the area of a section under the curve is

$$u_A = \sqrt{\left(u_v \frac{P}{2}\right)^2 + \left(u_p \frac{V}{2}\right)^2} \approx 5410057 \text{ kPa} \cdot \text{mm}^3$$

The maximum uncertainty in the area calculation is calculated at maximum pressure and volume with the uncertainty in volume, $u_v = \pm 4085 \text{ mm}^3$ (calculated in Section G.7) and the uncertainty in pressure, $u_p = \pm 31 \text{ kPa}$ (Section G.8).

The imep is calculated as:

$$imep = \frac{\sum A}{V_s}$$

where: V_s = swept volume

Since the uncertainty in volume has been accounted for in the uncertainty in area calculation it is not accounted for a second time in the imep uncertainty as V_s is assumed constant. However, the imep is calculated using a series of areas, therefore the worst case is the maximum uncertainty in area for all four areas considered.

$$u_{imep} = \frac{\sqrt{u_{a_1}^2 + (-u_{a_2})^2 + (-u_{a_3})^2 + (-u_{a_4})^2}}{V_s} = \frac{\sqrt{4(u_a)^2}}{V_s}$$

where $u_A \approx 5410057 \text{ kPa} \cdot \text{mm}^3$;

$$V_s = 285005 \text{ mm}^3.$$

Therefore, the u_{imep} is estimated as $\pm 38 \text{ kPa}$.

G.4 Air Flow Rate

As discussed in Section 4.1.3, air flow rates were determined using an Omega Hygrothermo anemometer, however, these results were notably higher than possible, giving equivalence ratios leaner than the ideal lean limit for gasoline combustion. Therefore, the equal area method was used as a secondary calibration standard (Appendix D).

The manometer readings were used to estimate the velocity profile and subsequently the flow rate by the following equations:

$$V(m/sec) = 44.72 \sqrt{\frac{h_{dynamic}}{\rho}} = 44.72 \sqrt{\frac{1.962 \times 0.001 \times 0.827 (P_{mm_{fluid}})}{\rho}}$$

where: ρ = air density as 298K = 1.1634 kg/m³

$$h_{dynamic} = 1.962 \times 0.001 P(\text{mm}_{\text{H}_2\text{O}})$$

$$P(\text{mm}_{\text{H}_2\text{O}}) = (P_{\text{mm}_{\text{fluid}}}) \times 0.827$$

The density of air is calculated as $\rho_{air} = \frac{P}{RT}$. The uncertainty associated with air density due to nonstandard room conditions is:

$$u_{\rho_{air}} = \sqrt{\left(u_{\rho} \frac{\partial \rho_{air}}{\partial P}\right)^2 + \left(u_T \frac{\partial \rho_{air}}{\partial T}\right)^2}$$

$$u_{\rho_{air}} = \sqrt{\left(u_{\rho} \frac{1}{RT}\right)^2 + \left(u_T \frac{-P}{RT^2}\right)^2}$$

$$u_T = \pm(T_{\text{max}} - 298), \text{ maximum room temperature reported was } 26^{\circ}\text{C}$$

$$u_T = \pm 26\text{K}$$

u_p = the uncertainty in room pressure is considered negligible.

$$\text{Therefore } u_{\rho} = \pm 0.018 \text{ kg/m}^3$$

The uncertainty in the manometer flow rate calculation is based on the errors associated with the manometer reading, $u_{p_{\text{mm}_{\text{fluid}}}}$.

$$u_{p_{\text{mm}_{\text{fluid}}}} = \pm 0.5 \text{ mm}_{\text{fluid}}$$

Therefore the uncertainty in the velocity and flow rate are:

$$u_v = \sqrt{\left(u_m \frac{\partial V}{\partial p_{mmfluid}}\right)^2 + \left(u_{\rho_{air}} \frac{\partial V}{\partial \rho_{air}}\right)^2} = \sqrt{(u_{v_p})^2 + (u_{v_{\rho_{air}}})^2}$$

$$u_{v_p} (m/sec) = \pm 44.72 \sqrt{\frac{1.962 \times 0.001 \times 0.827}{\rho}} \left(\frac{1}{2} \frac{1}{\sqrt{p_{mmfluid}}}\right) u_m = \pm 0.418 m/sec$$

$$u_{v_{\rho_{air}}} = -\frac{1}{2} \times 44.72 \times \frac{\sqrt{1.962 \times 0.001 \times 0.827 \times (P_{mmfluid})}}{\sqrt{\rho_{air}}^3} \times u_{\rho_{air}} = \pm 0.041 m/sec$$

Maximum $u_{v_{\rho_{air}}}$ will occur with the largest $P_{mmfluid}$ measured ($P_{mmfluid} = 10$ mm).

Finally,

$$u_v = \sqrt{(0.418)^2 + (0.041)^2} = 0.420 m/sec$$

And,

$$Q_{m,air} (m^3/sec) = \pi r^2 V$$

where: $Q_{m,air}$ = the flow rate calculated by manometer readings

$$\pi r^2 = \text{cross-sectional area of duct} = 0.00203 \text{ m}^2$$

The uncertainty in the radius measurement is neglected since the measurement error is on the scale of 0.001m, which is considerably small against the velocity uncertainty of 0.420 m/sec.

$$u_{Q_{m,air}} = \pi r^2 u_v = 0.00203 \times u_v = \pm 0.000853 m^3/sec$$

A linear relationship was determined between the anemometer readings and the manometer readings, by the following equation:

$$Q_{anem.air} = 1.3855Q_{m.air} + 0.1379$$

where: $Q_{m.air}$ is the corrected flow rate

$Q_{anem.air}$ is equal to the calculated flow rate based on the anemometer reading.

The uncertainty in $Q_{m.air}$ is related to the uncertainty in the resultant $Q_{anem.air}$ by

$$u_{anem.air} = \left(\frac{dQ_{m.air}}{dQ_{anem.air}} \right)_{x=\bar{x}} u_{Q_{m.air}}$$

$$u_{anem.air} = 1.3855 \times \pm 0.0008530 (\text{m}^3/\text{sec}) = \pm 0.00118 \text{m}^3/\text{sec} = 1.18 \text{L}/\text{sec}$$

G.5 Gasoline Flow Rate

The gasoline flow rate was measured using a 50 mL burette with 1 mL markings. The initial and final burette readings were recorded for a 30 second time interval as described in Section 4.1.4.

$$Q_f = \frac{V_2(\text{mL}) - V_1(\text{mL})}{30(\text{sec})}$$

Assuming that the uncertainty in the operation of the stopwatch was negligible, the uncertainty in the gasoline flow rate is based on the errors associated with the burette reading, u_v .

$$u_{v_1} = u_{v_2} = \pm 0.05 \text{mL}$$

and

$$u_{Q_f} = \sqrt{\left(u_{v_1} \left(\frac{\partial Q_f}{\partial V_1}\right)\right)^2 + \left(u_{v_2} \left(\frac{\partial Q_f}{\partial V_2}\right)\right)^2} = \sqrt{\left(u_{v_1} \left(-\frac{1}{t}\right)\right)^2 + \left(u_{v_2} \left(\frac{1}{t}\right)\right)^2} = \pm 0.0024 \text{ mL/s}$$

where $t=30$ sec.

Using the ideal gas law ($T=294\text{K}$ and 1 atm), the uncertainty factor was corrected for gasoline flow rates reported as a vapour. Therefore the $u_{Q_f} = \pm 0.00035$ L/s for gasoline vapour flow rates. The vapour flow rates, are used in the calculation of the equivalence ratio.

G.6 Equivalence Ratio

The equivalence ratio, ϕ , is calculated as:

$$\phi = \frac{FAR}{FAR_{stoic.}}$$

where: $FAR = \frac{Q_f}{Q_{air}}$

$$FAR_{stoic.} = 0.0168, \text{ Equation 4.6}$$

Therefore, the uncertainty in the equivalence ratio is a function of the uncertainty in the FAR calculation.

$$u_{\phi} = \frac{u_{FAR}}{0.0168}$$

$$\text{where: } u_{FAR} = \sqrt{\left(u_{Q_f} \frac{\partial FAR}{\partial Q_f}\right)^2 + \left(u_{Q_{air}} \frac{\partial FAR}{\partial Q_{air}}\right)^2} = \sqrt{\left(u_{q_f} \frac{1}{Q_{air}}\right)^2 + \left(u_{q_{air}} \frac{-Q_f}{Q_{air}^2}\right)^2}$$

and $u_{Q_f} = \pm 0.00035 \text{ L/s}$ (Section G.4)

$u_{Q_{air}} = 1.18 \text{ L/s}$ (Section G.3)

The uncertainty calculations are provided in Table G.2.

Table G.2 Equivalence ratio uncertainty calculations for each engine test completed

Test	Condition	Q_f	Q_{air}	FAR_{actual}	ϕ	U_{Qf}	U_{Qair}	U_{FAR}	u_ϕ
		L/s	L/s			L/s	L/s		
1	1	0.083	6.35	0.013	0.777	0.000350	1.180	0.00243	0.144
	2	0.084	6.29	0.013	0.795	0.000350	1.180	0.00251	0.149
	3	0.082	6.22	0.013	0.785	0.000350	1.180	0.00250	0.149
2	1	0.080	5.83	0.014	0.816	0.000350	1.180	0.00278	0.165
	2	0.078	5.72	0.014	0.812	0.000350	1.180	0.00281	0.168
	3	0.078	5.66	0.014	0.820	0.000350	1.180	0.00287	0.171
3	1	0.073	5.37	0.014	0.809	0.000350	1.180	0.00298	0.178
	2	0.072	5.24	0.014	0.818	0.000350	1.180	0.00310	0.184
	3	0.069	5.18	0.013	0.792	0.000350	1.180	0.00303	0.180
4	1	0.087	6.43	0.014	0.805	0.000350	1.180	0.00248	0.148
	2	0.086	6.29	0.014	0.814	0.000350	1.180	0.00257	0.153
	3	0.086	6.31	0.014	0.811	0.000350	1.180	0.00255	0.152
5	1	0.091	6.19	0.015	0.875	0.000350	1.180	0.00281	0.167
	2	0.092	6.12	0.015	0.895	0.000350	1.180	0.00290	0.173
	3	0.091	6.10	0.015	0.888	0.000350	1.180	0.00288	0.172
6	1	0.085	6.81	0.012	0.743	0.000350	1.180	0.00216	0.129
	2	0.085	6.74	0.013	0.751	0.000350	1.180	0.00221	0.131
	3	0.086	6.73	0.013	0.761	0.000350	1.180	0.00224	0.133
7	1	0.084	6.31	0.013	0.793	0.000350	1.180	0.00249	0.148
	2	0.083	6.36	0.013	0.777	0.000350	1.180	0.00242	0.144
	3	0.084	6.36	0.013	0.787	0.000350	1.180	0.00245	0.146
8	1	0.086	7.01	0.012	0.730	0.000350	1.180	0.00206	0.123
	2	0.085	6.93	0.012	0.730	0.000350	1.180	0.00209	0.124
	3	0.087	6.96	0.012	0.744	0.000350	1.180	0.00212	0.126
9	1	0.085	7.30	0.012	0.693	0.000350	1.180	0.00188	0.112
	2	0.084	7.16	0.012	0.698	0.000350	1.180	0.00193	0.115
	3	0.083	7.16	0.012	0.690	0.000350	1.180	0.00191	0.114
10	1	0.090	6.53	0.014	0.821	0.000350	1.180	0.00249	0.148
	2	0.083	6.41	0.013	0.770	0.000350	1.180	0.00238	0.142
	3	0.078	6.42	0.012	0.723	0.000350	1.180	0.00224	0.133
11	1	0.083	6.90	0.012	0.716	0.000350	1.180	0.00206	0.122
	2	0.081	6.75	0.012	0.714	0.000350	1.180	0.00210	0.125
	3	0.080	6.69	0.012	0.712	0.000350	1.180	0.00211	0.126

G.7 Encoder

The sources of uncertainty for the encoder include the uncertainty in the encoder, u_{encoder} , and the uncertainty being the alignment of the encoder TDC signal with the actual TDC, u_{TDC} . The u_{encoder} is based on the manufactures specification of $\pm 0.25^\circ$ (0.004363 radians).

The alignment of the encoder TDC signal and the actual piston TDC is likely to cause the larger source of error. First, the encoder is mounted on the shaft of the engine and connected to the data acquisition board. A light was connected to the data acquisition board, so when the encoder sent a TDC signal the light would illuminate. Before securing the encoder onto the engine shaft the actual piston TDC signal had to be located. To accomplish this the spark plug was replaced with a dial gage. A maximum reading on the dial gage represents the TDC. The encoder was secured to the shaft when both the dial gage was at its maximum reading and the light on the data acquisition board was illuminated. The uncertainty in determining the location of the TDC therefore depended on the uncertainty of the dial gage reading, which is $\pm 0.0127\text{mm}(\pm 0.0005'')$. To following equation was used to convert this uncertainty to degrees:

$$\sin \theta = 90 - \frac{(L/2) - \text{dial gage error}}{L/2}$$

where: L = compression stroke length = 70 mm

dial gage error = ± 0.0127 mm

Therefore, $u_{\text{TDC}} = \pm 1.54^\circ$ (0.02688 radians)

The overall uncertainty for the encoder is

$$u_{\theta} = \sqrt{u_{\text{TDC}}^2 + u_{\text{encoder}}^2} = \sqrt{1.54^2 + 0.25^2} = 1.56^\circ \text{ or } (0.0272 \text{ radians})$$

D.8 Cylinder Volume

The cylinder volume is calculated based on the Equations described in Chapter 4:

$$V = V_c + V_s \quad (4.9)$$

$$V_s = (l + a - s)\pi B^2 / 4 \quad (4.10)$$

$$s(\theta) = a \times \cos(\theta) + [l^2 - a^2 \times \sin^2(\theta)]^{1/2} \quad (4.11)$$

where l = connecting rod length (Briggs & Stratton 20HP Engine = 0.105 m)

a = crank radius = (Briggs & Stratton 20 HP Engine = 0.035 m)

B = cylinder bore (Briggs & Stratton 20HP Engine = 0.072 m)

s = stroke variation

The uncertainty in the volume is mainly a result of the uncertainty in the crank angle degree:

$$u_{s(\theta)} = u_\theta \frac{\partial s(\theta)}{\partial \theta} = u_\theta \left(-a \sin \theta + \frac{a^2 \sin \theta \cos \theta}{\sqrt{l^2 - a^2 \sin^2 \theta}} \right)$$

where: $u_\theta = 0.0272$ radians, as calculated in G.6

The largest uncertainty value is calculated at $\theta = 1.86$ radians

$$u_{s(\theta)} = \pm 1.004 \text{ mm}$$

Therefore, the uncertainty in the volume calculation is

$$u_{V_s} = u_{s(\theta)} \frac{\partial V_s}{\partial s} = u_{s(\theta)} (\pi B^2 / 4) = \pm 1.004 (\pi (72)^2 / 4) = \pm 4085 \text{ mm}^3$$

The uncertainty in volume, u_V is equal to u_{V_s} since the clearance volume, V_c , is constant.

$$u_V = u_{V_s} = \pm 4085 \text{ mm}^3$$

D.9 Data Acquisition System and Pressure Transducer

The data acquisition system used to collect the pressure data and encoder signals uses a 16-bit A/S with an input resolution error equal to [Wheeler and Ganji, 1996]:

$$\text{Input resolution error} = \pm 0.5 \left[\frac{V_m - V_n}{2^N} \right] = \pm 0.5 \left[\frac{10 - (-10)}{2^{16}} \right] = \pm 0.0001526 \text{ V}$$

Where: V_m = upper value of input range (10V)

V_n = lower value of input range (10V)

N = number of bits (16)

To convert the input resolution error into kPa Equation 4.12 is used

$$p(\text{kPa}) = \frac{V_{out} (\text{1pC/mV})(1000\text{mV/V})(6.895\text{kPa/psi})}{1.085\text{pC/psi}(10)} \quad (4.12)$$

$$p(\text{kPa}) = \frac{\pm 0.0001526(1\text{pC/mV})(1000\text{mV/V})(6.895\text{kPa/psi})}{1.085\text{pC/psi}(10)} = 0.097\text{kPa}$$

The pressure transducer was calibrated by PCB Piezotronics. The uncertainty due to the result of the uncertainty of the dead weight tester used in the calibration was $\pm 1\%$. The accuracy is the linearity specification, which is $\pm 0.15\%$ or ± 31.0 kPa. The pressure transducer is attached with a sensing line, via the spark plug allowing a conduit for the pressure transducer to measure the gas in the cylinder. There is an uncertainty associated with the damping effect caused by the sensing line, which is based on the natural frequency (f_n) of the system [Wheeler and Ganji, 1996]:

$$f_n = \frac{\omega_n}{2\pi} = \frac{C}{2\pi L_s \sqrt{0.5 + V_t/V_s}}$$

where: f_n = natural frequency, Hz

ω_n = undamped natural frequency, Hz

C = speed of sound in air (346 m/s at 298 K)

L_s = length of sensing line (≈ 20 mm)

$$V_s = L_s \frac{\pi(d_s)^2}{4} \approx 20 \frac{\pi(2)^2}{4} \approx 62.83 \text{ mm}^3 = \text{volume of sensing line}$$

$$V_t = L_t \frac{\pi(d_t)^2}{4} \approx 30 \frac{\pi(5)^2}{4} \approx 589.05 \text{ mm}^3 = \text{volume of transducer chamber}$$

L_t = length of transducer (≈ 30 mm)

d_s = diameter of sensing line (≈ 2 mm)

d_t = diameter of transducer (≈ 5 mm)

Therefore, by substituting in the values, $f_n = 880.66$ Hz

The damping ratio, ζ is equal to

$$\zeta = \frac{R_t L}{2\rho C} \sqrt{0.5 + \frac{V_t}{V_s}}$$

where: ρ = density of air (1.18 kg/m³ at 298 K and 1 atm)

$R_f = 32\nu/d_s^2$ = fluid resistance offered by the sensing line

ν = air viscosity (1.8*10⁻⁵ Ns/m²)

d_s = diameter of sensing line (\approx 2 mm)

Substituting in the correct values gives, $\zeta = 0.0076$

The error in amplitude is determined by the equation

$$\text{Error in amplitude} = \left[\left(1 - \frac{\omega^2}{\omega_n^2} \right) + \left(\frac{2\zeta\omega}{\omega_n} \right)^2 \right]^{-1/2}$$

Where: ω_n = undamped natural angular frequency in rad/s or

$$\omega_n = f_n 2\pi = (880.67)(2\pi) = 5533 \text{ rad/s}$$

ω = actual angular frequency (greatest error occurs with highest speed, 3600 rpm)

$$\omega = (3600 \text{ rpm})(1 \text{ min}/60 \text{ sec})(2\pi \text{ rad/rev})(1 \text{ cycle}/2\text{rev})=188 \text{ rad/sec.}$$

The error in amplitude based on this equation and data provided above = 1.0012. This indicates that the amplitude of the output signal will be at most 0.1% higher than the ideal output pressure due to the damping effect, $u_{damping} = 0.1\%$.

As the pressure transducer ages, drift may occur which would become apparent in the pressure-volume diagram. The pressure recorded over the compression stroke should remain consistent for each cycle with the pressure trace only varying after the spark due to the variation in combustion. This drift was not apparent in the p-V diagrams created during data analysis, and is therefore assumed to be negligible.

The total uncertainty in the pressure measurement, u_p , includes the uncertainty in the transducer, $u_{\text{transducer}}$ (1%), accuracy, u_{accuracy} (31 kPa), damping effect, u_{damping} (0.1%), and the data acquisition system, u_{data} (0.097kPa). However, the uncertainty values determined for the transducer, the damping effect and data acquisition system are insignificant when compared to the accuracy uncertainty, which is equal to ± 31 kPa.

G.10 Burn Duration

The pressure rise in a cylinder is caused by two factors, combustion and change in volume due to piston motion. The pressure rise due to combustion only, Δp or mass fraction burnt (mfb) is calculated by subtracting the unfired cycle's pressure trace, $\Delta p_{\text{unfired}}$, from the fired cycle's pressure trace, Δp_{fired} . The uncertainty associated with the calculation of Δp includes the uncertainty in the pressure measurements, $u_p = \pm 31$ kPa and the standard deviation of the unfired cycles for each test. The largest standard deviation in the averaged unfired cycles was 47.3. Therefore, the uncertainty in Δp is

$$u_{\Delta p} = \sqrt{u_{p_{\text{unfired}}}^2 + u_{p_{\text{fired}}}^2 + (st.dev._{\text{unfired}})^2} = \sqrt{(31)^2 + (31)^2 + (47.3)^2} = \pm 64.5$$

The difference in pressure was then normalized to a constant volume as in Equation 4.18.

$$\Delta p_{ci} = \Delta p_i \frac{V_i}{V_c}$$

Then the maximum uncertainty is calculated by

$$u_{\Delta p_{ci}} = \left(\sqrt{u_{\Delta p_i} \left(\frac{V_i}{V_c} \right)^2 + \left(u_{V_i} \left(\frac{\Delta p_i}{V_c} \right) \right)^2} \right)$$

for $u_v = \pm 4085 \text{ mm}^3$

$V_i =$ a maximum of 323205 mm³ at crank angle degree 540°

$V_c = 38200$ mm³

$u_{\Delta p_i} = \pm 64.5$ kPa

By substituting in the appropriate values, the maximum $u_{\Delta p_i}$ ($u_{\Delta p_i} = \pm 64.5$ kPa) occurs at the BDC (maximum volume). The uncertainty in the crank angle was then established by determining the corresponding number of crank angles associated with the maximum $u_{\Delta p_i}$. The uncertainty in the crank angle, u_{CAD} , is ± 2 CAD.

G.11 Gas Analysis

The IMR 2800P was calibrated on December, 2002 before use and has the following measurement range and accuracy as noted in Table G.3.

Table G.3 IMR 2800P Gas Analyser measurement and range

Parameter	Principal	Accuracy	Measuring Range	Measuring Resolution
O ₂	Electrochemical sensor	Z	0-20.9 %	0.1 %
CO	Electrochemical sensor	Z	1000 – 100000 ppm	1 ppm
NO	Electrochemical sensor	Z	100 – 4000 ppm	1 ppm
Gas temperature	Thermocouple	± 1 %	1200 °C	± 1 °C

Note: Z = ± 1 % of the end value of the range for 0 – 20 % of the measuring range.

Z = ± 5 % of the measured value for 20 – 100 % of the measuring range.

The ENERAC 3000E was calibrated on July 2 and July 17, 2003. The measurement range and accuracy of the unit is provided in Table G.4

Table G.4 ENERAC 3000E Gas Analyser measurement and range

Parameter	Principal	Accuracy	Measuring Range	Measuring Resolution
O ₂	Electrochemical sensor	±2 %	0-5 %	0.1 %
CO	Electrochemical sensor	±2 %	0 – 20000 ppm	1 ppm
NO	Electrochemical sensor	±2 %	0 – 4000 ppm	1 ppm
NO ₂	Electrochemical sensor	±2 %	0 – 500 ppm	1 ppm
HC	Infrared Sensor	±5 %	0 – 30000 ppm	1 ppm
Ambient Temperature	IC Sensor	3 °F	66 °C	1 °C
Gas temperature	Thermocouple	5 °F	1100 °C	1 °C

G.12 Electrolysis Products Flow Rate

The flow rate of the electrolysis products was measured using a mini-Buck M-30 flow calibrator. The mini-Buck is capable of measuring flows between 100 cc/min and 30 L/min. The manufactures specifications for the mini-Buck calibrator note an accuracy of ±0.5 % of the displayed reading.

$$u_{Buck} = \pm 0.5\%$$

VITA AUCTORIS

Name	Karina Joan Richters
Place of Birth	Windsor, Ontario, Canada
Date of Birth	November 20, 1975
Education	Oakwood Elementary School Windsor, Ontario, Canada 1989
	Massey Secondary School Windsor, Ontario, Canada 1994
	University of Windsor Windsor, Ontario, Canada Bachelor of Applied Science Environmental Engineering 1998
	University of Windsor Windsor, Ontario, Canada Candidate for Masters of Applied Science Environmental Engineering 2004